

CONTRACT NAS8-11101

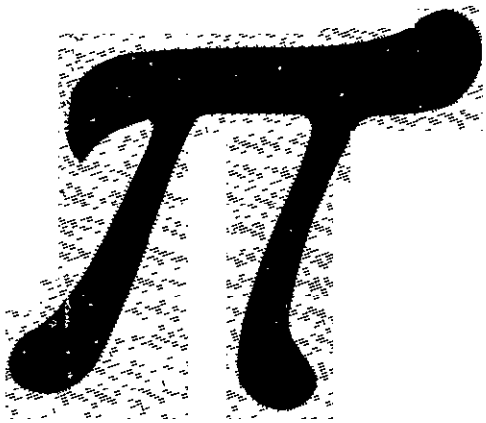
MCR-68-87
Copy No

Martin

USE OF DYNAMIC SCALE MODELS TO DETERMINE LAUNCH VEHICLE CHARACTERISTICS

FINAL REPORT

VOLUME II EXPERIMENTAL INVESTIGATION



FACILITY FORM 602	(ACCESSION NUMBER) N69-11165	(THRU)
	(PAGES) 57-102280	(CODE)
	(NASA CR OR TMX OR AD NUMBER)	(CATEGORY)
		32

AUGUST 1969

prepared for NATIONAL AERONAUTICS AND SPACE ADMINISTRATION
GEORGE G. MARSHALL SPACE FLIGHT CENTER
HUNTSVILLE, ALABAMA 35812

Reproduced by the
CLEARINGHOUSE
for Federal Scientific & Technical
Information Springfield Va. 22151

MARTIN MARIETTA CORPORATION

MCR-68-87

CONTRACT NAS8-21101


USE OF DYNAMIC SCALE MODELS
TO DETERMINE
LAUNCH VEHICLE CHARACTERISTICS
FINAL REPORT
VOLUME II. EXPERIMENTAL INVESTIGATION

August 1969

Author

F. A. Penning

Approved


George Morosow
Program Manager

FOREWORD

This volume presents the results of an experimental study performed from May 18, 1968 through July 31, 1969 on the use of dynamic scale models to determine launch vehicle characteristics. The investigation was conducted by the Denver Division of the Martin Marietta Corporation, Denver, Colorado, for the National Aeronautics and Space Administration, George C. Marshall Space Flight Center, Huntsville, Alabama, under extension of Contract No. NAS8-21101. Mr. L. Kiefling was the principal representative for the contracting office.

Mr. George Morosow was the Program Manager for the Denver Division and all work was performed under the direction of Mr. Morosow and Mr. Francis A. Penning, Principal Investigator. Significant contributions were provided by C. Forsyth, D. A. Stang, and J. T. Thompson of the Denver Division. In addition, Mr. Thomas H. Cooper, President, Plasticrafts, Inc., Denver, Colorado, provided many valuable discussions regarding model fabrication.

An analytical study, completed May 17, 1968, is presented in Volume I.

The contractor's designation of this report is MCR-68-87.

ABSTRACT

This study considers the use of distorted models to provide experimental information regarding prototype behavior. Of the many tests performed on launch vehicles, this report details the free vibrations of cylindrical and conical shells. The structures are individual segments of the second stage of the Saturn V rocket. Test conditions are clamped boundary conditions and no pressure nor axial loads.

From the governing differential equations for shell vibrations the important parameters are identified. These are scaled for exact dynamic similitude then are manipulated to produce distorted models. By using the laws of similitude and from numerical values of scaled quantities vibration studies of models are related directly to the prototype.

CONTENTS

	<u>Page</u>
Foreword	ii
Abstract	iii
Contents	iv thru viii
Summary	ix
I. Introduction	I-1
Symbols	I-3 thru I-4
II. Shell Vibrations	II-1 thru II-11
III. Similitude	III-1 thru III-11
IV. Prototype Properties	IV-1 thru IV-7
V. Modeling	V-1
A. Model Dimensions	V-1
B. Material Selection	V-1
C. Skin-Stringer Cylinder Models	V-8
D. Skin-Stringer Cone Models	V-11
E. Gridwork Cylinder Models	V-12
F. Gridwork Cone Models	V-17
G. Summary of Model Designs	V-18 thru V-28
VI. Distorted Models	VI-1 thru VI-8

	<u>Page</u>
VII. Experimental Procedure	VII-1
A. Model Construction	VII-1
1. Cellulose Acetate Models	VII-1
2. Flexible Polyvinyl Chloride Models	VII-2
3. Summary of Cylinder and Cone Models	VII-9
B. Boundary Conditions	VII-11
C. Excitation and Measuring	VII-13 thru VII-18
VIII. Results	VIII-1
A. Experimental Data	VIII-1
B. Comparisons with Other Data	VIII-4
C. Conclusions	VIII-9
IX. References	IX-1

Figure

II-1 Internal Forces and Moments on Shell Element	II-3
II-2 Elastic Relations for an Orthotropic Material	II-6
II-3 Notation for Stiffened Shells--..	II-9
II-4 Free Vibration Modes for Simply Supported Cylindrical Shells	II-11
III-1 Ratio of Model Time to Prototype Time for 1/10 and 1/20 Scale Models	III-10
IV-1 Portions of Saturn V, Second Stage Used in Modeling.	IV-1
IV-2 Saturn V, Second Stage, Tank Wall, Skin Stringer	IV-5
IV-3 Saturn V, Second Stage, Forward Skirt Skin Stringer	IV-6
IV-4 Saturn V, Adapter, Second to Third Stage, Skin Stringer	IV-7
V-1 Dimensions of the Three Model Shells	V-1

<u>Figure</u>		<u>Page</u>
V-2	Modulus of Elasticity as a Function of Specific Gravity for Model Material	V-5
V-3	Modulus of Elasticity and Specific Gravity for Metals and Wood	V-6
V-4	Section of Composite Gridwork Shell	V-13
V-5	Details of Skin-Stringer Cylinder and Cone Models .	V-21
V-6	Details of Developed Surface for Composite Gridwork Shells	V-26
V-7	Reinforcing Details of Composite Gridwork Shells . .	V-27
V-8	Details of Cone C Dimensions and Developed Surface .	V-28
VI-1	Alternate Sections for a Uniform Section	VI-2
VI-2	Permissible Regions for Cruciform and H-Section to Provide Rigidities	VI-4
VI-3	The Several Wall Thicknesses for Cellulose Acetate .	VI-6
VI-4	Several Wall Thicknesses for Cylinder A Made of Flexible PVC	VI-8
VII-1	Cellulose Acetate Cylinders and Cone	VII-3
VII-2	Cardboard Structure for Support of Plaster Mandrel .	VII-5
VII-3	Steps in Applying Glass Filaments on Cone C	VII-6
VII-4	Cylinders A and B on Mandrel After Glass Filaments Wound at Intervals	VII-7
VII-5	Flexible Polyvinyl Chloride Cylinders and Cone . . .	VII-8
VII-6	Clamping Plates Showing Cylinder on Left Side and Cone on Right Side	VII-12
VII-7	Schematic of Instrumentation and Acoustic Speaker .	VII-14
VII-8	Baffle and Horn in Front of Speaker Cone	VII-16

<u>Figure</u>		<u>Page</u>
VII-9	Cylinder A in Test Setup with Associated Measuring Devices	VII-17
VII-10	Electronics Equipment for Exciting and Measuring Dynamic Response	VII-18
VIII-1	Frequencies for Cylinder A, Cellulose Acetate	VIII-5
VIII-2	Frequencies for Cylinder B, Cellulose Acetate	VIII-6
VIII-3	Frequencies for Cone C, Cellulose Acetate as an Equivalent Cylinder	VIII-7
VIII-4	Frequencies for Simply Supported Aluminum Cylinders with Internal, External and No Stiffeners	VIII-8

Table

II-1	Internal Forces and Moments in Terms of Rigidities and Deformations	II-4
II-2	Shell Rigidities in Terms of Elastic Constants and Geometry	II-8
III-1	Independent and Dependent Variables	III-2
III-2	Scale Factors for Modeling	III-9
IV-1	Saturn V Second Stage Extensional and Flexural Rigidities	IV-2
IV-2	Saturn V, Second Stage π Terms for Extensional and Flexural Rigidities	IV-3
V-1	Calculated and Actual Shell Dimensions and Rigidities	V-19
V-2	Scaled and Unscaled Terms	V-20
V-3	Calculated and Design Shell Dimensions and Reinforcing for Composite Gridwork Shells	V-22
V-4	Scaled and Unscaled π Terms for Composite Gridwork Shell Models	V-23
V-5	Composite Moduli Time Scales, and Gravity Factors for Gridwork Shells	V-24

<u>Table</u>		<u>Page</u>
VII-1	Summary for Cellulose Acetate Models	VII-9
VII-2	Summary for Flexible PVC Models	VII-10
VIII-1	Observed Frequencies for Cellulose Acetate Shells .	VIII-2
VIII-2	Observed Frequencies for Flexible PVC Shells	VIII-3

SUMMARY

Each of the several portions of the multiphased problem of dynamic similitude of shell structures are presented; analysis, design, fabrication, and experiment. Orthotropic cylinders and cones are modeled using dissimilar materials both as isotropic materials and composite materials.

Shell vibrations and ring vibrations in extensional and inextensional modes are studied to identify the material and geometry parameters that are important. Basic dimensions of the vibration problem are mass, length and time; therefore, these are isolated by three arbitrary scale factors. Dependent and independent variables are made nondimensional and evaluated for the prototype. Models are designed to provide the same numerical values for corresponding nondimensional terms.

From the designs models are fabricated. One group is skin-stringer construction made of cellulose-acetate. The other group is gridwork construction made of a composite consisting of flexible polyvinyl chloride, steel wire, and glass filaments. After fabrication the models are held circular and fixed at the boundaries and excited using an acoustic driving system.

Resonance is found and wave shape determined. Comparisons are made between theoretical predicted and measured frequencies. Conclusions and recommendations are given based on the knowledge gained during this study.

I. INTRODUCTION

Dynamic models are used in the research and development phases of aerospace vehicles. Models serve to supplement or in some cases to completely replace dynamic tests of the full scale prototype launch vehicles. They are used to verify analytical methods of vibration analysis, for loads and stability analyses and to determine the aeroelastic characteristics of launch vehicles.

This study concerns the use of distorted models to provide experimental information regarding prototype behavior. Of the many tests performed on aerospace structures, we have considered only the free vibrations of shells. Further, the structures are individual shell segments of the second stage of the Saturn V rocket, tested with clamped boundary conditions, and not subjected to loads or pressures. From the differential equations describing shell vibrations we obtain the several factors important to the problem. By using the laws of similitude and from properly scaled quantities, identified in the differential equations, vibration studies of models are related directly to the prototype.

Several classes of problems occur in the study of large aerospace structures. Significant differences in the response and modeling requirements are imposed by continuity of structure, aeroelastic response, liquid fuel slosh effects, flight or ground conditions, loaded and unloaded structure, plus other loads and environments. For some of these conditions certain scaling conditions can be ignored between model and prototype such as modulus to density ratio, or gravity force, or liquid densities and viscosities, depending on their relative importance. Without specific knowledge of the modeling requirements, it is not possible to classify certain parameters as always being important. The identical prototype structure being modeled to obtain response information for several kinds of loadings may need models made of material different than the prototype, or tested in a centrifuge, or simulated by an equivalent beam, or other such requirements imposed by numerically matching nondimensional factors.

Among the more renowned factors are the Reynolds number and the Mach number used in aerodynamic model studies. No correspondingly "named" numbers have appeared for structures to be modeled for vibration or buckling other than mention of the length to radius of gyration ratio for an Euler column. Nonetheless, the requirements that have established the well known numbers are steeped in the same basic physical law requirements when applied to either solid or fluid mechanics problems.

The physical size and geometric scaling factor of launch vehicle dynamic models vary over a broad range: some are the size of intermediate range ballistic missiles, while others have diameters of only a few inches. Scale factors range from 2.5% to 20% of the full-scale vehicle. The manufacturing technology required to construct such models varies considerably depending on the accuracy requirements. When a dynamic model is used primarily to verify the analysis of the full-scale vehicle, exact scaling of the prototype may not be necessary. When the data acquired in the model test program are used directly to predict or verify full-scale flight article characteristics, a more precise approach to model scaling, design, and manufacturing is needed.

Two basic philosophies are prevalent in the design of dynamic models of launch vehicles; direct geometric scaling, and distorted geometric scaling. Both approaches preserve the external geometry of the vehicle. However, the more general modeling approach of building mechanical analog structures of dissimilar shape has not gained, thus far, a significant role in any launch vehicle program.

Direct geometric scaling, using similar materials for model and prototype, satisfies more easily the nondimensional terms, and is a more common approach to launch vehicle modeling. Direct scaling however is limited by manufacturing and tolerance control problems when shell skin gages become unmanageably thin and by the inability to simulate coupled structural-slosh modes of the boost phase. Another area where the direct scaling approach has limited use is wind tunnel testing of aeroelastic models.

The distorted scaling approach, as applied to typical launch vehicles, may neglect scaling parameters of small influence in order to preserve important parameters. Thus, the use of distorted models, in general, is oriented toward a particular type of test program. Frequently, both the materials and the construction techniques used to build a distorted model are different from those used in the prototype. When such different technologies are used, verification of the model scaling, and construction techniques is essential. Such verification is accomplished by comparing test results of simple model structures with the known properties of full-scale structures or of analysis.

A related problem area, is the correlation of structural damping of models and full-scale launch vehicle structures.

Experimental values of structural damping obtained from full-scale launch vehicle tests follow an empirical equation. This can serve as a basis for correlating measured model damping data with full-scale damping

Symbols found in the analysis are identified in the following tabulation.

Symbol

A	stiffener or rib area
a	cylinder radius of reference surface
b	stiffener or rib spacing
c	centroid of area from reference surface
D	flexural rigidity
E	modulus of elasticity
G	shear modulus
g	gravitational constant
h	shell wall thickness
I	moment of inertia of stiffener or rib
J	polar moment of inertia of stiffener or rib
K	extensional rigidity
l	shell length
M	unit moment
m	number of axial half waves
N	unit stress resultant
n	number of circumferential waves
n_i	independent scale factor ($i = 1, 2, 3$)
r_i	ratio number ($i = 1, 2, 3, 4$)
S	rigidity moment
t	time, also stringer or rib width
u,v,w	displacements

x	axial direction
γ	weight density
Δ	nondimensional frequency
ϵ	strain
ν	Poisson ratio
π_i	nondimensional factor ($i = 1, 2, 3 \dots$)
ρ	mass density
σ	stress
τ	shear stress
ϕ	circumferential direction
ω	frequency

Subscript

m	model
p	prototype
x	x direction
ϕ	ϕ direction
$x\phi$	in a plane normal to x and in ϕ direction
ϕx	in a plane normal to ϕ and in x direction

II. SHELL VIBRATIONS

Analytical development of dynamic response of circular structures has a relatively long history. Rings were studied by R. Hoppe in 1871, inextensional vibrations of cylinder by Lord Rayleigh in 1881, and general vibrations of cylinders by Arnold and Warburton in 1943. These and other studies show the recurrence of geometry and material parameters that determine frequencies and wave numbers.

For rings of circular cross section, c , frequency for wave number n is [1]*

$$\text{freq.} = \frac{c}{4\pi a^2} \sqrt{\frac{E}{\rho}} \frac{n(n^2-1)}{\sqrt{n^2+1}} \quad (\text{where } \rho = \frac{\gamma}{g})$$

For cylinders undergoing inextensional vibrations [1] we have for circular frequency

$$\text{freq.} = \frac{h}{2\pi a^2} \sqrt{\frac{E}{\rho(1-\nu^2)}} \frac{n(n^2-1)}{\sqrt{n^2+1}}$$

Studies by Arnold and Warburton [2] show for the more general case

$$\text{freq.} = \frac{1}{2\pi a} \sqrt{\frac{E}{\rho(1-\nu^2)}} \sqrt{\Delta}$$

in which the factor $\sqrt{\Delta}$ is a function of material, geometry, boundary conditions, and vibration modes. In these equations modulus E and unit mass density ρ are combined in the ratio $\sqrt{E/\rho}$ (the dilatational wave velocity of circular rods). It will be shown that this ratio occurs in each term of the dynamic differential equations for gridwork, stiffened, and monocoque cylinders. Although this affects the nondimensionalization of independent scale factors the general treatment will consider modulus and density as being independent.

Any physical problem that can be formulated mathematically, as has been done for shell vibrations, will yield the complete set of physical parameters that influence the phenomena [3].

*Numbers in brackets are references in Section IX.

Similitude requirements can be calculated for these physical parameters therefore the number of properly scaled, poorly scaled and neglected independent variables can be determined. The differential equations describing a freely vibrating cylinder are given by Flügge [4] in terms of forces and moments and are presented as Equations (II-1). Generally the last of Equations (II-1) is neglected because of small differences in $N_{x\phi}$ and $N_{\phi x}$.

$$\frac{\partial N_x}{\partial x} + \frac{1}{a} \frac{\partial N_{\phi x}}{\partial \phi} = \rho h \frac{\partial^2 u}{\partial t^2} \quad (\text{where } \rho = \frac{\gamma}{g}) \quad (\text{II-1a})$$

$$\frac{1}{a} \frac{\partial N_\phi}{\partial \phi} + \frac{\partial N_{x\phi}}{\partial x} - \frac{\partial M_\phi}{\partial \phi} - \frac{1}{a} \frac{\partial M_{x\phi}}{\partial x} = \rho h \frac{\partial^2 v}{\partial t^2} \quad (\text{II-1b})$$

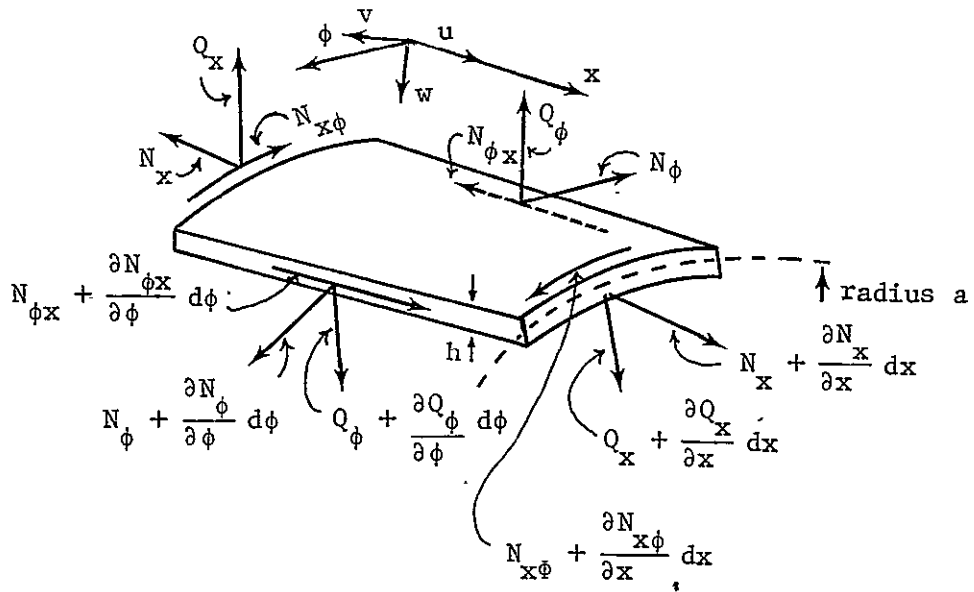
$$\frac{1}{a^2} \frac{\partial^2 M_\phi}{\partial \phi^2} + \frac{1}{a} \frac{\partial^2 M_{x\phi}}{\partial x \partial \phi} + \frac{\partial^2 M_x}{\partial x^2} + \frac{1}{a} N_\phi = -\rho h \frac{\partial^2 w}{\partial t^2} \quad (\text{II-1c})$$

$$a N_{x\phi} - a N_{\phi x} + M_{\phi x} = 0 \quad (\text{II-1d})$$

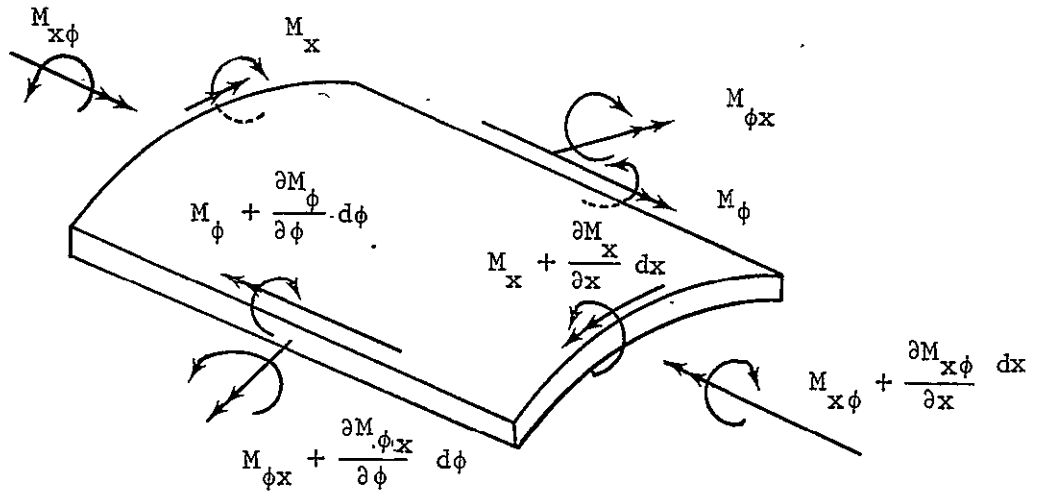
Forces and moments appearing in these equations are shown acting on the shell element of Fig. II-1. The free vibrations of the several kinds of cylindrical shells are described by these equations. In Table II-1 the internal forces and moments as produced by reference surface deformation are given for gridwork, ring and stringer, skin-stringer and monocoque cylindrical shells. Details of construction, such as distribution of material in stiffened shells, produce differences in the internal equilibrium system of the respective shells. Because our interest is in prototype shells made of a single isotropic material we are not including constructions such as sandwich and filament-winding.

For shell analysis three assumptions are made regarding the behavior of the shell and its material. These are reviewed to provide guidance in the event distorted scaling may tend to invalidate these conditions.

1. Points on a normal to the middle surface remain on the normal after deformation;
2. Any point z away from the middle surface is unaffected by deformations and remains at distance z ;



a. Internal Forces on Shell Element



b. Internal Moments Acting on Shell Element

Fig. II-1 Internal Forces and Moments on Shell Element

Table II-1 Integral Forces and Moments in Terms of Rigidities and Deformations

Stress Result	Dimensions		Type of Cylindrical Shell			
	Engr	MLT	Gridwork	Ring and Stringer	Skin-Stringer	Monocoque
N_{ϕ}	$\frac{lb}{in.}$	MT ⁻²	$\frac{K_{\phi}}{a} \left(\frac{\partial v}{\partial \phi} + w \right) + \frac{S_{\phi}}{a^2} \frac{\partial^2 w}{\partial \phi^2}$	$\frac{K_{\phi}}{a} \left(\frac{\partial v}{\partial \phi} + w \right) + K_{\nu} \frac{\partial u}{\partial x} + \frac{S_{\phi}}{a^2} \frac{\partial^2 w}{\partial \phi^2}$	$\frac{K_{\phi}}{a} \left(\frac{\partial v}{\partial \phi} + w \right) + K_{\nu} \frac{\partial u}{\partial x}$	$\frac{K}{a} \left(\frac{\partial v}{\partial \phi} + w + \nu a \frac{\partial u}{\partial x} \right)$
N_x	$\frac{lb}{in.}$	MT ⁻²	$K_x \frac{\partial u}{\partial x} + S_x \frac{\partial^2 w}{\partial x^2}$	$K_x \frac{\partial u}{\partial x} + \frac{K_{\nu}}{a} \left(\frac{\partial v}{\partial \phi} + w \right) + S_x \frac{\partial^2 w}{\partial x^2}$	$K_x \frac{\partial u}{\partial x} + \frac{K_{\nu}}{a} \left(\frac{\partial v}{\partial \phi} + w \right) + S_x \frac{\partial^2 w}{\partial x^2}$	$\frac{K}{a} \left(a \frac{\partial u}{\partial x} + \nu \frac{\partial v}{\partial \phi} + \nu w \right)$
$N_{\phi x}$	$\frac{lb}{in.}$	MT ⁻²	$\frac{K_{\phi x}}{a} \left(\frac{\partial u}{\partial \phi} + a \frac{\partial v}{\partial x} \right) + \frac{D_{\phi x}}{a^2} \frac{\partial^2 w}{\partial x \partial \phi}$	$\frac{K_{\phi x}}{a} \left(\frac{\partial u}{\partial \phi} + a \frac{\partial v}{\partial x} \right) + \frac{D_{\phi x}}{a^2} \frac{\partial^2 w}{\partial x \partial \phi}$	$\frac{K_{\phi x}}{a} \left(\frac{\partial u}{\partial \phi} + a \frac{\partial v}{\partial x} \right) + \frac{D_{\phi x}}{a^2} \frac{\partial^2 w}{\partial x \partial \phi}$	$\frac{K}{2a} (1 - \nu) \left(\frac{\partial u}{\partial \phi} + a \frac{\partial v}{\partial x} \right)$
$N_{x\phi}$	$\frac{lb}{in.}$	MT ⁻²	$\frac{K_{\phi x}}{a} \left(\frac{\partial u}{\partial \phi} + a \frac{\partial v}{\partial x} \right)$	$\frac{K_{\phi x}}{a} \left(\frac{\partial u}{\partial \phi} + a \frac{\partial v}{\partial x} \right)$	$\frac{K_{\phi x}}{a} \left(\frac{\partial u}{\partial \phi} + a \frac{\partial v}{\partial x} \right)$	$\frac{K}{2a} (1 - \nu) \left(\frac{\partial u}{\partial \phi} + a \frac{\partial v}{\partial x} \right)$
M_{ϕ}	1b	MLT ⁻²	$\frac{D_{\phi}}{a^2} \frac{\partial^2 w}{\partial \phi^2} + \frac{S_{\phi}}{a} \left(\frac{\partial v}{\partial \phi} + w \right)$	$\frac{D_{\phi}}{a^2} \frac{\partial^2 w}{\partial \phi^2} + K_{\nu} \frac{\partial^2 w}{\partial x^2} + \frac{S_{\phi}}{a} \left(\frac{\partial v}{\partial \phi} + w \right)$	$\frac{D_{\phi}}{a^2} \frac{\partial^2 w}{\partial \phi^2} + K_{\nu} \frac{\partial^2 w}{\partial x^2}$	$\frac{D}{a^2} \left(\frac{\partial^2 w}{\partial \phi^2} + \nu a^2 \frac{\partial^2 w}{\partial x^2} \right)$
M_x	1b	MLT ⁻²	$D_x \frac{\partial^2 w}{\partial x^2} + S_x \frac{\partial u}{\partial x}$	$D_x \frac{\partial^2 w}{\partial x^2} + \frac{D_{\nu}}{a^2} \frac{\partial^2 w}{\partial \phi^2} + S_x \frac{\partial u}{\partial x}$	$D_x \frac{\partial^2 w}{\partial x^2} + \frac{D_{\nu}}{a^2} \frac{\partial^2 w}{\partial \phi^2} + S_x \frac{\partial u}{\partial x}$	$\frac{D}{a^2} \left(a^2 \frac{\partial^2 w}{\partial x^2} + \nu \frac{\partial^2 w}{\partial \phi^2} \right)$
$M_{\phi x}$	1b	MLT ⁻²	$\frac{D_{\phi x}}{a} \frac{\partial^2 w}{\partial x \partial \phi}$	$\frac{D_{\phi x}}{a} \frac{\partial^2 w}{\partial x \partial \phi}$	$\frac{D_{\phi x}}{a} \frac{\partial^2 w}{\partial x \partial \phi}$	$\frac{D}{a} (1 - \nu) \frac{\partial^2 w}{\partial x \partial \phi}$
$M_{x\phi}$	1b	MLT ⁻²	$\frac{D_{\phi x}}{a} \frac{\partial^2 w}{\partial x \partial \phi}$	$\frac{D_{\phi x}}{a} \frac{\partial^2 w}{\partial x \partial \phi}$	$\frac{D_{\phi x}}{a} \frac{\partial^2 w}{\partial x \partial \phi}$	$\frac{D}{a} (1 - \nu) \frac{\partial^2 w}{\partial x \partial \phi}$

MCR-68-87

3. Displacements are small with respect to the radius and their first derivatives are much smaller than unity.

The first two assumptions presuppose the shell to be made of an artificial anisotropic material for which the modulus of elasticity, E_3 , in the thickness direction and the shear moduli G_{13} and G_{23} (for the shearing obtains γ_{13} and γ_{23}) are infinite, as identified on the element in the coordinate system of Fig. II-2. Furthermore, the Poisson ratios ν_{13} and ν_{23} are required to be zero.

For an orthotropic material the elastic moduli and the Poisson's ratio are related by

$$E_1 \nu_{12} = E_2 \nu_{21}$$

$$E_1 \nu_{13} = E_3 \nu_{31}$$

$$E_2 \nu_{23} = E_3 \nu_{32}$$

Shell theory assumes the following relations hold

$$E_3 \rightarrow \infty$$

$$G_{13} \rightarrow \infty$$

$$G_{23} \rightarrow \infty$$

$$\nu_{13} = \nu_{23} = 0$$

$$\epsilon_3 = \gamma_{31} = \gamma_{23} = 0$$

Therefore, the corresponding stress relations for shells are different from those shown in Fig. II-2 and are given by

$$\sigma_{11} = E_1 \epsilon_1 + E_2 \nu_{21} \epsilon_2$$

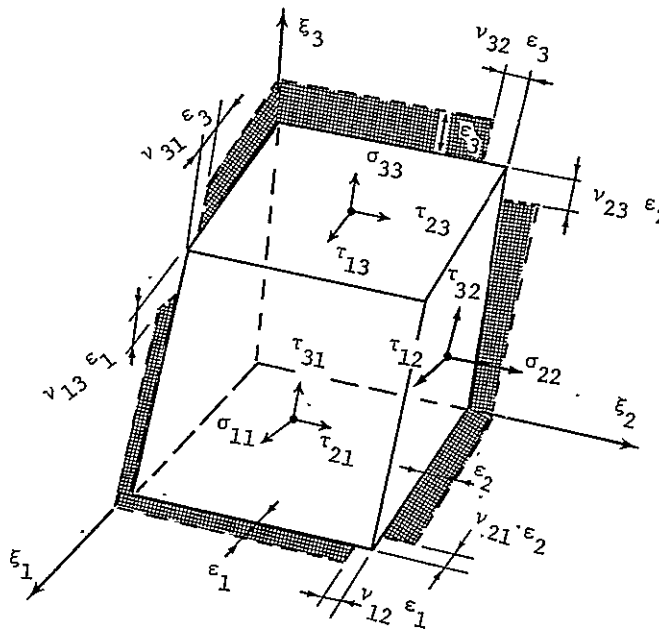
$$\sigma_{22} = E_1 \nu_{12} \epsilon_1 + E_2 \epsilon_2$$

$$\sigma_{33} = 0$$

$$\tau_{23} = 0$$

$\sigma_{11} =$	$E_1 \epsilon_1$	$+ E_2 \nu_{21} \epsilon_2$	$+ E_3 \nu_{31} \epsilon_3$			
$\sigma_{22} =$	$E_1 \nu_{12} \epsilon_1$	$+ E_2 \epsilon_2$	$+ E_3 \nu_{32} \epsilon_3$			
$\sigma_{33} =$	$E_1 \nu_{13} \epsilon_1$	$+ E_2 \nu_{23} \epsilon_2$	$+ E_3 \epsilon_3$			
$\tau_{23} =$				$G_{23} \gamma_{23}$		
$\tau_{31} =$					$G_{31} \gamma_{31}$	
$\tau_{12} =$						$G_{12} \gamma_{12}$

a. Hooke's Law for an Orthotropic Material



b. Element of Orthotropic Material

Fig. II-2 Elastic Relations for an Element of Orthotropic Material

$$\tau_{31} = 0$$

$$\tau_{12} = G_{12} \gamma_{12}$$

In order to completely formulate Equations (II-1) the several rigidities are required. Again considering gridwork, ring and stringer, skin-stringer and monocoque cylindrical shells, their respective extensional rigidities, rigidity moments, and bending rigidities are shown in Table II.2. Notation used in this table is illustrated by a portion of a stiffened shell shown in Fig. II-3. By incorporating the rigidities into the stress resultants in Table II.1 and operating on them as shown in Equations (II-1) it is possible to formulate the free vibration differential equation in terms of displacements, elastic constants, and radius to thickness ratio. The simplest form of these equations (for monocoque shells) are shown as Eqs. (II-2) to indicate the quantities to be scaled that will provide dynamic similitude in models.

$$K \frac{\partial^2 u}{\partial x^2} + G \frac{h}{2a^2} \frac{\partial^2 u}{\partial \phi^2} + \frac{E}{2(1-\nu)} \frac{h}{a} \frac{\partial^2 v}{\partial x \partial \phi} + \frac{E\nu}{1-\nu^2} \frac{h}{a} \frac{\partial w}{\partial x} = h\rho \frac{\partial^2 u}{\partial t^2} \quad (\text{II-2a})$$

$$\frac{E}{2(1-\nu)} \frac{h}{a} \frac{\partial^2 u}{\partial x \partial \phi} + \frac{G}{2} h \frac{\partial^2 v}{\partial x^2} + K \frac{1}{a^2} \frac{\partial^2 w}{\partial \phi^2} + K \frac{1}{a^2} \frac{\partial w}{\partial \phi} = h\rho \frac{\partial^2 v}{\partial t^2} \quad (\text{II-2b})$$

$$K \frac{\nu}{a} \frac{\partial}{\partial x} + K \frac{1}{a} \frac{\partial v}{\partial \phi} + K \frac{1}{a^2} w + DV^4 w = -h\rho \frac{\partial^2 w}{\partial t^2} \quad (\text{II-2c})$$

The terms K, G, and D each contain the elastic modulus E as shown in Table II.2, therefore each of the terms on the left-hand side of Eqs. (II-2) contain the ratio E/ρ. Consideration of boundary conditions gives one more parameter not shown in the equations, ℓ, the length of the cylinder. Displacement functions that satisfy boundary conditions at x=0 and x=ℓ are of the form

$$u = f(mx/\ell, n\phi, \omega t) \quad (\text{II-3a})$$

$$v = g(mx/\ell, n\phi, \omega t) \quad (\text{II-3b})$$

$$w = h(mx/\ell, n\phi, \omega t) \quad (\text{II-3c})$$

Table II-2 Shell Rigidities in Terms of Elastic Constants and Geometry

II-8

Type	Dimensions		Stiffened Cylindrical Shells				Unstiffened Cylinders	
	Engr	MLT	Symbol	Gridwork	Ring and Stringer	Skin-Stringer	Symbol	Monocoque
Extensional Rigidity	1b/in.	MLT ⁻²	K_ϕ	$\frac{EA_\phi}{b_1}$	$\frac{Eh}{1-\nu^2} + \frac{EA_\phi}{b_1}$	$\frac{Eh}{1-\nu^2}$		$\frac{Eh}{1-\nu^2}$
			K_x	$\frac{EA_x}{b_2}$	$\frac{Eh}{1-\nu^2} + \frac{EA_x}{b_2}$	$\frac{Eh}{1-\nu^2} + \frac{EA_x}{b_2}$		
			K_ν		$\frac{Eh\nu}{1-\nu^2}$	$\frac{Eh\nu}{1-\nu^2}$		
			$K_{x\phi}$	$\frac{12}{b_1 b_2} \left(\frac{b_2}{EI_r} + \frac{b_1}{EI_s} \right)^{-1}$	$\frac{Eh}{2(1+\nu)}$	$\frac{Eh}{2(1+\nu)}$	Gh	$\frac{Eh}{2(1+\nu)}$
Rigidity Moment	lb	MLT ⁻²	S_ϕ	$\frac{EA_\phi c_\phi}{b_1}$	$\frac{EA_\phi c_\phi}{b_1}$			
			S_x	$\frac{EA_x c_x}{b_2}$	$\frac{EA_x c_x}{b_2}$	$\frac{EA_x c_x}{b_2}$		
Bending Rigidity	in.-lb	ML ² T ⁻²	D_ϕ	$\frac{E(I_\phi + A_\phi c_\phi^2)}{b_1}$	$\frac{Eh^3}{12(1-\nu^2)} + \frac{E(I_\phi + A_\phi c_\phi^2)}{b_1}$	$\frac{Eh^3}{12(1-\nu^2)}$	D	$\frac{Eh^3}{12(1-\nu^2)}$
			D_x	$\frac{E(I_x + A_x c_x^2)}{b_2}$	$\frac{Eh^3}{12(1-\nu^2)} + \frac{E(I_x + A_x c_x^2)}{b_2}$	$\frac{Eh^3}{12(1-\nu^2)} + \frac{E(I_x + A_x c_x^2)}{b_2}$		
			D_ν		$\frac{Eh^3 \nu}{12(1-\nu^2)}$	$\frac{Eh^3 \nu}{12(1-\nu^2)}$		
			$D_{\phi x}$	$\frac{GJ_\phi}{b_1}$	$\frac{Eh^3}{12(1+\nu)} + \frac{GJ_\phi}{b_1}$	$\frac{Eh^3}{12(1+\nu)}$		
			$D_{x\phi}$	$\frac{GJ_x}{b_2}$	$\frac{Eh^3}{12(1+\nu)} + \frac{GJ_x}{b_2}$	$\frac{Eh^3}{12(1+\nu)} + \frac{GJ_x}{b_2}$		

MCR-68-87

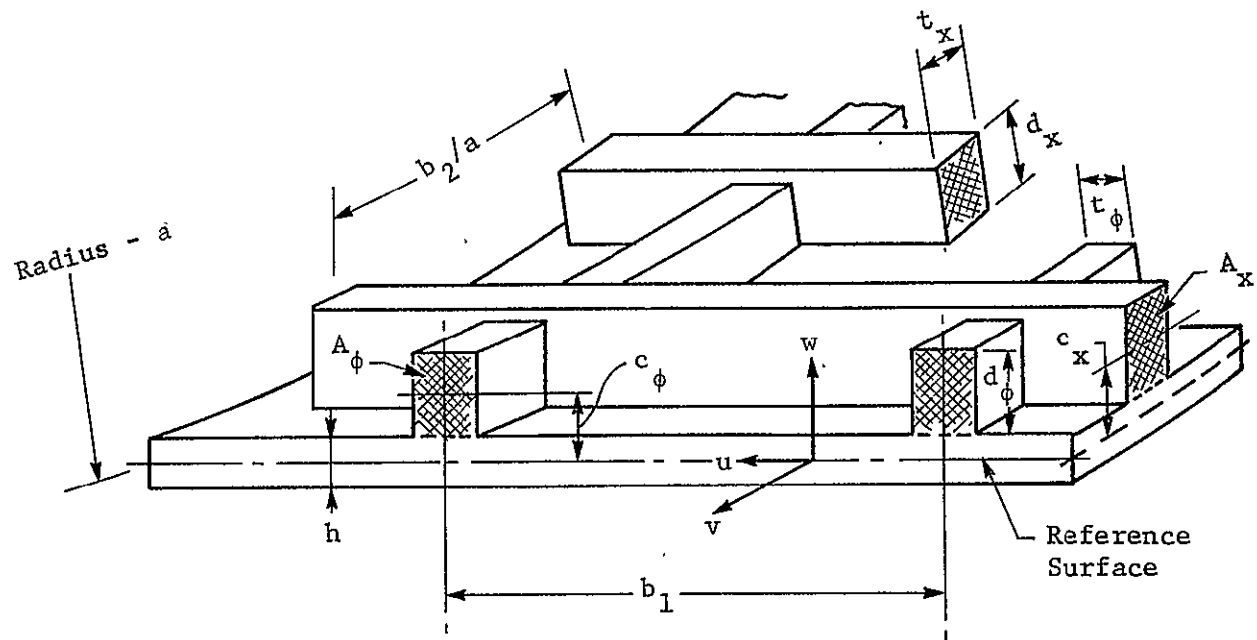
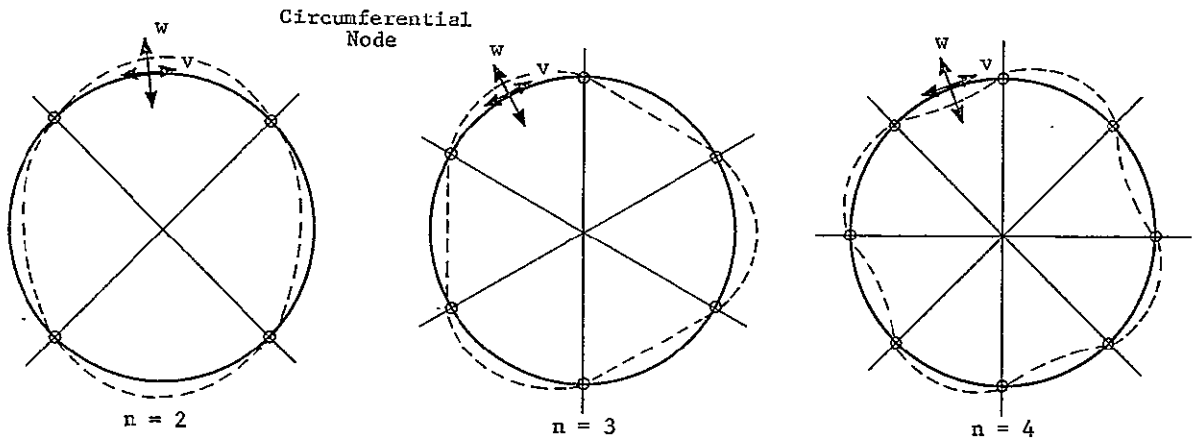


Fig. II-3 Notation for Stiffened Shells

The modes of free vibration that have been found analytically and experimentally for simply supported cylinders are shown in Fig. II-4. At each end the cylinder is maintained as a circular section. The number of axial half waves is designated by m and the number of full waves in the circumferential direction is n . Orthogonal modal lines occur along the generators and on planes normal to the axis. (See Ref. 2)

Although the discussion has been for circular cylinders the physical quantities and the vibrating phenomena also apply to conical shells as well as other shells of revolution. Portions of this report will consider the case of modeling a vibrating cone and it will be treated as an equivalent cylinder.

Circumferential Waves



Axial Waves

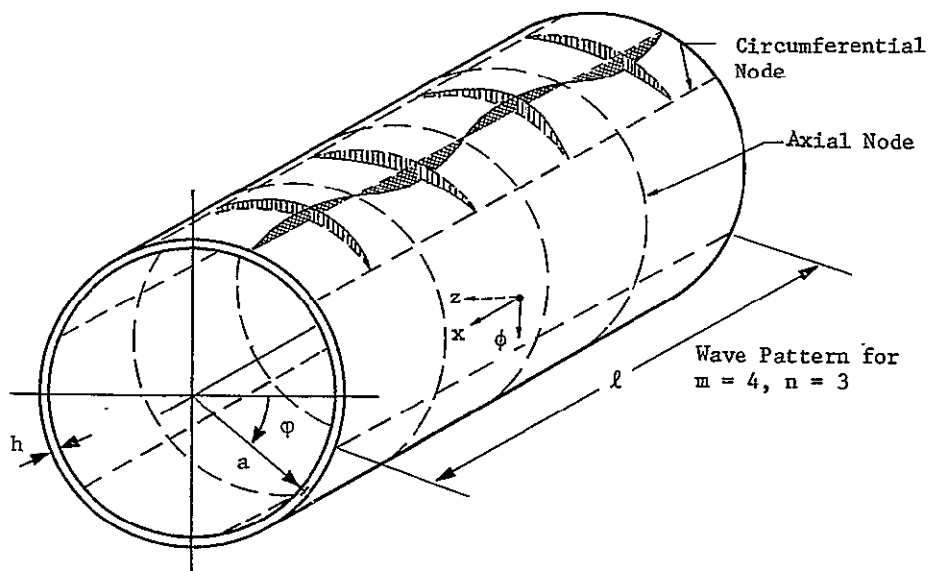
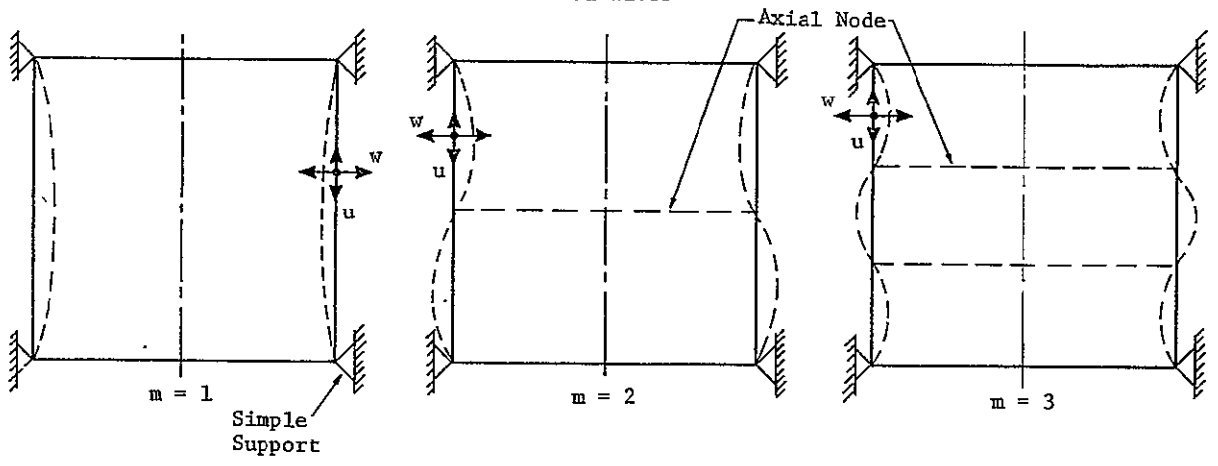


Fig. II-4 Free Vibration Modes for Simply Supported Cylindrical Shells

III. SIMILITUDE

Shell vibrations as well as many other physical phenomena can be analyzed as a physical system with dimensions that are multiples of the basic quantities, mass (M) length (L), and time (T). After we identify all important physical quantities, and if through the laws of scaling we create a model physical system whose physical quantities when evaluated nondimensionally are numerically identical to the prototype system then we can predict the response of the prototype by studying the model.

Our interest here is to design model shells that when undergoing free vibrations their frequencies and mode shapes will give information regarding the prototype shells. Of further interest will be model distortion whereby the appearance of the model shell will not be identical with the prototype. In Section II on shell vibrations the important physical quantities have been identified from the mathematical formulation of this problem. Using information from the equations and the previous tables the important quantities are given in Table III-1.

Frequency ω , a dependent variable is a function of at least all the quantities listed as independent variables. From Buckingham's Pi theorem we can reduce the number of independent variables that must be scaled by the number of basic dimensions shown here to be three (M, L and T). We can select three arbitrary scale factors from the independent parameters to which we can assign convenient ratios and also obtain a means of consistently nondimensionalizing all the independent variables. These arbitrary scale factors must be chosen so that in combination they can produce ratios of only mass, length, and time for model and prototype. Once chosen these values cannot be changed arbitrarily.

The arbitrary length scale factor n_1 is based on the ratio of the shell radii

$$n_1 = \frac{a_m}{a_p} = \frac{L_m}{L_p} \quad (\text{III-1})$$

so that model length is related to prototype length by

$$L_m = n_1 L_p \quad (\text{III-2})$$

Another arbitrary scale factor is unit mass density so that we chose for model and prototype

Table III-1 Independent and Dependent Variables

<u>Quantity</u>	<u>Symbol</u>	<u>Dimension</u>	
		<u>Engineering Units</u>	<u>MLT</u>
<u>Independent Variables</u>			
Length	l	in	L
Radius	a	in	L
Thickness	h	in	L
Spacing	b	in	L
Eccentricity	c	in	L
Area	A	in^2	L^2
Moment of Inertia	I, J	in^4	L^4
Modulus of Elasticity	E	lb/in^2	$ML^{-1}T^{-2}$
Unit Mass Density	ρ	$\text{lb sec}^2/\text{in}^4$	ML^{-3}
Unit Weight Density	γ	lb/in^3	$ML^{-2}T^{-2}$
Extensional Rigidity	K	lb/in	MT^{-2}
Bending Rigidity	D	in lb	ML^2T^{-2}
Rigidity Moment	S	lb	MLT^{-2}
Coordinate Angle	ϕ	--	--
Wave Number	m, n	--	--
Poisson Ratio	ν	--	--
<u>Dependent Variables</u>			
Displacements	u, v, w	in	L
Stress/Unit Length	N	lb/in	MT^{-2}
Moment/Unit Length	M	lb	MLT^{-2}
Frequency	ω	$1/\text{sec}$	T^{-1}

$$n_2 = \frac{\rho_m}{\rho_p} = \frac{M_m L_m^{-3}}{M_p L_p^{-3}} \quad (\text{III-3})$$

From this we establish mass ratios so that

$$M_m = n_1^3 n_2^3 M_p \quad (\text{III-4})$$

For the third arbitrary scale factor, selected so that the remaining basic dimension, time, can be acquired, we chose the elastic modulus ratios such that

$$n_3 = \frac{E_m}{E_p} \quad (\text{III-5})$$

from which the time ratio for model to prototype becomes

$$T_m = n_1 n_2^{1/2} n_3^{-1/2} T_p \quad (\text{III-6})$$

From Equation (III-6) the well known frequency relation is apparent when scaling with identical materials for model and prototype $n_2 = 1$, $n_3 = 1$ so that $\omega_m/\omega_p = L_p/L_m$.

Nondimensional π terms from the remaining independent variables (a , ρ , E selected arbitrarily) are the result of the following arbitrary choice of nondimensional combinations.

$$\begin{aligned} \pi_1 &= \frac{a}{l} \\ \pi_2 &= \frac{a}{h} \\ \pi_3 &= \frac{a}{b} \\ \pi_4 &= \frac{a}{c} \\ \pi_5 &= \frac{A}{a^2} \\ \pi_6 &= \frac{I}{a^4} \\ \pi_7 &= \frac{J}{a^4} \end{aligned}$$

$$\begin{aligned}
 \pi_8 &= \frac{E}{\gamma_a} \\
 \pi_9 &= \frac{K}{\gamma_a^2} \\
 \pi_{10} &= \frac{D}{\gamma_a^4} \\
 \pi_{11} &= \frac{S}{Ka} \\
 \pi_{12} &= 1 = \frac{\phi_m}{\phi_p} \\
 \pi_{13} &= 1 = \frac{m_m}{m_p} \\
 \pi_{14} &= 1 = \frac{n_n}{n_p} \\
 \pi_{15} &= 1 = \frac{v_m}{v_p}
 \end{aligned} \tag{III-7}$$

For proper scaling it is necessary for corresponding independent terms for model and prototype to be numerically identical, therefore with subscript m for model and p for prototype

$$\begin{aligned}
 \pi_{1m} &= \pi_{1p} \\
 \pi_{2m} &= \pi_{2p} \\
 \vdots & \quad \quad \quad \vdots \\
 \vdots & \quad \quad \quad \vdots \\
 \vdots & \quad \quad \quad \vdots \\
 \pi_{15m} &= \pi_{15p}
 \end{aligned} \tag{III-8}$$

The above $\pi_m = \pi_p$ terms can be rewritten as

$$\begin{aligned}
 \pi_1 &= \frac{a_m}{l_m} = \frac{a_p}{l_p} \text{ or, } l_m = l_p \frac{a_m}{a_p} \\
 \pi_2 &= \frac{a_m}{b_m} = \frac{a_p}{b_p} \text{ or, } b_m = b_p \frac{a_m}{a_p}
 \end{aligned}$$

$$\begin{aligned} \pi_3 &= \frac{a_m}{h_m} = \frac{a_p}{h_p} \quad \text{or,} \quad h_m = h_p \frac{a_m}{a_p} \\ \pi_4 &= \frac{a_m}{c_m} = \frac{a_p}{c_p} \quad \text{or,} \quad c_m = c_p \frac{a_m}{a_p} \\ \pi_5 &= \frac{\frac{A_m}{2}}{a_m} = \frac{\frac{A_p}{2}}{a_p} \quad \text{or,} \quad A_m = A_p \left(\frac{a_m}{a_p} \right)^2 \\ \pi_6 &= \frac{\frac{I_m}{4}}{a_m} = \frac{\frac{I_p}{4}}{a_p} \quad \text{or,} \quad I_m = I_p \left(\frac{a_m}{a_p} \right)^4 \\ \pi_7 &= \frac{\frac{J_m}{4}}{a_m} = \frac{\frac{J_p}{4}}{a_p} \quad \text{or,} \quad J_m = J_p \left(\frac{a_m}{a_p} \right)^4 \\ \pi_8 &= \frac{\frac{E_m}{\gamma_m a_m}}{\gamma_m a_m} = \frac{\frac{E_p}{\gamma_p a_p}}{\gamma_p a_p} \quad \text{or,} \quad \gamma_m = \gamma_p \frac{a_p}{a_m} \frac{E_m}{E_p} \quad (\text{III-9}) \\ \pi_9 &= \frac{\frac{K_m}{\gamma_m a_m^2}}{\gamma_m a_m^2} = \frac{\frac{K_p}{\gamma_p a_p^2}}{\gamma_p a_p^2} \quad \text{or,} \quad K_m = K_p \left(\frac{a_m}{a_p} \right)^2 \frac{\gamma_m}{\gamma_p} \\ \pi_{10} &= \frac{\frac{D_m}{\gamma_m a_m^4}}{\gamma_m a_m^4} = \frac{\frac{D_p}{\gamma_p a_p^4}}{\gamma_p a_p^4} \quad \text{or,} \quad D_m = D_p \left(\frac{a_m}{a_p} \right)^4 \frac{\gamma_m}{\gamma_p} \\ \pi_{11} &= \frac{\frac{S_m}{K_m a_m}}{K_m a_m} = \frac{\frac{S_p}{K_p a_p}}{K_p a_p} \quad \text{or,} \quad S_m = S_p \frac{a_m}{a_p} \frac{K_m}{K_p} \\ \pi_{12} &= 1 = \frac{\phi_m}{\phi_p} \quad \text{or,} \quad \phi_m = \phi_p \\ \pi_{13} &= 1 = \frac{n_m}{n_p} \quad \text{or,} \quad n_m = n_p \end{aligned}$$

$$\pi_{14} = 1 = \frac{n_n}{n_p} \quad \text{or,} \quad n_n = n_p$$

$$\pi_{15} = 1 = \frac{v_m}{v_p} \quad \text{or,} \quad v_m = v_p$$

We can continue to define model properties by using the MLT dimensions previously shown for the 15 π terms. This further manipulation explains why the terms n_1 , n_2 , and n_3 have been established. As we have shown L_m , T_m , and T_m can be expressed as functions of n_1 , n_2 and n_3 and if given complete freedom of choice of the numerical value of these n terms (arbitrary scale factors) any prototype can be modeled into any size and with any material. Our particular problem does not permit this complete freedom as will be shown, however that does not detract from the general presentation of providing similitude. Using the MLT dimensions and the model quantities we continue by direct substitution from Table III.1 to establish

$$\ell_m = \ell_p \frac{L_m}{L_p}$$

$$b_m = b_p \frac{L_m}{L_p}$$

$$h_m = h_p \frac{L_m}{L_p}$$

$$c_m = c_p \frac{L_m}{L_p}$$

$$A_m = A_p \left(\frac{L_m}{L_p} \right)^2$$

$$I_m = I_p \left(\frac{L_m}{L_p} \right)^4$$

$$J_m = J_p \left(\frac{L_m}{L_p} \right)^4$$

$$\gamma_m = \gamma_p \frac{L_m^{-1}}{L_p^{-1}} \frac{M_m L_m^{-1} T_m^{-2}}{M_p L_p^{-1} T_p^{-2}} = \gamma_p \left(\frac{L_m}{L_p} \right)^2 \frac{M_m}{M_p} \left(\frac{T_m}{T_p} \right)^{-2}$$

$$K_m = K_p \left(\frac{L_m}{L_p} \right)^2 \frac{M_m L_m^{-2} T_m^{-2}}{M_p L_p^{-2} T_p^{-2}} = K_p \frac{M_m}{M_p} \left(\frac{T_m}{T_p} \right)^{-2}$$

$$D_m = D_p \left(\frac{L_m}{L_p} \right)^4 \frac{M_m L_m^{-2} T_m^{-2}}{M_p L_p^{-2} T_p^{-2}} = D_p \left(\frac{L_m}{L_p} \right)^2 \frac{M_m}{M_p} \left(\frac{T_m}{T_p} \right)^{-2}$$

$$S_m = S_p \frac{L_m}{L_p} \frac{M_m T_m^{-2}}{M_p T_p^{-2}} = S_p \frac{L_m}{L_p} \frac{M_m}{M_p} \left(\frac{T_m}{T_p} \right)^{-2}$$

$$\phi_m = \phi_p$$

$$m_m = m_p$$

$$n_m = n_p$$

$$v_m = v_p$$

If all these model quantities are satisfied then the dependent value of model frequency can be related to the prototype simply as

$$\pi_{\omega m} = \pi_{\omega p}$$

or choosing quite arbitrarily from the variables to give

$$\pi_{\omega} = \omega \left(\frac{\rho}{K} h^3 \right)^{1/2}$$

and continuing as before to satisfy similitude

$$\omega_m \left(\frac{\rho_m}{K_m} h_m^3 \right)^{1/2} = \omega_p \left(\frac{\rho_p}{K_p} h_p^3 \right)^{1/2}$$

This gives for the model frequency

$$\omega_m = \omega_p \left(\frac{\rho_p}{\rho_m} \right)^{1/2} \left(\frac{K_m}{K_p} \right)^{1/2} \left(\frac{h_p}{h_m} \right)^{3/2}$$

Using the MLT dimensions for mass density, extensional stiffness and thickness we can write as we did for the independent terms above

$$\omega_m = \omega_p \left(\frac{\frac{M L}{P P}^{-3}}{\frac{M L}{m m}^{-3}} \right)^{1/2} \left(\frac{\frac{M T}{m m}^{-2}}{\frac{M T}{P P}^{-2}} \right)^{1/2} \left(\frac{\frac{L}{P}}{\frac{L}{m}} \right)^{3/2}$$

$$\omega_m = \omega_p \frac{T_m^{-1}}{T_p^{-1}}$$

and from Eq. (III-6)

$$\omega_m = (n_1^{-1} n_2^{-1/2} n_3^{1/2}) \omega_p \quad (\text{III-10})$$

By continuing in the manner just described, all the independent variables can be scaled using the three arbitrary scale factors. If the numerical values of n_1 , n_2 and n_3 are established and faithfully maintained as constants then the resulting model will provide dynamic similitude. Such a model will provide reliable quantitative data that can be applied to the prototype. The result of the algebraic manipulations with the MLT terms and their corresponding n terms is shown in Table III-2 giving the scale factors for modeling.

In those cases where the three scale factors are perfectly arbitrary the model can be designed to meet constraints imposed by time scale, or length restrictions, or perhaps model mass. Our equation for time (III-6) can be used to investigate how the physical dimensions such as size and mass affect the time scale or conversely how a selected time scale factor designs the model properties. In Fig. III-1, T_m/T_p is plotted against model mass to prototype mass for 1/10 and 1/20 scale models. Selection of unit mass density, elastic modulus and size produces a wide choice in time scale. It should be noted, however, that for smaller than prototype masses and for both higher and lower elastic moduli the model time is less than the prototype time for the conditions shown here.

Table III-2 Scale Factors for Modeling

<u>Quantity</u>	<u>Symbol</u>	<u>Scaling Relationship for Model</u>
Length	ℓ	$\ell_m = n_1 \ell_p$
Radius	a	$a_m = n_1 a_p$ (See Eq. III-1)
Thickness	h	$h_m = n_1 h_p$
Spacing	b	$b_m = n_1 b_p$
Eccentricity	c	$c_m = n_1 c_p$
Area	A	$A_m = n_1^2 A_p$
Moment of Inertia	I, J	$I_m = n_1^4 I_p, J_m = n_1^4 J_p$
Modulus of Elasticity	E	$E_m = n_3 E_p$ (See Eq. III-5)
Unit Mass Density	ρ	$\rho_m = n_2 \rho_p$ (See Eq. III-3)
Unit Weight Density	γ	$\gamma_m = n_1^{-1} n_3 \gamma_p$
Extensional Rigidity	K	$K_m = n_1 n_3 K_p$
Bending Rigidity	D	$D_m = n_1^3 n_3 D_p$
Rigidity Moment	S	$S_m = n_1^2 n_3 S_p$
Coordinate Angle	ϕ	$\phi_m = \phi_p$
Wave Number	m, n	$n_m = m_p, n_m = n_p$
Poisson Ratio	ν	$\nu_m = \nu_p$
Frequency	ω	$\omega_m = n_1^{-1} n_2^{-1/2} n_3^{1/2} \omega_p$ (See Eq. III-10)

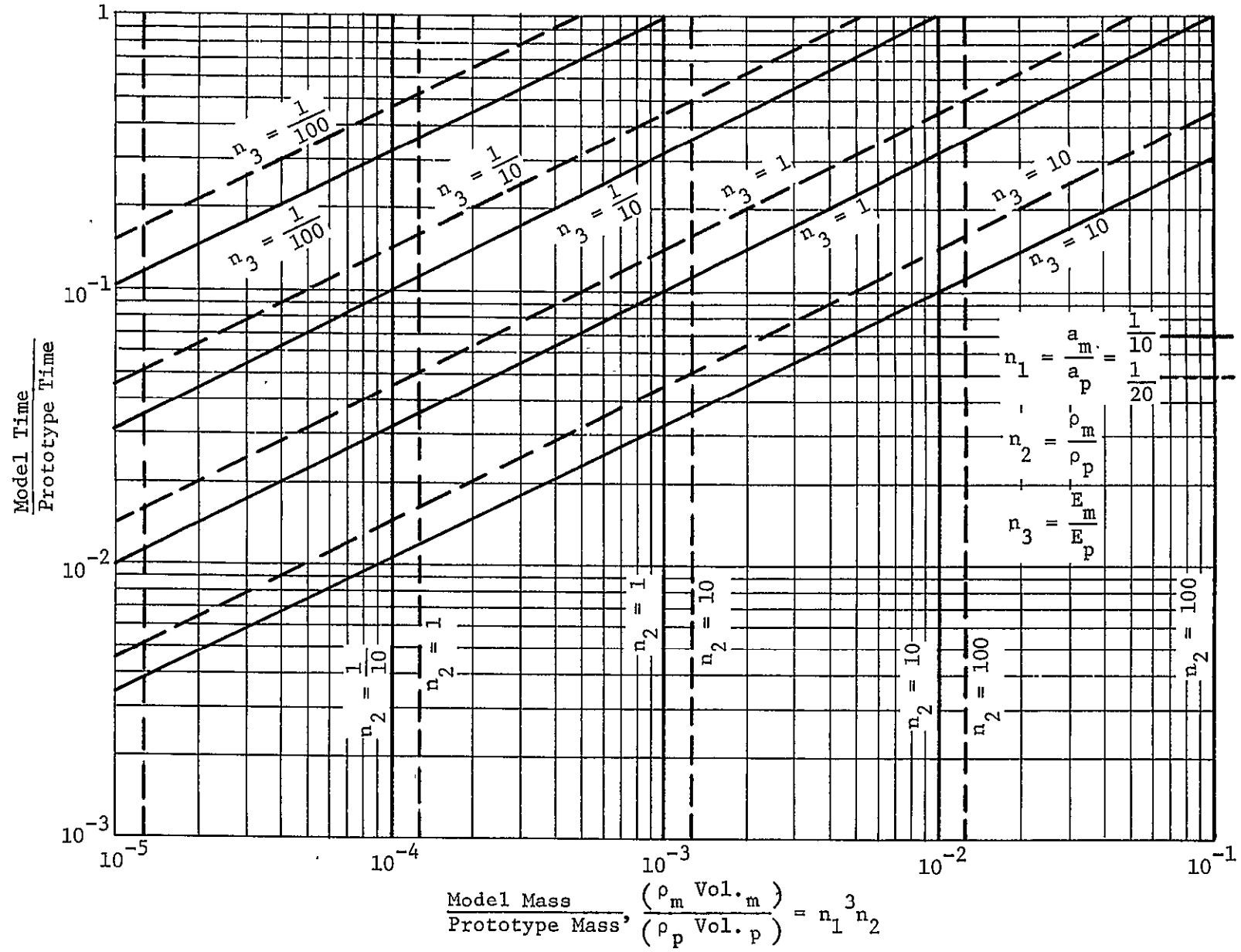


Fig. III-1 Ratio of Model Time to Prototype Time for $\frac{1}{10}$ and $\frac{1}{20}$ Scale Models

Although the above treatment for scaling is general, the problem of free vibrations of a shell with no masses attached to it and in turn the subject shell not fastened to other flexible members requires restrictions on our n_1 , n_2 , and n_3 terms defined in this section. As will be shown the term E/ρ assumes the role of an independent variable and neither E nor ρ can be selected arbitrarily. This restriction does not apply if there are other larger masses attached to the shell whereby the shell mass becomes insignificant.

IV. PROTOTYPE PROPERTIES

Dynamically scaled models are analyzed and fabricated for three of the shell structures that are a portion of the second stage of Saturn V. These sections are second stage tank-hereafter referred to as Cylinder A, second stage forward skirt to be called Cylinder B, and adapter second to third stage and designated here as Cone C. Overall dimensions and relative positions are shown in Fig. IV-1.

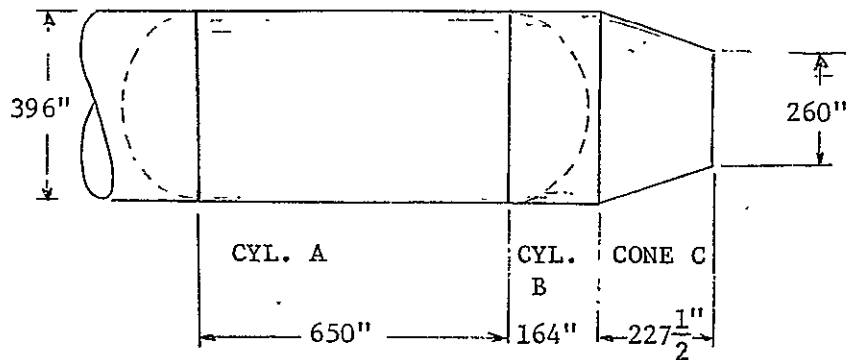


Fig. IV-1 Portions of Saturn V, Second Stage Used in Modeling

In reference [5] Saturn V designs are given for flight conditions accounting for the skin temperatures that produce changes in elastic modulus. Our conditions will be room temperature and all rigidities will be for material at room temperature. A summary of the design data and the modifications for room temperature are shown in Table IV-1.

From the definitions of the π terms given in Equations (III-7) the extensional rigidity π_9 and flexural rigidity π_{10} are calculated for Saturn V, second stage at room temperature. These are listed in Table IV-2 using the numbers given in Table IV-1. Conversion factors are given for the two cylinders and the cone as part of the table.

A brief examination of either table reveals large differences in the shell rigidities both in the x and ϕ directions. These differences occur within a shell and between the shells. The orthotropic nature of these structures is readily apparent.

Table IV-1 Saturn V, Second Stage Extensional and Flexural Rigidities

Component	Temp (°F)	Extensional Rigidities		Flexural Rigidities	
		K_x (lb/in.)	K_ϕ (lb/in.)	D_x (in. lb)	D_ϕ (in. lb)
Second Stage Tank	-423 ⁽¹⁾	2.33×10^6	2.24×10^6	93.0×10^3	5.19×10^3
Cylinder A	+78 ⁽⁴⁾	2.07×10^6	1.99×10^6	82.8×10^3	4.61×10^3
Second Stage Forward Skirt	+300 ⁽²⁾	1.61×10^6	0.73×10^6	414×10^3	$.247 \times 10^3$
Cylinder B	+78 ⁽⁴⁾	1.69×10^6	0.77×10^6	435×10^3	$.257 \times 10^3$
Adapter 2nd to 3rd Stage	+400 ⁽³⁾	1.68×10^6	0.729×10^6	453×10^3	$.281 \times 10^3$
Cone C	+78 ⁽⁴⁾	1.86×10^6	0.808×10^6	502×10^3	$.311 \times 10^3$
<u>For 2014-T6 Al</u>					
(1) $E = 11.90 \times 10^6$ psi at -423°F					
(2) $E = 10.10 \times 10^6$ psi at $+300^\circ\text{F}$ $\nu = 0.33$					
(3) $E = 9.56 \times 10^6$ psi at $+400^\circ\text{F}$ $\gamma = 0.101$ lb/in. ³					
(4) $E = 10.60 \times 10^6$ psi at $+78^\circ\text{F}$					

Table IV-2 Saturn V, Second Stage π Terms for Extensional and Flexural Rigidities

Component	Extensional π Terms		Flexural π Terms	
	π_{9xp}	$\pi_{9\phi p}$	π_{10xp}	$\pi_{10\phi p}$
Second Stage Tank (Cyl A)	525	505	0.534×10^{-3}	0.0298×10^{-3}
Second Stage Frwd Skrt (Cyl B)	427	194	2.81×10^{-3}	0.00166×10^{-3}
Adapter 2nd to 3rd Stage (Cone C)	686	298	6.89×10^{-3}	0.00426×10^{-3}

For Cylinders A and B

$$\pi_{9p} = \frac{K}{\gamma a^2} = \frac{K}{0.101 \times 198^2} = \frac{K}{3960}$$

$$\pi_{10p} = \frac{D}{\gamma a^4} = \frac{D}{0.101 \times 198^4} = \frac{D}{155.2 \times 10^6}$$

For Cone C (Equivalent Cylinder Average Radius = 164 in.)

$$\pi_{9p} = \frac{K}{\gamma \left(\frac{a_1 + a_2}{2} \right)^2} = \frac{K}{0.101 \times 164^2} = \frac{K}{2716}$$

$$\pi_{10p} = \frac{D}{\gamma \left(\frac{a_1 + a_2}{2} \right)^4} = \frac{D}{0.101 \times 164^4} = \frac{D}{73.06 \times 10^6}$$

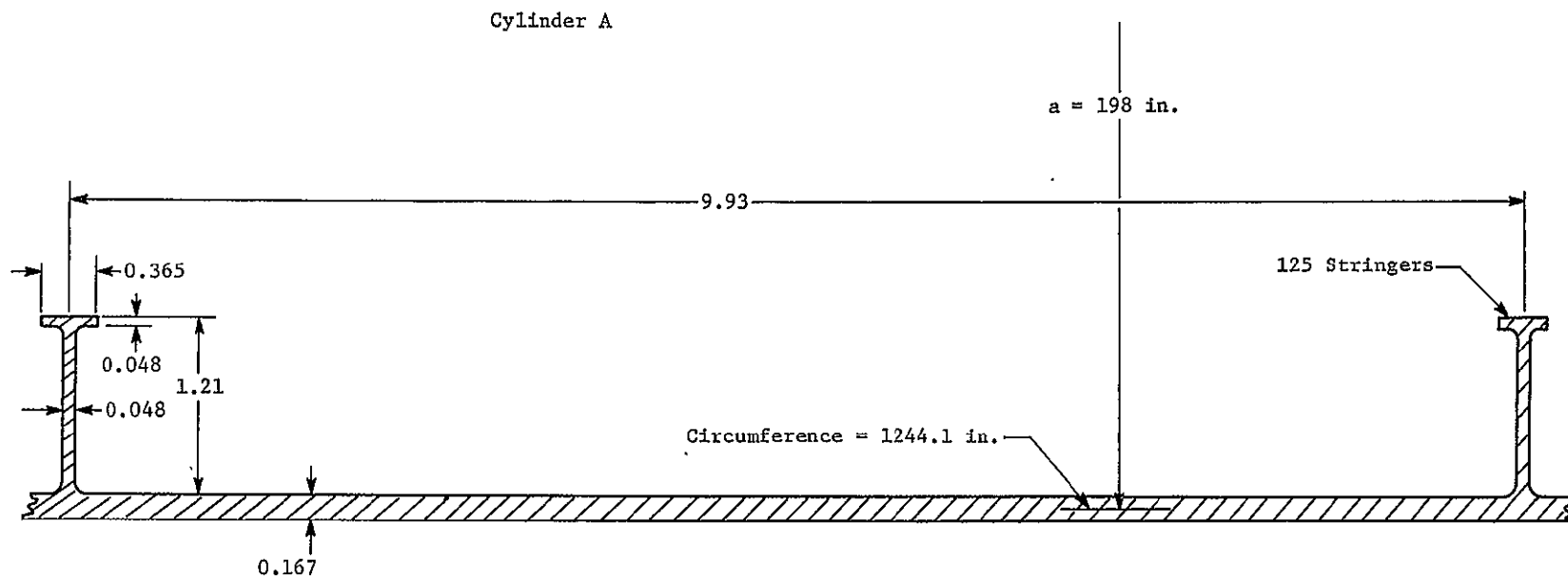
Large size sections through the stiffened shell (looking in the x direction) are sketched in Fig. IV-2 for cylinder A, Fig. IV-3 for cylinder B, and Fig. IV-4 for cone C. Cylinder A is reinforced with a T shaped integral stiffener and the prototype is a pressurized shell filled with liquid. Both cylinder B and cone C are not pressurized and are stiffened with hat sections running longitudinally. Laboratory tests of the models of these three shell types are performed with clamped boundary conditions, no axial loads, and no pressure loads.

A small discrepancy occurs in calculating the K_x extensional rigidity when comparing that quantity defined in Reference [5] and Flügge's definition for skin stringer shells given in Table II-2.

$$\text{From [5]} \quad K_x = \frac{E}{1-\nu^2} \left(h + \frac{A_x}{b_2} \right)$$

$$\text{From Table II-2} \quad K_x = \frac{Eh}{1-\nu^2} + \frac{EA_x}{b_2}$$

Because the $1-\nu^2$ term is close to 1 and for nominal amounts of reinforcing the differences are slight we shall disregard the discrepancy and chose the rigidity given in Reference [5]. It is this reference that provides the design data for the prototype structures and therefore, the models will be scaled consistently with the prototype, in this particular regard. It should be mentioned that the integral stiffener in cylinder A departs most from the behavior ascribed to it in Reference [5] in participating in the longitudinal extensional rigidity. The hat sections of cylinder B and cone C act more as shell-like elements because of their shape and method of fastening. These sections are better represented by the Reference [5] description of their action than the integral stiffener. Numerically the differences are slight, using either formula.



MCR-68-87

Fig. IV-2 Saturn V, Second Stage, Tank Wall, Skin Stringer

Cylinder B

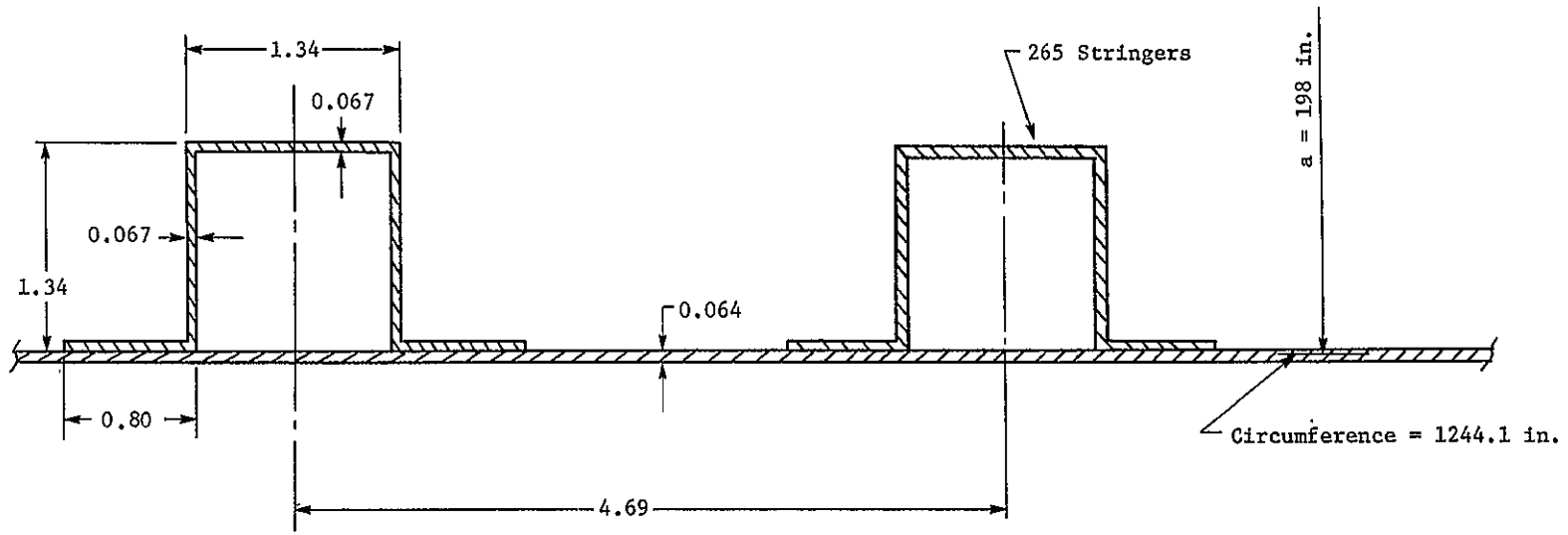
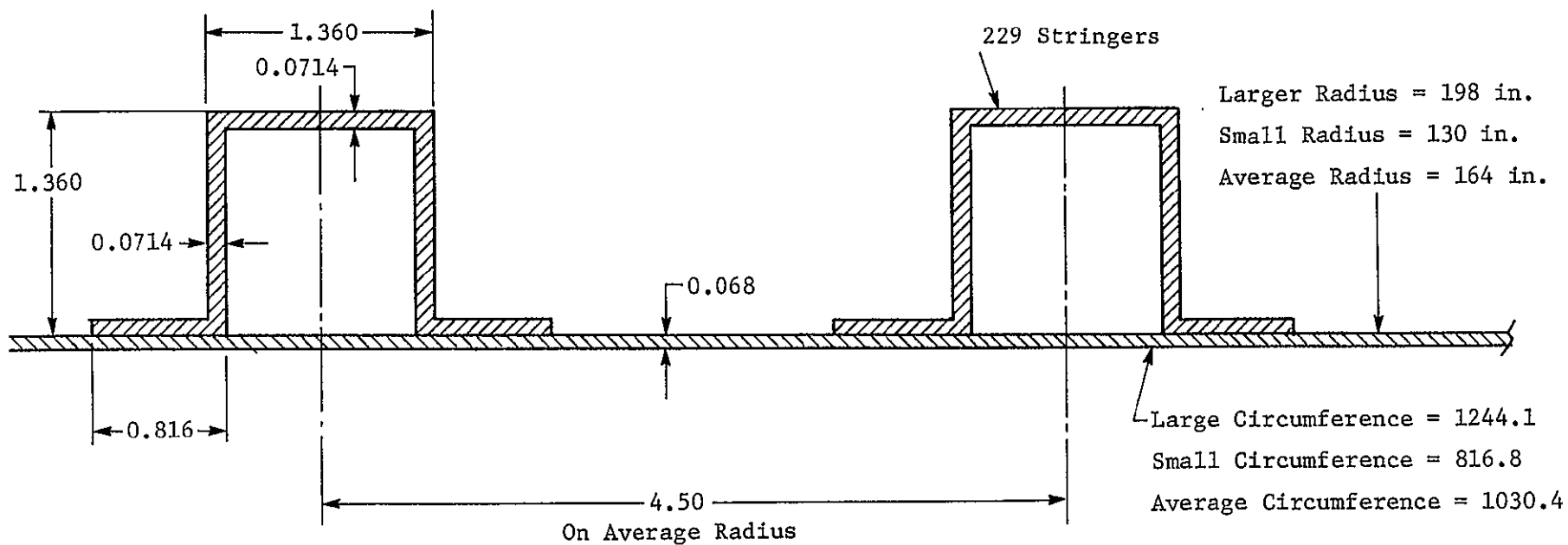


Fig. IV-3 Saturn V, Second Stage, Forward Skirt, Skin Stringer

Cone C



MCR-68-87

Fig. IV-4 Saturn V, Adapter, 2nd to 3rd Stage, Skin Stringer

V. MODELING

A. MODEL DIMENSIONS

Of the three arbitrary scale factors n_1 , n_2 , and n_3 given in Section III, the one with the greatest influence is n_1 , the size scale factor. For this study n_1 has been selected as $1/20$ thereby establishing the size of the model. Preserving π_1 from Eq. (III-7) and satisfying boundary conditions of Eq. (II-3) requires the length to radius ratio to remain the same. Model dimensions are shown in Fig. V-1.

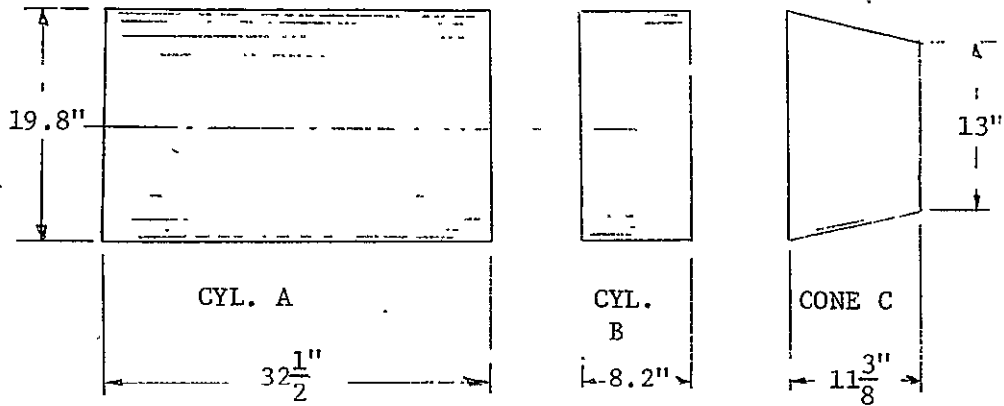


Fig. V-1 Dimensions of the Three Model Shells

B. MATERIAL SELECTION

To create models of these dimensions that can provide meaningful data we are led to examine the differential equations of Section II. As mentioned earlier we have, for completeness, selected arbitrary scale factors to isolate ratios of model to prototype mass, length, and time in terms of arbitrary numbers n_1 , n_2 , and n_3 . This is shown as Equations (III-2), (III-4), and (III-6). However, examination of the equations in Section II reveals that all terms on the left hand side contain the quantity E/ρ . Therefore, n_2 and n_3 , material scale factors, cannot be

selected in an arbitrary manner. Their ratio in nondimensional form, must be kept constant for model and prototype. This combination of E/ρ was anticipated from the equations of ring vibrations in Section II. Not all shell problems will contain this restriction, such as the problems of static loading, buckling, thermal stresses, and others. Our particular problem, because of the right hand side of Eq. (II-1) restricts the selection of ρ . This is the only physical quantity in the problem that can isolate the time. In Table III-1 each elastic constant contains a T^{-2} term in addition to M and L terms. Only ρ contains M and L without T thereby permitting T to be expressed in terms of n_1 , n_2 and n_3 . To isolate the E/ρ term we will define unit mass density as

$$\rho_m = \frac{\gamma_m}{g_m}, \quad \text{and} \quad \rho_p = \frac{\gamma_p}{g_p} \quad (\text{V-1})$$

in which g is a constant, the acceleration due to gravity. Using this definition of ρ the ratio E/γ becomes equivalent to E/ρ for model and prototype when their respective g terms are equal. Substituting for ρ from Eq. (V-1) and recalling π_8 from Eq. (III-7) we have

$$\pi_8 = \frac{E}{\gamma a} = \frac{E}{\rho g a}$$

For similitude using our previously established laws requires

$$\pi_{8m} = \pi_{8p}$$

so that

$$\frac{E_m}{\rho_m g_m a_m} = \frac{E_p}{\rho_p g_p a_p}$$

thereby giving the relationship

$$\frac{E_m}{E_p} = \frac{a_m}{a_p} \frac{\rho_m}{\rho_p} \frac{g_m}{g_p}$$

or from Eqs. (III-1), (III-3) and (III-5)

$$n_3 = n_1 n_2 \frac{g_m}{g_p}$$

and for the same gravitational constants $g_m = g_p$ we have the relationship that

$$n_1 = n_2^{-1} n_3 \quad (V-2)$$

This result restricts the combination of n_3/n_2 to be the same number as the arbitrary scale factor n_1 . Both n_3 and n_2 determine what materials are appropriate for modeling.

Using the result of Eq. (V-2) into the time equation relating model and prototype time we find

$$T_m = n_1^{1/2} T_p \quad (V-3)$$

or for the quantity of interest to vibrating shells

$$\omega_m = n_1^{-1/2} \omega_p, \quad (V-4)$$

thereby setting for our 1/20 models the relationship that the model frequency becomes 4.47 times higher than the prototype frequency for corresponding modes.

Material selection is based on dynamically scaling a prototype structure 2014-T6 aluminum into another structure 1/20 that size. For the model material we have from π_8

$$E_m = \frac{E_p}{\gamma_p} \frac{a_m}{a_p} \gamma_m$$

For 2014 T-6 aluminum and a 1/20 model,

$$E_m = \frac{10.6 \times 10^6}{0.101} \times \frac{1}{20} \times \gamma_m \quad (V-5)$$

We convert the above equation by using the factor

$$1 \text{ gm/cm}^3 = 0.0361 \text{ lb/in}^3$$

to a relationship for model modulus and specific gravity (making metric mass density and specific gravity equal) such that

$$E_m \text{ (lb/in}^2\text{)} = 1.90 \times 10^5 \times \text{sp. gr.} \quad (\text{V-6})$$

This linear relationship is shown in Fig. V-2 for the specific gravity varying from 0.8 to 1.6. Several materials taken from Reference [6] having values of modulus that satisfy this modeling requirement are represented by numbered bars. Of the several materials, No. 7, Cellulose Acetate, ASTM Grade H4-1 is the most attractive. It is available in sheet form, can be joined by cementing and its range of modulus appears to be small compared to other classes of plastic materials.

Not many materials qualify for the relationship given in Eq. (V-6). Unreinforced plastics have a small range of specific gravity when compared to metals and of all the types of plastics very few have the desired modulus. It is interesting that any material that can provide the proper modulus to specific gravity ratio will produce a shell satisfying dynamic similitude. Furthermore, each of the 1/20 scale models will respond with corresponding frequencies 4.47 times higher than the aluminum prototype.

As an indication of how very small this group of plastics is, we have enlarged the modulus and specific gravity scales and included both metals and wood for comparison with the modulus line of Fig. V-2. This is shown in Fig. V-3. The modulus and specific gravity values are taken from Reference [7]. Along the bottom of the graph the line from Eq. (V-6) is plotted to a specific gravity of 30. In the lower left hand corner, the region covered by Fig. V-2 is shown as a shaded area. The small domain of this region is obvious when examining Fig. V-3.

Wood is included by using the empirical formula for its longitudinal modulus as

$$E_{\text{wood}} = 2.80 \times 10^6 \times \text{sp. gr.}$$

At corresponding specific gravities the longitudinal modulus of wood is too high by an order of magnitude, but in addition wood is orthotropic whereas aluminum, the prototype material, is isotropic.

Of the several metals shown in Fig. V-3 lead is surprisingly close to the desired E/sp. gr. ratio. Values taken from

T = Tensile modulus
 F = Flexural modulus
 C = Compressive modulus
 (min-max subscripts indicate range)

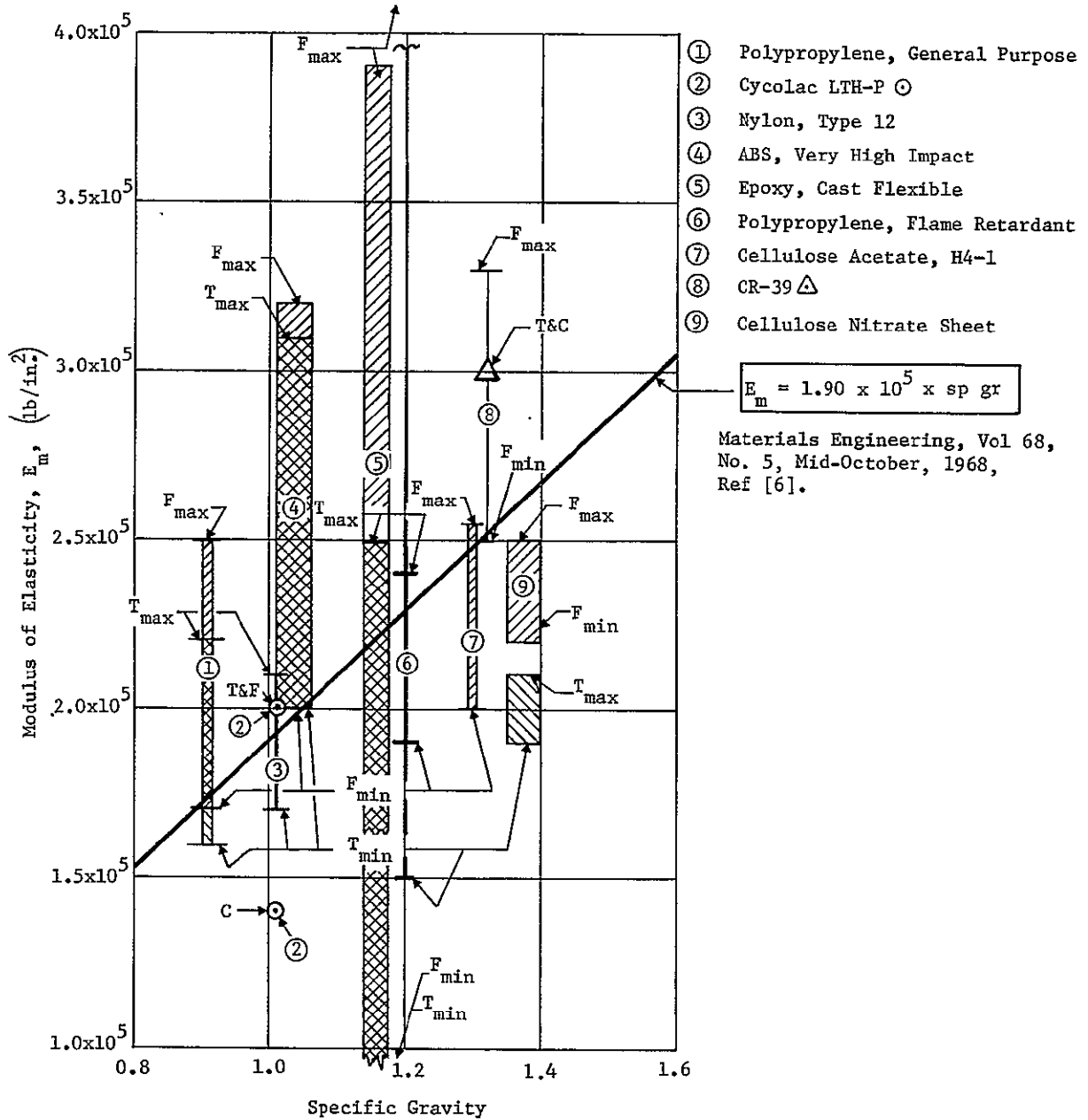


Fig. V-2 Modulus of Elasticity as a Function of Specific Gravity for Model Material

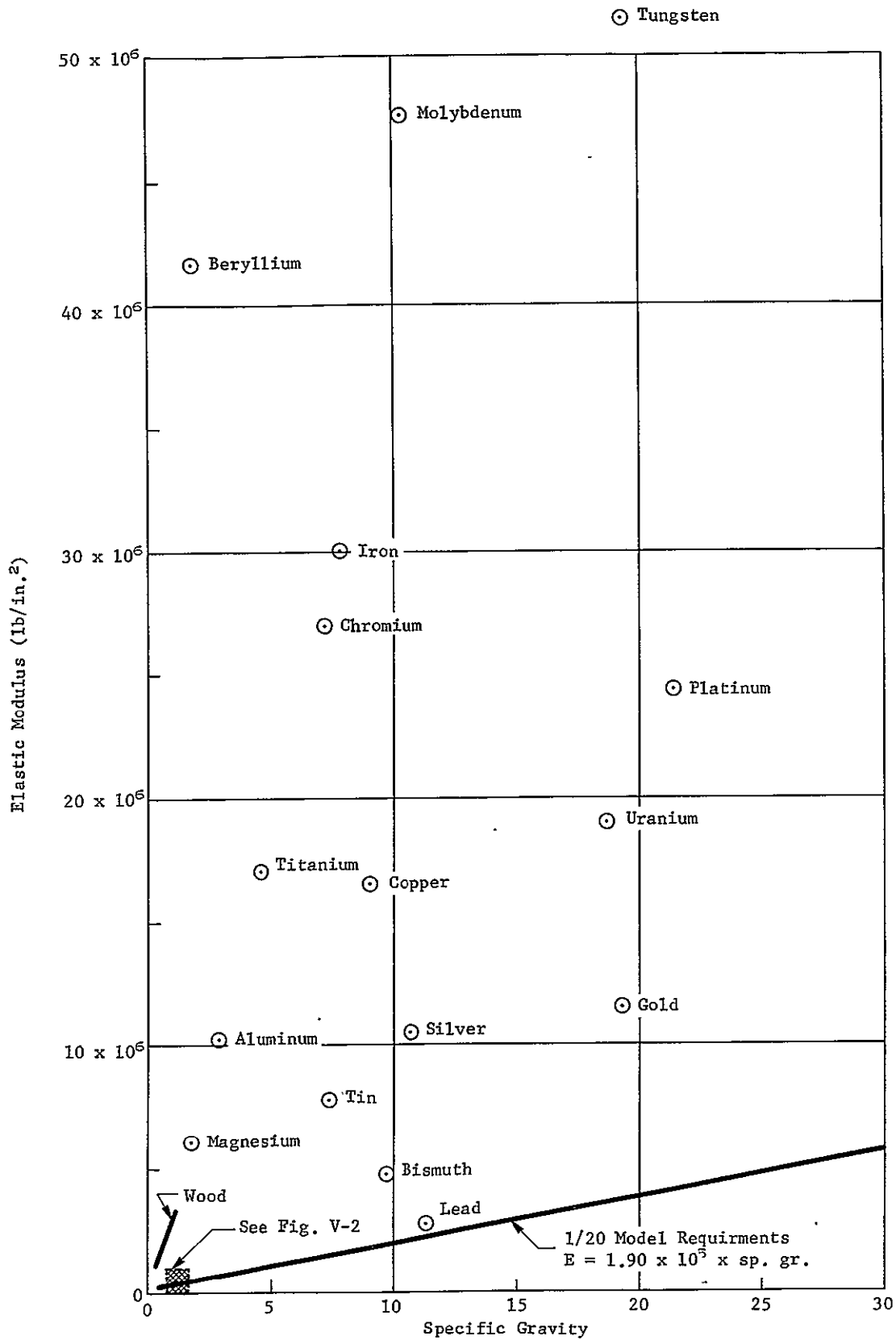


Fig. V-3 Modulus of Elasticity and Specific Gravity for Metals and Wood

Reference [7] for lead are $E = 2.56 \times 10^6 \text{ lb/in}^2$ and density = 11.34 g/cm^3 . Depending on purity and other factors the modulus of lead can cover a broad range and at times may be difficult to define.

Because the elastic modulus of a material cannot be changed at room temperature the use of many of these materials is not feasible without doing one of two things; either increasing the apparent specific gravity by attaching additional mass or performing the experiments in a centrifuge as discussed by Sedov [3]. Use of the centrifuge to increase the weight density (for $\rho_m = \rho_p$, $g_m > g_p$) of dynamically scaled models began in the early 1930's. With a relatively large centrifuge arm and a sufficiently small model the centrifugal force can be a good approximation to an increased gravity condition. The earth's gravity component, however, is not changed during the time a model is being centrifuged.

The required increase in weight density to approach the 1/20 model line is very great for most materials as shown by Fig. V-3. All points (because modulus remains constant) must move to the right until they intercept the 1/20 model line. As mentioned earlier the points in Fig. V-3 could be moved down by heating the models (not changing weight density) thereby decreasing elastic modulus. Other than saying this is possible and probably quite unreliable when compared to a centrifuge no other discussion of this method will be made.

It should be kept in mind that the identification of acceptable materials shown in Fig. V-2 based on Eq. (V-6) is applicable only to a 2014-T6 aluminum prototype structure undergoing free vibrations, without additional masses and being scaled using a size factor of 1/20. Other materials, other loads, other responses, or other sizes will produce their particular numerical coefficient for Eq. (V-6). Furthermore in this study $g_m = g_p$. The effects of any linear accelerations, other gravity fields, or centrifuge conditions must be taken into account (or deliberately manipulated) when satisfying the nondimensional term $\pi_8 = \frac{E}{\gamma a}$.

C. SKIN-STRINGER CYLINDER MODELS

Several departures from the fifteen π terms identified as influencing the free vibrations of cylindrical and conical shells will result in, by definition, a distorted model. This model will have the general appearance of a skin-stringer prototype, however, stringer spacing, stringer shape (affecting polar moment of inertia, and rigidity moment) will not be modeled geometrically. Skin-stringer combinations will be required to satisfy longitudinal extensional and flexural rigidities, modulus to density requirements and length to radius ratios. The skin will be required to satisfy the circumferential extensional and flexural rigidities and the radius to thickness ratios as well as modulus to density ratio. We will assume the value of Poisson's ratio for the model material to be 0.3. The model shell radius $a = 9.9$ in.

To find the wall thickness of the model, h_m , we must satisfy the nondimensional extensional rigidity in the ϕ direction so that $\pi_{9\phi m} = \pi_{9\phi p}$. From the definition of $\pi_{9\phi}$

$$\pi_{9\phi p} = \frac{K_{\phi m}}{\gamma_m a_m^2}$$

Referring to Table II-2 for K_{ϕ} for a skin-stringer shell

$$\pi_{9\phi p} = \frac{E_m h_m}{1-\nu_m^2} \frac{1}{\gamma_m a_m^2}$$

From Eq. (V-5) we can substitute numerical values so that

$$\pi_{9\phi p} = \frac{1}{1-.3^2} \times \frac{10.6 \times 10^6}{0.101} \times \frac{1}{20} \times \frac{h_m}{9.9^2}$$

Solving for h_m and combining the numbers gives for the wall thickness of the model shell

$$h_m \text{ (in)} = \frac{\pi_{9\phi p}}{5.90 \times 10^4} \quad (V-7)$$

An earlier calculation and tabulation lists in Table IV-2 the values of $\pi_{9\phi p}$ for cylinder A and cylinder B. Substitution from this

table determines the wall thicknesses. Examination of the results of Eq. (V-7) shows that $\pi_2 = a/h$ is satisfied as well.

We can determine the stringer area A_{xm} from the $\pi_{9xm} = \pi_{9xp}$ requirement and proceeding in a similar manner from the definition of π_{9x}

$$\pi_{9xp} = \frac{K_{xm}}{\gamma_m a_m^2}$$

Referring to Reference [5] for K_x for a skin-stringer shell

$$\pi_{9xp} = \frac{EM}{1-\nu_m^2} \left(h_m + \frac{A_{xm}}{b_{2m}} \right) \frac{1}{\gamma_m a_m^2}$$

From Eq. (V-5) we substitute for E/γ and arbitrarily select

$$b_{2m} = \frac{2\pi a}{\text{no. stringers}} = \frac{2\pi 9.9}{60} = 1.038 \text{ in./stringer.}$$

For faithful adherence to scaling we should insist that

$$\pi_3 = \frac{9.93}{20} = 0.496 \text{ in./stringer.}$$

Obviously the angular spacing of stringers is more than twice as great on the model as on the prototype. This violates the π_{12} term for angle coordinate ϕ . To proceed with the development of stringer area

$$\pi_{9xp} = \frac{1}{1-.3^2} \times \frac{10.6 \times 10^6}{0.101} \times \frac{1}{20} \left(\frac{\pi_{9\phi p}}{5.90 \times 10^4} + \frac{A_{xm}}{1.038} \right)$$

Solving for A_{xm} we can establish

$$A_{xm} = \frac{\pi_{9xp} - \pi_{9\phi p}}{5.68 \times 10^4} \quad (V-8)$$

Both values, π_{9xp} and $\pi_{9\phi p}$, are tabulated in Table IV-2. Although the stringer area is established by Eq. (V-8) the shape of the stringer is not defined. We will prescribe a rectangular section, thereby violating π_4 , π_7 and π_{11} . To find the dimensions of the

rectangle we can use π_{10} , the nondimensional factor containing stringer moment of inertia, I_x .

For similitude we enforce the following equality as we have for the π_9 terms, namely $\pi_{10xm} = \pi_{10xp}$. From the previously given definitions we can require

$$\pi_{10xp} = \frac{D_{xm}}{\gamma_m a_m^4}$$

From the rigidity definition this becomes for skin-stringer shells as given in Table II-2

$$\pi_{10xp} = E_m \left(\frac{h_m^3}{12(1-\nu_m)^2} + \frac{I_{xm} + A_{xm} c_{xm}^2}{b_{2m}} \right) \frac{1}{\gamma_m a_m^4}$$

Because the stringer shape is rectangular we can write

$$\pi_{10xp} = \frac{E_m}{\gamma_m a_m^4} \left[\frac{h_m^3}{12(1-\nu_m)^2} + \frac{\frac{A_{xm} d_{xm}^2}{12} + A_{xm} \left(\frac{d_{xm} + h_m}{2} \right)^2}{b_{2m}} \right] \quad (V-9)$$

The only unknown in Eq. (V-9) is the depth of the stringer d_{xm} . The factor E_m/γ_m is evaluated in Eq. (V-5). From the length scale factor $a_m = 9.9$ in. Thickness h_m is found from Eq. (V-7), and ν_m is defined as 0.3 for all materials. The area A_{xm} comes from Eq. (V-8), b_{2m} has been established as 1.038 in. and π_{10xp} is given in Table IV-2. Therefore d_{xm} appears in quadratic form and affords a simple solution. Using the notation established in Fig. II-3 stringer width is simply $t_{xm} = A_{xm}/d_{xm}$. A table, presented in Section V.G, summarizes these calculations.

D. SKIN-STRINGER CONE MODELS

The cone for this study has been treated as an equivalent cylinder with an average radius defined as the large radius plus the small radius divided by two. Wall thickness, stringer area, and rectangular stringer dimensions have been calculated as described in the preceding Section V.C outlining the design of skin-stringer cylinder models. For the equivalent a the numerical value becomes $(9.9 + 6.5)/2 = 8.2$ in. Other dimensions^m for the model are shown in Fig. V-1.

A table presented as Section V.G compares the calculated and design dimensionsof cone C.

E. GRIDWORK CYLINDER MODELS

Skin-stringer model distortion has been accomplished by using a composite gridwork shell to represent an orthotropic shell (by virtue of material distribution) made of an isotropic material. The composite materials are selected for their large differences in elastic modulus. Flexible PVC with a very low modulus has been designed to provide flexural rigidity by being relatively thick. Glass filaments or steel music wire; both with a relatively high elastic modulus, have been designed to provide extensional rigidity. No interaction between the two materials is assumed.

Retaining the notation previously established in Fig. II-3 but adding the composite construction features we see in Fig. V-4 a section through the composite gridwork shell. The analysis based on the stated assumptions determines the amount of glass or wire reinforcing and the depth of the rib sections d_x and d_ϕ .

Design of the gridwork shell is based on providing numerical equality for the extensional π term (π_9) and the flexural term (π_{10}). Properties of the two materials (E and γ) will be used with no regard for matching $\pi_8 = EY/a$. Certain grid dimensions have been selected arbitrarily, and are as follows:

$$\begin{aligned} b_1 &= 1 \text{ in.} \\ t_\phi &= \frac{b_1}{2} = \frac{1}{2} \text{ in.} \\ b_2 &= 1 \text{ in.} \\ t_x &= \frac{b_2}{2} = \frac{1}{2} \text{ in.} \end{aligned}$$

The selected material flexible PVC, S-Glass, and music wire are assumed to have the following properties;

Flexible PVC:	$E = 1,200 \text{ lb/in}^2$
	$\gamma = 0.05 \text{ lb/in}^3$
S-Glass Roving:	$E = 12 \times 10^6 \text{ lb/in}^2$
(204 filaments per single end roving)	$\gamma = 0.10 \text{ lb/in}^3$
	area = $15 \times 10^{-6} \text{ in}^2/\text{single end}$

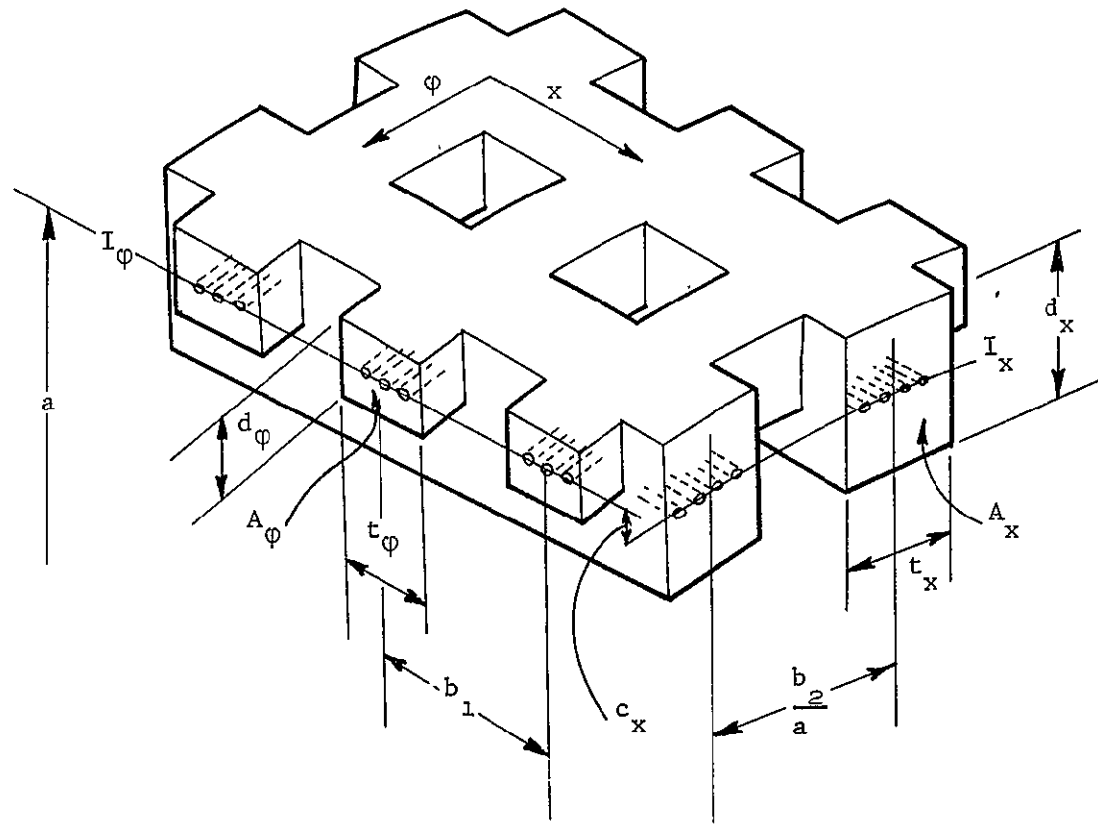


Fig. V-4 Section of Composite Gridwork Shell

$$\begin{aligned} \text{Music Wire:} \quad E &= 29 \times 10^6 \text{ lb/in}^2 \\ \gamma &= 0.284 \text{ lb/in}^3 \end{aligned}$$

Thicknesses d_ϕ and d_x are determined by providing numerical equivalence for their respective flexural rigidity π terms. For d_ϕ , symmetrical about the reference surface, (the eccentricity $c_\phi \equiv 0$)! we require $\pi_{10\phi m} = \pi_{10\phi p}$. Using the definitions previously established and tabulated and using flexible PVC properties for E_m and γ_m

$$\pi_{10\phi p} = \frac{D_{\phi m}}{\gamma_m a_m^4}$$

For a gridwork shell from Table II-2 we have

$$\pi_{10\phi p} = \frac{E_m (I_{\phi m} + A_{\phi m} c_{\phi m}^2)}{b_{1m} \gamma_m a_m^4}$$

and for rectangular sections and for our selected geometry of the gridwork pattern it follows that

$$\pi_{10\phi p} = \frac{E_m}{\gamma_m a_m^4} \frac{d_{\phi m}^3}{24} \quad (V-10)$$

All terms except $d_{\phi m}$ are known therefore this simple calculation provides one of the thicknesses.

Continuing in a similar manner we find the longitudinal rib thickness, however, we must take into account the eccentricity c_x . Again we require that $\pi_{10xm} = \pi_{10xp}$ and it follows that

$$\pi_{10xp} = \frac{D_{xm}}{\gamma_m a_m^4}$$

For a gridwork shell from Table II-2 we can write

$$\pi_{10xp} = \frac{E_m (I_{xm} + A_{xm} c_{xm}^2)}{b_{2m} \gamma_m a_m^4}$$

For rectangular sections and using our previously described geometry it can be shown that

$$\pi_{10xp} = \frac{E_m}{\gamma_m a_m^4} \left(\frac{d_{xm}^3}{6} - \frac{d_{xm}^2 d_{\phi m}}{4} + \frac{d_{xm} d_{\phi m}^2}{8} \right) \quad (V-11)$$

Again all terms except d_{xm} are known, $d_{\phi m}$ having been determined by Eq. (V-10). Solving for both thicknesses gives all the information required to produce that portion of the shell for which the flexural rigidities have the same nondimensional numerical values.

Using a different class of material, to complete the composite structure, the extensional rigidities (π_9) are satisfied by using S-Glass filaments or steel music wire. It is assumed that there is no interaction between either of the composite materials each working independently of the other and fulfilling its designated function. The requirement on scaling is made so that

$$\pi_{9\phi m} = \pi_{9\phi p}$$

from which we have

$$\pi_{9\phi p} = \frac{K_{xm}}{\gamma_m a_m^2}$$

For a gridwork shell from Table 11-2 we see that

$$\pi_{9\phi} = \frac{E_m A_{\phi m}}{b_{im} \gamma_m a_m^2}$$

or quite directly, the area required per rib is

$$A_{\phi m} = \frac{\pi_{9\phi p} b_{im} \gamma_m a_m^2}{E_m} \quad (V-12)$$

(For Glass or Music Wire/Rib)

And without additional discussion we can write directly for the other area

$$A_{xm} = \frac{\pi g_{xp} b_{2m} \gamma_m a_m^2}{E_m} \quad (V-13)$$

(For Glass or Music Wire/Rib)

Several interesting features of this modeling technique are discussed in Section V.G wherein a summary of model dimensions and characteristics is made.

X

F. GRIDWORK CONE MODEL

The cone model made as a composite gridwork cone has been treated as an equivalent cylinder with an average radius defined as the average of the large and small radii. Grid dimensions are somewhat smaller than for the cylinders. Thicknesses and reinforcing areas are calculated in the same manner as for the cylinders in the previous section.

A table in Section V.G provides numerical information regarding the cone designs.

G. SUMMARY OF MODEL DESIGNS

Design information developed for skin-stringer and composite gridwork shells has been used to determine sizes, spacings, etc. of the 1/20 models. Calculated thicknesses and specified thicknesses are shown in tabular form as well as comments regarding the scaled and unscaled π terms. Whether a π term is greater or less between model and prototype has no particular meaning. Each of these terms is equally as correct when used as its inverse. Therefore, a term too large can arbitrarily be made too small and vice versa, doing this of course to both model and prototype. A close examination of each term is required before any conclusion might be drawn regarding its effect when not precisely scaled.

Skin-stringer model designs are summarized in Tables V-1 and V-2. The first of these tables gives calculated and design shell dimensions and rigidities. Comments regarding the attempt to scale or not scale the 15 π terms are made in the second of these tables. Earlier discussions have given more detailed explanations of the summary made here. Full scale portions of the three shells are sketched in Fig. V-5. These are 1/20 scale dynamic model representations of the prototype shells shown in the figures of Section IV.

In a similar manner Table V-3 lists calculated and design data for the composite gridwork models. Both glass fiber reinforcement and steel music wire reinforcement are shown. Table V-4 lists the scaled and unscaled π terms with comments. Many more terms are left unscaled using this construction when compared to the skin-stringer models. Discussions in the text give more details and more reasons for the comments in the table.

Many π terms are left unscaled and in addition composite values of density and modulus can be defined for the combination of flexible PVC with either glass or steel. From the law of mixtures a composite modulus, analogous to the isotropic material elastic modulus can be calculated. Results of such calculations are given in Table V-5. From the previously specified numbers for PVC and glass and steel, we see many numbers. None of these are close to the values used in scaling and a large spread of values occurs. Using the composite modulus for the n_3 term and applying our time scaling factor we see the large differences in model and prototype, all influenced by a varying modulus, and similarly for the effect of gravity. When previously we forced the gravity constant to be the same for model and prototype, we see the contradictory requirements of model gravity being less or

Table V-1 Calculated and Actual Shell Dimensions and Rigidities

Shell	h_m (in.)		d_{xm} (in.)		t_{xm} (in.)		Extensional Rigidity				Flexural Rigidity			
	Calc	Use	Calc	Use	Calc	Use	π_{9xm}	π_{9xp}	$\pi_{9\phi m}$	$\pi_{9\phi p}$	π_{10xm}	π_{10xp}	$\pi_{10\phi m}$	$\pi_{10\phi p}$
Cyl A	0.00868	0.009	0.0790	0.080	0.0044	0.004	542	525	525	505	0.456 $\times 10^{-3}$	0.534 $\times 10^{-3}$	0.0361 $\times 10^{-3}$	0.0298 $\times 10^{-3}$
Cyl B	0.00333	0.003	0.0524	0.50	0.094	0.090	425	427	175	194	2.13 $\times 10^{-3}$	2.81 $\times 10^{-3}$	0.00134 $\times 10^{-3}$	0.00166 $\times 10^{-3}$
Cone C	0.00351	0.004	0.0583	0.060	0.067	0.070	756	686	340	298	7.46 $\times 10^{-3}$	6.89 $\times 10^{-3}$	0.00674 $\times 10^{-3}$	0.00426 $\times 10^{-3}$

MCR-68-87

Table V-2 Scaled and Unscaled Terms

π Terms	Form	Scaled		Comments
		Yes	No	
π_1	a/l	x		Required for boundary conditions
π_2	a/h	x		Result of providing extensional rigidity and realizing E/ρ as a factor
π_3	a/b		x	1/2 - 1/4 as many stringers
π_4	a/c		x	Eccentricity function of shape
π_5	A/a^2	x		From extensional rigidity
π_6	I/a^4	x		From flexural rigidity
π_7	J/a^4		x	Not scaled; however quantity is provided
π_8	$E/\gamma a$	x		Coefficient on all terms of D.E.
π_9	$K/\gamma a^2$	x		Extensional rigidity
π_{10}	$D/\gamma a^4$	x		Flexural Rigidity
π_{11}	S/Ka		x	Function of eccentricity
π_{12}	ϕ	x		Dimensionless coordinate
π_{13}	m	x		Dimensionless wave number
π_{14}	n	x		Dimensionless wave number
π_{15}	ν	x		0.33 on prototype, 0.3 assumed

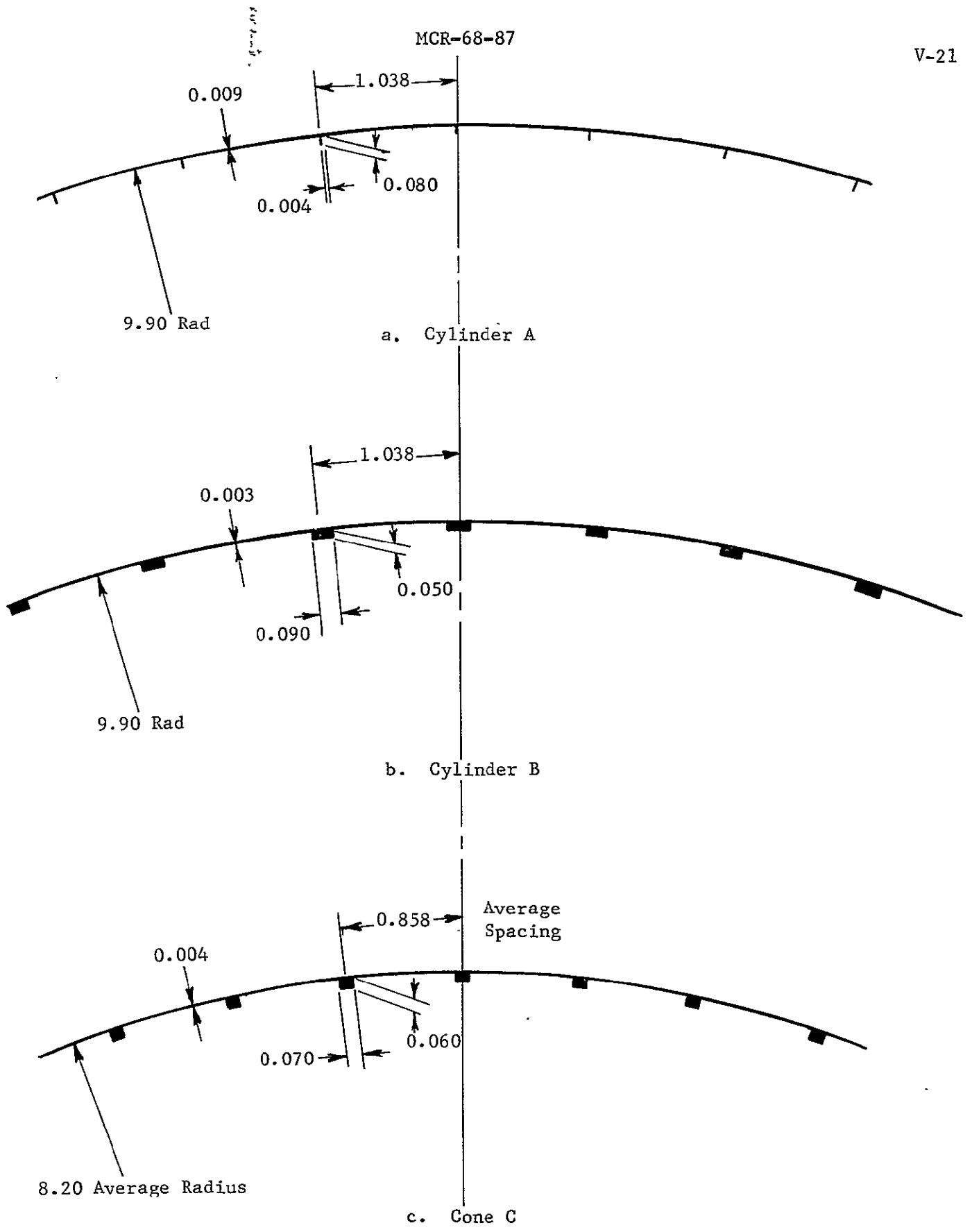


Fig. V-5 Details of Skin-Stringer Cylinder and Cone Models

Table V-3. Calculated and Design Shell Dimensions and Reinforcing for Composite Gridwork Models

Shell	d _{φm} ⁽¹⁾ (in.)		d _{xm} ⁽¹⁾ (in.)		φ direction (circumferential)				x direction (longitudinal)			
	Calc.	Use	Calc.	Use	S-Glass Roving (2)		Music Wire		S-Glass Roving		Music Wire	
					Calc.	Use	Calc.	Use	Calc.	Use	Calc.	Use
Cyl A	0.0659	0.066	0.141	0.140	28.6	30	5.10	5- 2Ga ⁽³⁾	29.6	30	3.80	4- 4Ga ⁽⁴⁾
Cyl B	0.0254	0.025	0.202	0.200	10.9	11	1.92	2- 2Ga	24.1	24	3.09	3- 4Ga
Cone C	0.0268	0.027	0.212	0.210	9.5	10	1.09	1- 5Ga ⁽⁵⁾	22.0	22	2.92	3- 4Ga

(1) Flexible PVC (E = 1,200 psi)

(2) Number of strands of single end roving (204 filaments/end) in each rib

(3) No. 2 Gage Music Wire 0.011 in. diameter

(4) No. 4 Gage Music Wire 0.013 in. diameter

(5) No. 5 Gage Music Wire 0.014 in. diameter

Table V-4 Scaled and Unscaled Π Terms for Composite Gridwork Shell Models

Π Terms	Form	Scaled		Comments
		Yes	No	
Π_1	a/l	✓		Required for boundary conditions.
Π_2	a/h		✓	Gridwork shell has no shell wall
Π_3	a/b		✓	1/2 - 1/4 as many stringers
Π_4	a/c		✓	Eccentricity is function of shape
Π_5	A/a^2		✓	Composite construction provides 2 areas
Π_6	I/a^4	✓		Assuming that materials behave independently
Π_7	J/a^4		✓	Not scaled, however quantity provided
Π_8	$E/\gamma a$		✓	Completely disregarded, two materials used
Π_9	$K/\gamma a^2$?		A numerically correct value provided
Π_{10}	$D/\gamma a^4$?		A numerically correct value provided
Π_{11}	S/Ka		✓	Function of eccentricity
Π_{12}	ϕ		✓	Angular location of comparable quantities not possible
Π_{13}	m	✓		Dimensionless wave number
Π_{14}	n	✓		Dimensionless wave number
Π_{15}	ν		✓	Not used in gridwork theory

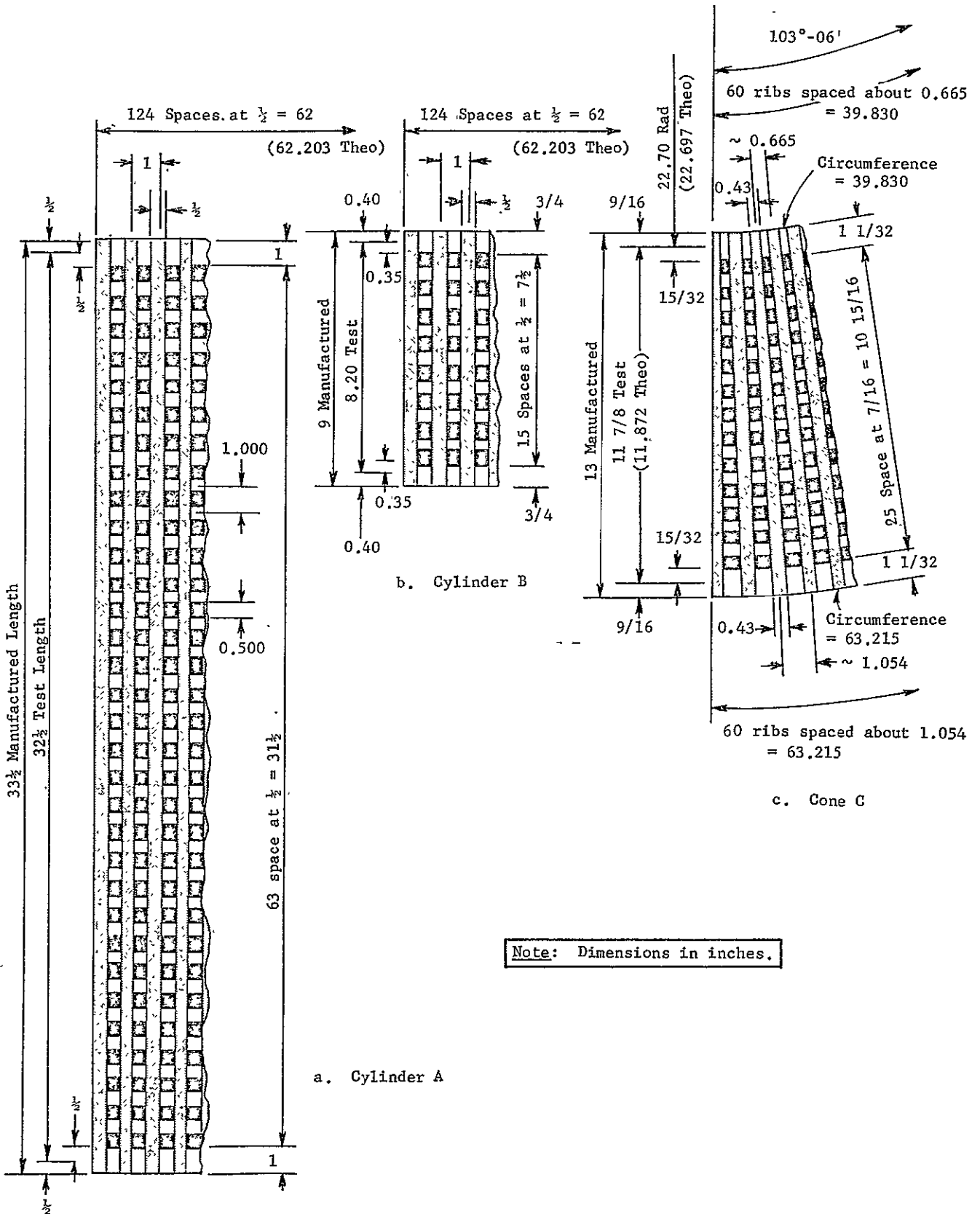
Table V-5 Composite Moduli, Time Scales, and Gravity Factors for Gridwork Shells

Shell	Composite Moduli (lb/in. ²)				Time Scale, T _m				Gravity Factor, g _m			
	PVC + Glass		PVC + Wire		PVC + Glass		PVC + Wire		PVC + Glass		PVC + Wire	
	φ-dir	x-dir	φ-dir	x-dir	φ-dir	x-dir	φ-dir	x-dir	φ-dir	x-dir	φ-dir	x-dir
Cyl A	165,000	80,000	415,000	220,000	0.29 T _p	0.41 T _p	0.18 T _p	0.25 T _p	0.62 g _p	0.29 g _p	1.6 g _p	0.82 g _p
Cyl B	155,000	45,000	435,000	115,000	0.29 T _p	0.54 T _p	0.17 T _p	0.34 T _p	0.59 g _p	0.17 g _p	1.6 g _p	0.44 g _p
Cone C	150,000	45,000	375,000	130,000	0.30 T _p	0.54 T _p	0.19 T _p	0.32 T _p	0.57 g _p	0.17 g _p	1.4 g _p	0.49 g _p

more than prototype gravity and different in both directions x and ϕ . Only experiment can decide the influence of this approach to scaling.

Details of the composite gridwork shells are shown as sketches. Fig. V-6 contains details of the developed surfaces. Full-scale sections through the composite shells are given in Fig. V-7.

Cone geometry has been developed in Fig. V-8 from which spacings and dimensions have been used in the model designs.



Note: Dimensions in inches.

Fig. V-6 Details of Developed Surface for Composite Gridwork Shells

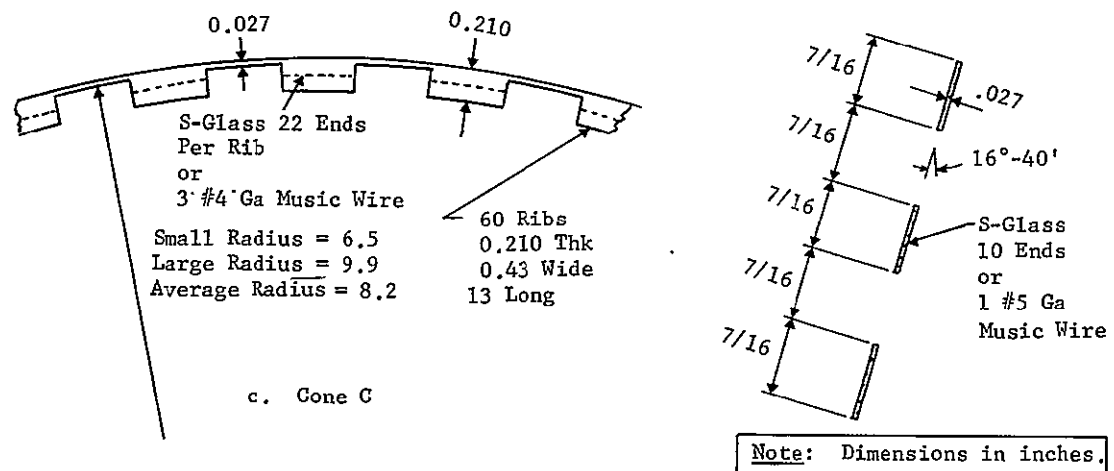
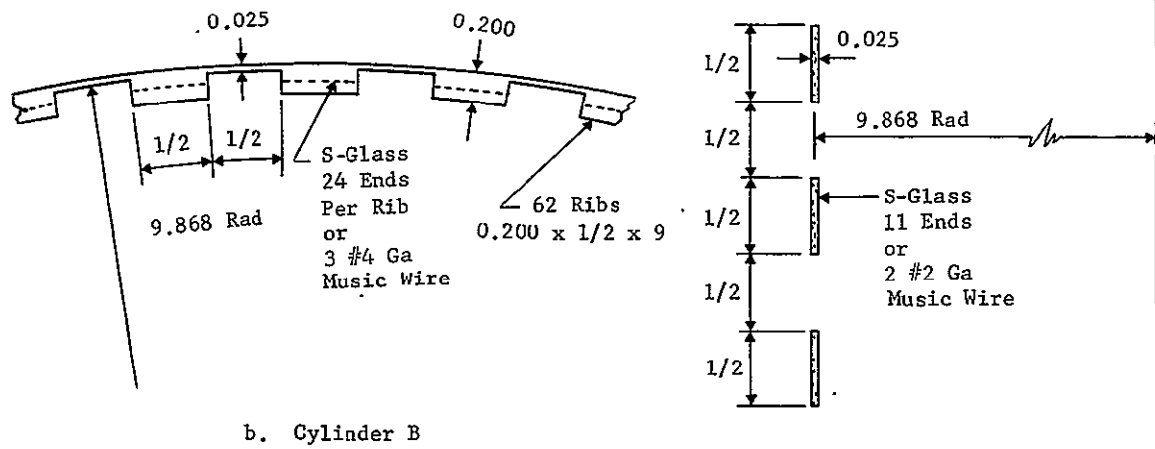
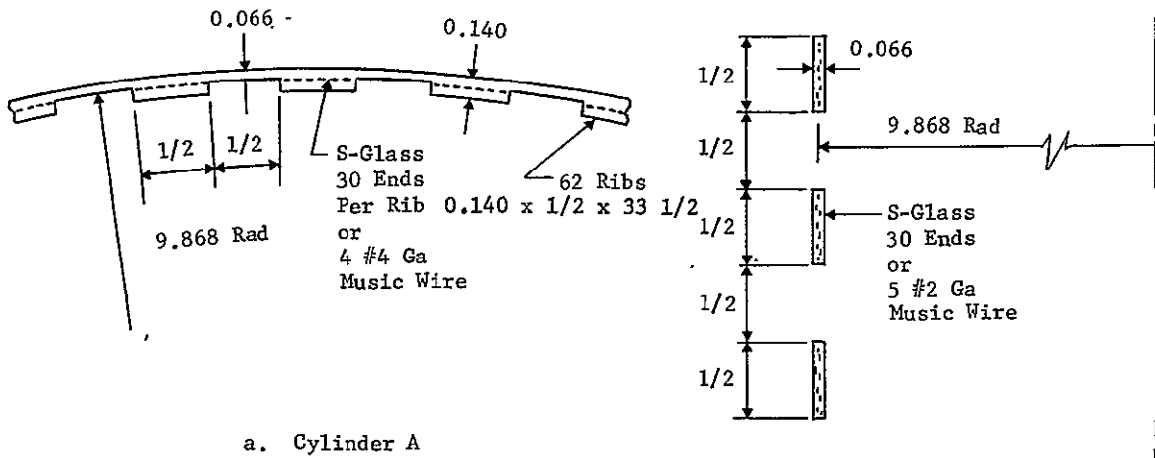


Fig. V-7 Reinforcing Details of Composite Gridwork Shells

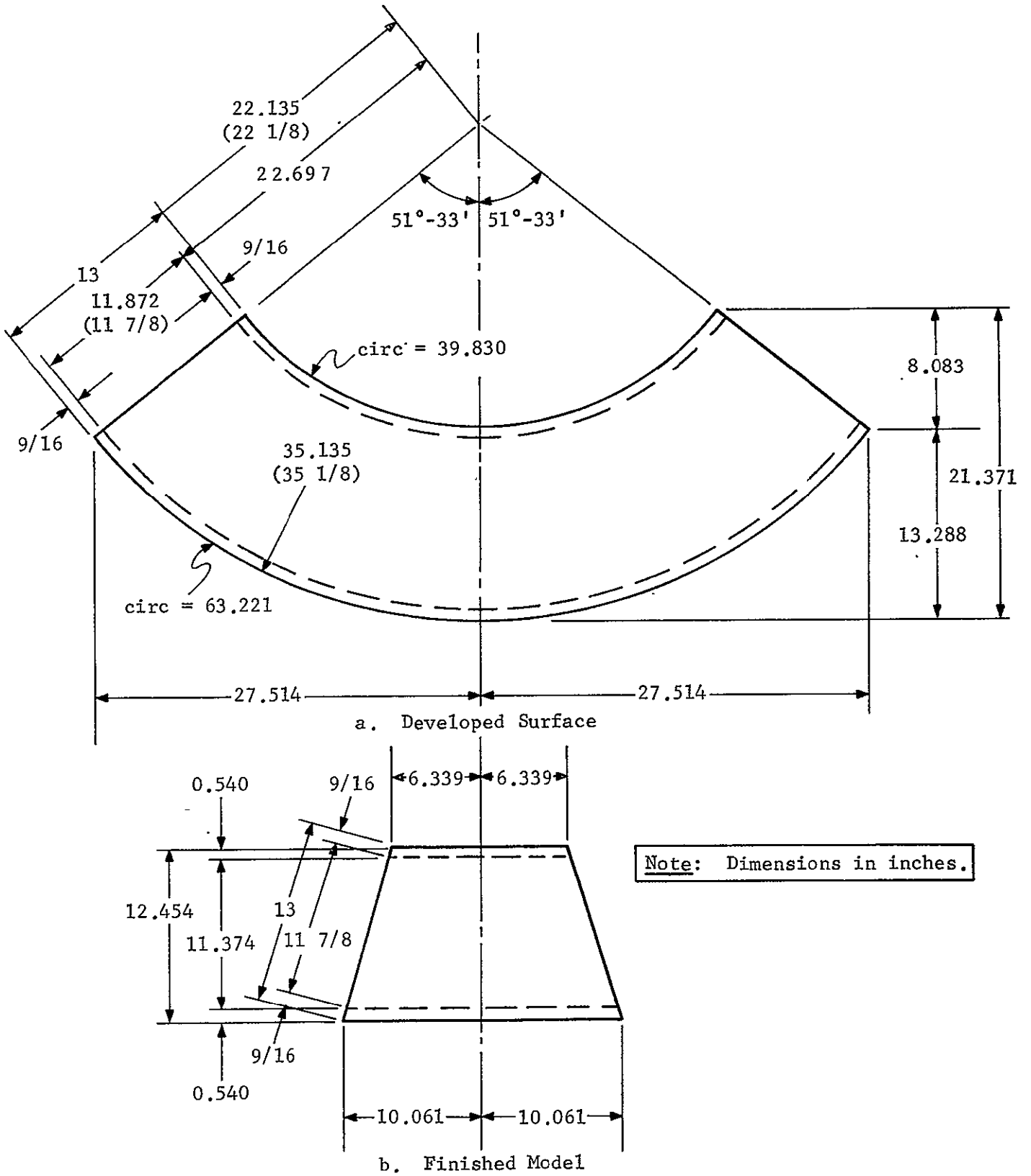


Fig. V-8 Details of Cone C Dimensions and Developed Surface

VI. DISTORTED MODELS

Any attempt to model an isotropic structure, such as a monocoque cylinder by discrete structural elements in the form of bars or rods requires that several rigidity requirements be met. As shown in Eqs. (II-2) in addition to radius to thickness ratios the quantities that require similitude (E and ρ selected as arbitrary scale factors (See Eqs. III-3 and III-5)) are extensional rigidity K and flexural rigidity D . Considering a skin-stringer structure modeled by discrete structural elements, it is easily verified that the shell modeling requirement normal to the stringers (in the ϕ direction) are the same as for monocoque shells. See, for example, rigidities in the ϕ direction for such shells in Table II-2. Shells stiffened in two directions x and ϕ can be approximated by grid work shells.

Assuming that a monocoque shell has been faithfully modeled by replica scaling and that this model is to be distorted using bars or rods or cruciform or H-sections we will have the following requirements. Using the notation from Fig. VI-1, the requirement for bending rigidity become for the bars

$$\frac{Ebh^3}{12(1-\nu^2)} = E_{\text{bar}} \frac{r_2^b (r_1 h)^3}{12}$$

and for the stretching rigidity

$$\frac{Ehb}{1-\nu^2} = E_{\text{bar}} r_1 h r_2^b$$

so that

$$r_2^b = \frac{Ehb}{(1-\nu^2) E_{\text{bar}} r_1 h}$$

which give

$$r_1 = 1, \quad r_2 = \frac{E}{E_{\text{bar}} (1-\nu^2)}$$

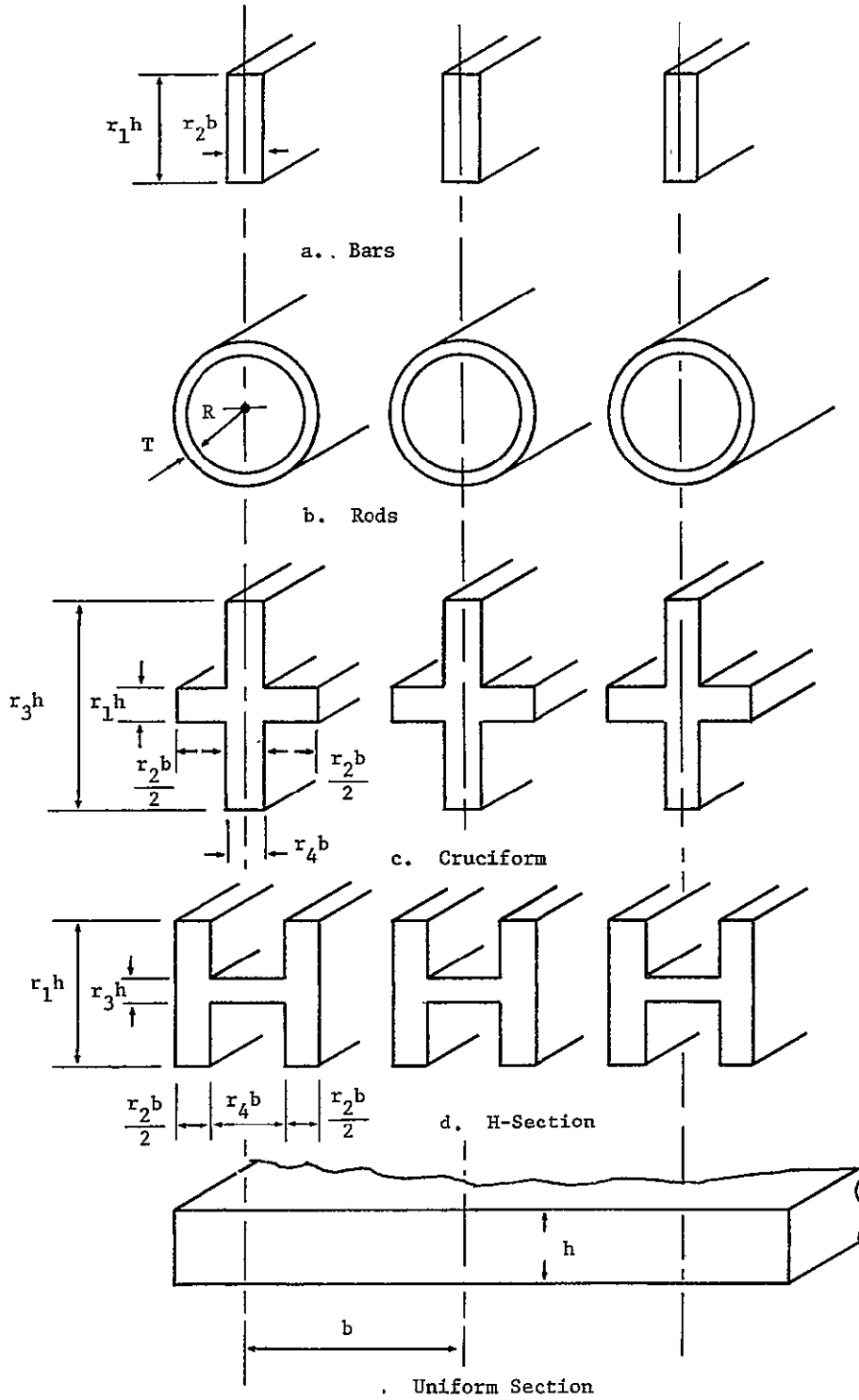


Fig. VI-1 Alternate Sections for a Uniform Section

This means the bar is the same thickness as the plate, depending on material the widths are matched but for individual bars the rigidities are matched in one direction only.

Similarly for the rods shown in Fig. VI.1b matching of rigidities (in one direction only) requires that

$$R < 0.41 h$$

producing a condition whereby the distorted model is thinner than the replica model.

A summary of the cruciform and H-sections that can provide both extensional and flexural rigidities in one direction is shown in Fig. VI-2. Procedure for determining this is exactly the same as outlined for the bars. In all cases the final width of either the cruciform or the H-section is wider than the original width b . Therefore, overlapping of pieces would be required in any one direction and another overlapping layer would be required in the transverse direction. There would be no shear rigidity in such a system without fastening crossing layers. This would then provide additional rigidities in flexural and extension to each of the layers, thereby destroying any attempt to match a replica scaled model by a distorted model consisting of discrete structural elements.

Distorted modeling in which some of the physical quantities are properly scaled can be achieved with composite materials. This development presented in Section V with details for such a set of models.

An indication of the orthotropic nature of skin-stringer shell construction can be obtained by attempting to model an orthotropic shell with an isotropic shell. By finding monocoque shell wall thicknesses that can independently satisfy the several rigidities, we can evaluate the feasibility of ignoring rigidity requirements. If the thicknesses are nearly the same, an averaged value may produce an acceptable distorted model. If, however, the calculated thicknesses are significantly different, then a distorted model (isotropic shell for orthotropic construction) cannot provide this similitude requirement.

We will satisfy g -scaling with a material so that

$$g_m = n_1^{-1} n_2^{-1} n_3 g_p$$

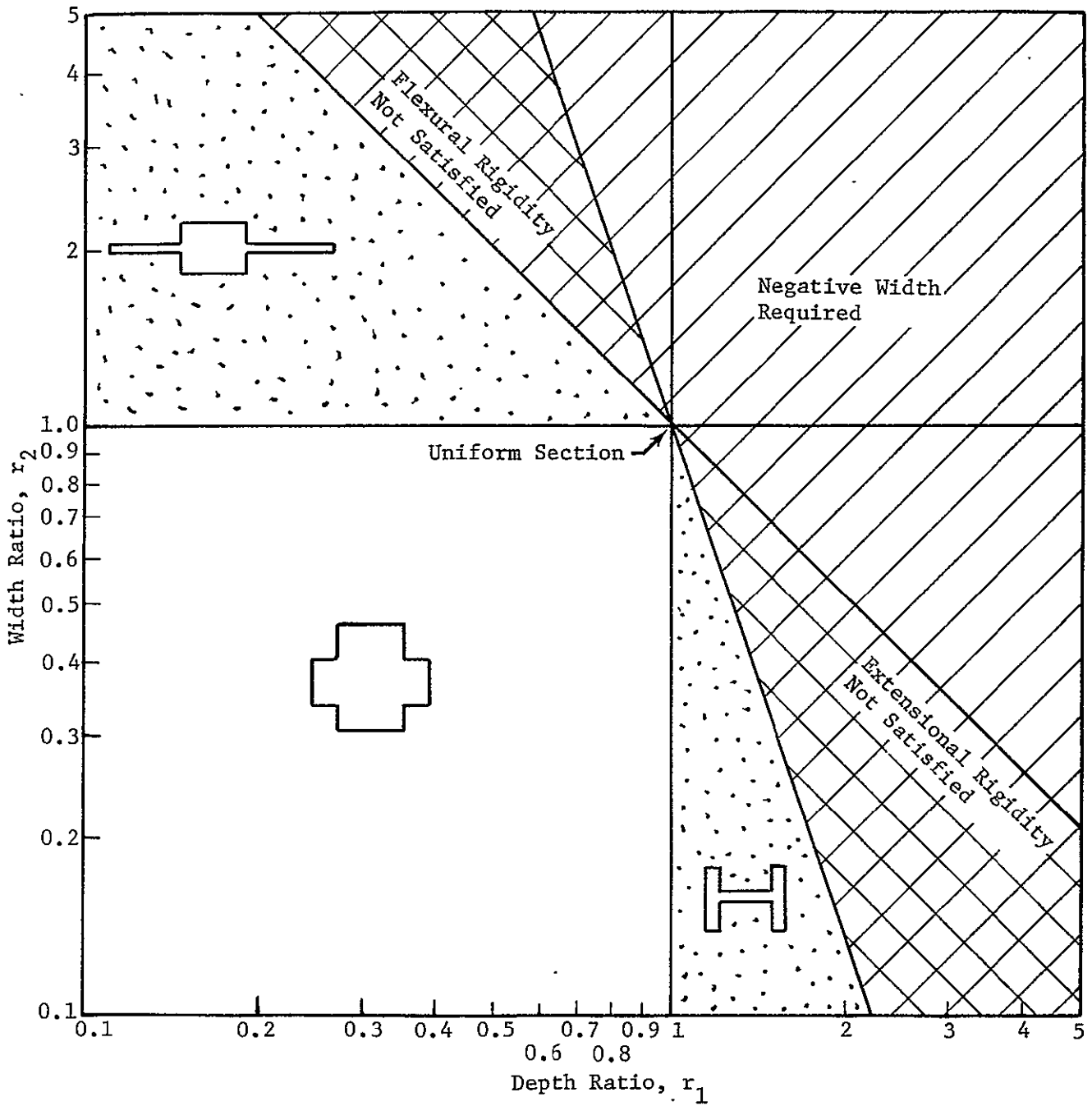


Fig. VI-2 Permissible Regions for Cruciform and H-Section to Provide Rigidities

or
$$n_1^{-1} n_2^{-1} n_3 = 1$$

for $n_1 = 1/20$, (a 1/20 scale model). For a material such as cellulose acetate we will specify

$$\gamma_m = 0.05 \text{ lb/in}^3, \quad E_m = 0.26 \times 10^6 \text{ lb/in}^2, \quad \text{and} \quad \nu_m = 0.3.$$

$$n_2 = \frac{\rho_m}{\rho_p} = \frac{0.05/\text{g}_m}{0.101/\text{g}_p} = \frac{1}{2}$$

$$n_3 = \frac{E_m}{E_p} = \frac{0.26 \times 10^6}{10.6 \times 10^6} = \frac{1}{40}$$

Using the density and modulus values, we find the following thickness relationships for the cylinders.

$$h_{9xm} = \frac{\pi_{9xp}}{58,200}$$

$$h_{9\phi m} = \frac{\pi_{9\phi p}}{58,200}$$

$$h_{10xm} = \left(\frac{\pi_{10xp}}{49.8} \right)^{1/3}$$

$$h_{10\phi m} = \left(\frac{\pi_{10\phi p}}{49.8} \right)^{1/3}$$

Values of the π terms are as previously tabulated. Solving for the four h terms, and including the cone as an equivalent cylinder the several thicknesses are given as a bar graph in Fig. VI-3. The conflicting requirements for thickness show ratios as high as 10 to 1 and as low as 2 to 1. It seems apparent that an orthotropic shell cannot be successfully modeled with a monocoque shell, even when satisfying the modulus to density requirements.

As a further illustration of the difficulties involved in attempting distorted shell models, a calculation is made for flexible PVC. Ignoring the modulus to density requirement and using the flexible PVC properties (as assumed for the composite gridwork shells) $\gamma_m = 0.05 \text{ lb/in}^3$, $E_m = 1,200 \text{ lb/in}^2$, and $\nu_m = 0.3$

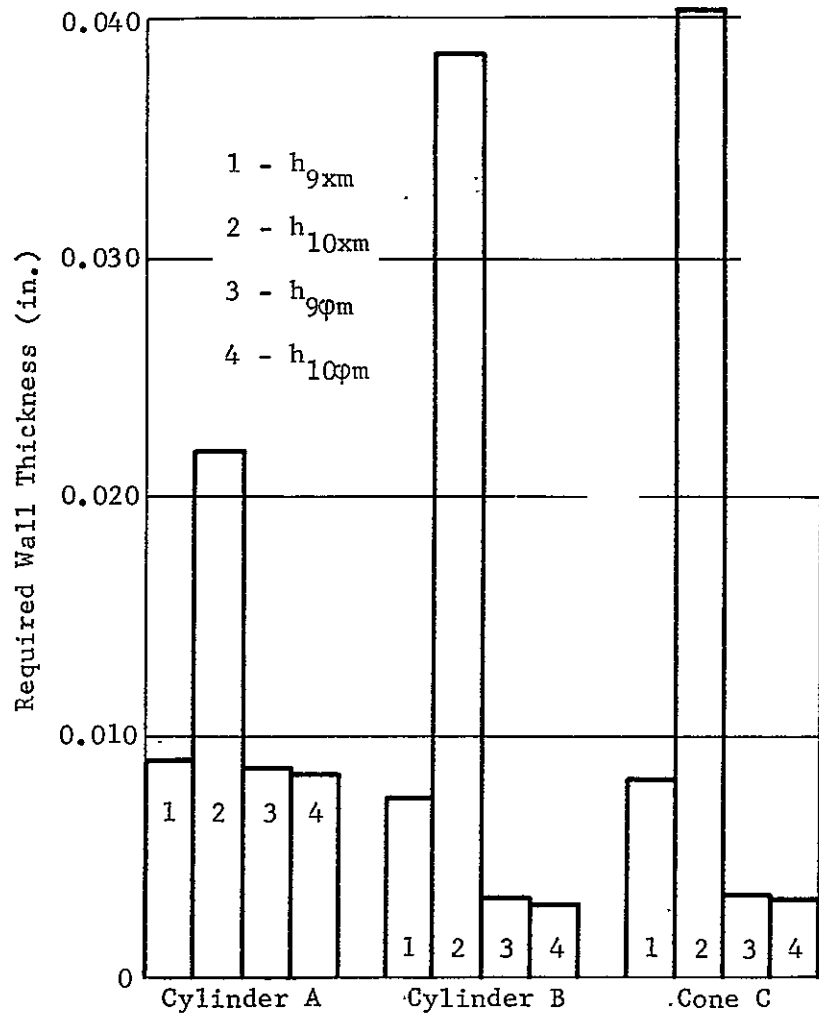


Fig. VI-3 The Several Wall Thicknesses for Cellulose Acetate

the several thicknesses are calculated proceeding in the same manner as for cellulose acetate. Figure VI-4 illustrates the four very different thicknesses required of a single shell. The ratios for this material, shown only for cylinder A, are much larger than for cellulose acetate.

Satisfying the extensional and flexural rigidities as well as the modulus to density ratio puts severe restrictions on dynamic scale models. Several other similitude requirements are automatically satisfied such as thickness to radius ratios, spacings and other ratios as the model shell more nearly reproduces the prototype shell. Not all structures impose this requirement on modeling. Shell structures because of their curvature (or curvatures) demand that models be more similar to their prototypes.

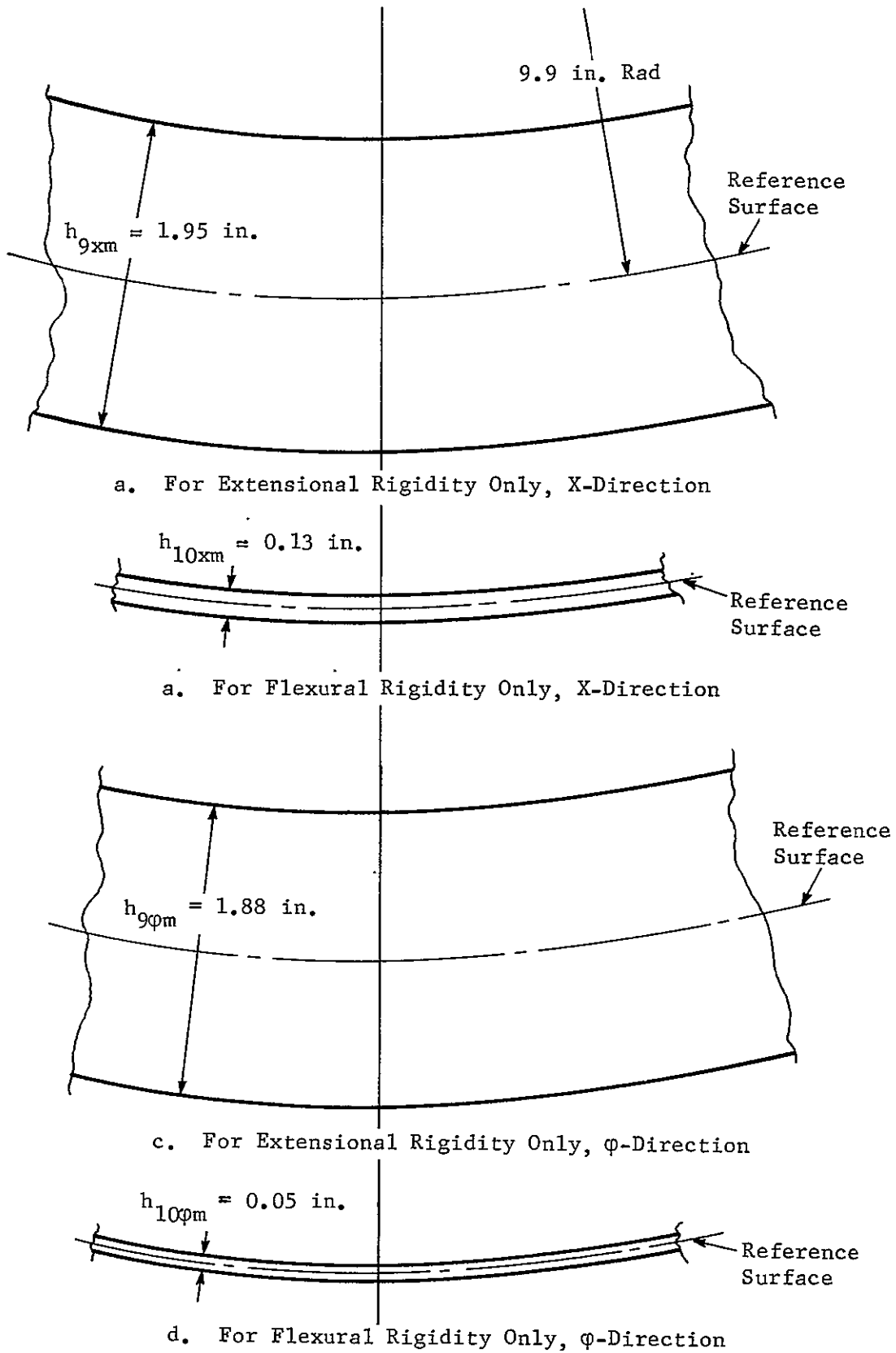


Fig. VI-4 Several Wall Thicknesses for Cylinder A Made of Flexible PVC

VII. EXPERIMENTAL PROCEDURE

A. MODEL CONSTRUCTION

Models of cellulose acetate (CA) and flexible polyvinyl chloride (PVC) were fabricated by personnel of the Martin Marietta Corporation, Denver Division, Structures and Materials Research Department. Detailed drawings were made from the design information in Section V and from the details given in Figures V-5 through V-8. Several deviations from these drawings are noted in the discussion of each model.

1. Cellulose Acetate Models

Sheet material of clear cellulose acetate of the appropriate thickness was used to form one each of Cylinder A, Cylinder B, and Cone C. In addition, a monocoque model with a 0.010 inch skin thickness was fabricated to have the same thickness, length, and diameter as Cylinder A. This model was used to establish handling and measuring techniques prior to testing the scaled skin-stringer and gridwork shells.

Material for the three shell skins and the stringers for Cylinder A were cut by using a sharp blade guided by a straight edge. A band saw with a fine blade was used to cut the relatively heavy stringers of Cylinder B and Cone C. Sawing left a slightly rough edge that was made smooth by pulling the cut edge over fine sand paper.

Bonding was accomplished by using acetone introduced through a hypodermic needle and syringe. Stringers on Cylinder A were located by using a metal template with two parallel lines scribed the length of the cylinder (33 1/2-in.) and spaced one-inch apart. To maintain the stiffener perpendicular to the shell wall and straight along the scribe lines a one-inch thick metal block was used at each end to provide a normal clamping surface and a tightening device to hold the stringers straight until the acetone evaporated. Good bonding was achieved for the full length of the stringer and no stringer failures were observed during vibration testing. Because of the small size of the stringer (.005 x .080-in. with the .005-in edge bonded) an additional amount of acetone was required and resulted in local softening of the wall that produced some distortion in the finished article.

Cylinder B and Cone C were made using a full scale paper drawing of each shell. The transparent cellulose acetate was

placed over the drawing and wall size and shape were cut and stringers bonded at appropriate locations. This technique prevented part of the distortion found in Cylinder A.

Cellulose acetate Cylinder B and Cone C are shown on top of the .010-in. wall monocoque cylinder in Fig. VII-1. The white rings are epoxy clamping rings used for the fixed boundary conditions and are discussed later.

All cellulose acetate material was acquired from the Celanese Plastics Company, a division of Celanese Corporation. The material was extruded diacetate sheeting No. 704 and is made in thicknesses from .003-in and greater. Models were constructed from .005 and .010-in. S-704 extruded film and .040 and .060-in. S-704 AA sheet. A tensile test from the material showed linear stress-strain behavior and a modulus of 2.5×10^5 lb/in².

2. Flexible Polyvinyl Chloride Models

Composite construction consisting of flexible polyvinyl chloride for flexural rigidity, music wire for axial extensional rigidity, and glass filaments for circumferential extensional rigidity were combined into gridwork shells. Distorted scale models required many more steps in construction, took longer to fabricate, and demanded a wide variety of fabrication equipment and special tooling.

Material in sheet form was acquired from the Norton Company in 1/32, 1/16, and 3/32-in. thicknesses. Design dimensions and wire embedment were achieved by laminating thin sheets. Several solvents were used to find the most efficient bonding agent. The most satisfactory agent was cyclohexanone and required 16 hours at room temperature to achieve bond while contact pressure was applied to the laminate. Occasionally after removing pressure it was discovered that edges were not bonded and the process was repeated.

Ribs for Cylinder A were formed in groups of five using the room temperature process. Wires were held on a large sheet of PVC at each rib location by templates consisting of a positioning hole and a tightening peg for each wire. Rib were cut to width and centered over the wires. It was necessary to ensure that wires did not leave the ribs when pressure (from weights) was applied. The cyclohexanone and softened flexible PVC made a slippery environment for the wires until set began to occur. This model, after all ribs were attached, was placed in an oven for several hours at 100 to 110°F to evaporate any remaining solvent.

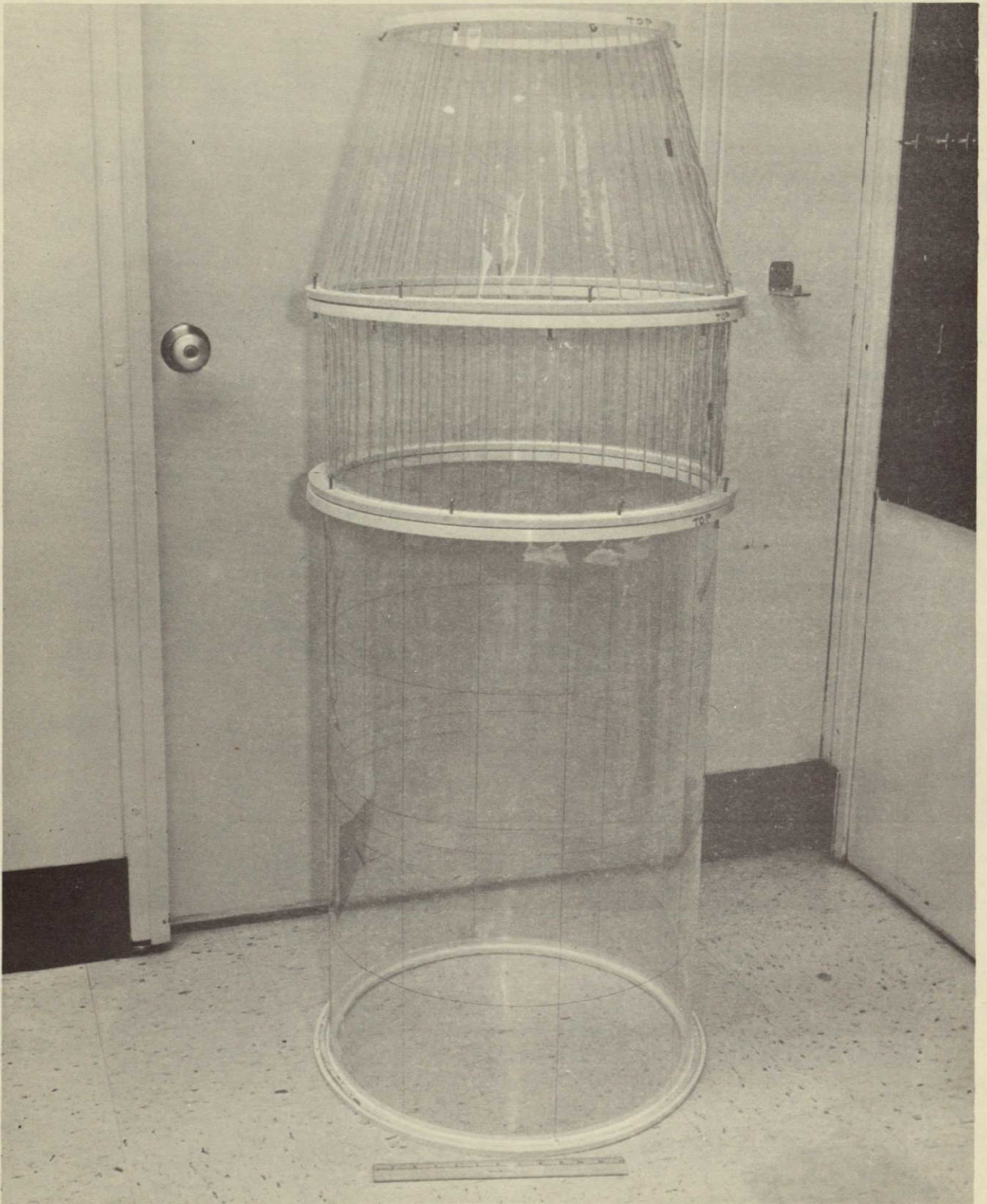


Figure VII-1 Cellulose Acetate Cylinders and Cone

Ribs for Cylinder B and Cone C were made in an open top mold of the desired dimensions with pegs at each end to tighten and position the wires. PVC, wires, and PVC were placed in the mold and the assembly was placed in a preheated platten press at 350°F. Sufficient force was applied to compact the laminate and held at 350°F for 15 minutes. Ribes were removed from the mold after cooling to room temperature.

Paper drawings of the full size model were used to cut the skin portion of the model and to locate the ribs. Cyclohexanone at room temperature was used to bond the ribs to the skin and weights were used to apply a bonding pressure. The difficulty encountered in Cylinder A when ribs and wires tended to shift was not encountered when bonding PVC ribs (with wires in the rib) only to the PVC skin.

Extensional rigidity was supplied by glass filaments wound at rings spaced at one-inch centers. Because of the extremely low modulus (1,400 lb/in²) and relatively large thicknesses the shells behaved in a very limp fashion. Mandrels made to the geometry of the finished part were constructed by using a cardboard skeletal structure on which plaster was applied and swept to a final dimension. Fig. VII-2 is a detail of such a structure for Cone C. Further steps in the fabrication of the cone are shown in Figures VII-3 a, b, and c. In Fig. VII-3a the plaster has been applied and cured to produce a mandrel on which the PVC cone will be fitted. In Fig. VII-3b the cone is on the mandrel and tapered wooden strips have been fitted between the ribs to provide a smooth surface for winding. The reason for the filler strips, can be observed in Fig. V-7. Glass filaments are shown wound on the cone in Fig. VII-3c. A room temperature cureable epoxy was applied as a very thin coat to bond the glass to itself and to the PVC surface. Although the cone has been discussed and shown in detail cylinders A and B were treated in the same manner and they are shown on their mandrel in Fig. VII-4. The cylinders and cone were removed from plaster mandrels by removing the cardboard supporting structure and breaking the plaster. After attempting to provide square holes for the gridwork shells, it was found more expedient to drill round holes using a cork borer. These holes were drilled prior to breaking the plaster mandrels.

Completed Cylinder A, Cylinder B and Cone C are shown stacked atop each other in Fig. VII.5. Clamping rings made of epoxy have been applied to the ends to maintain each end as a circle. Flexible PVC being very soft and showing almost no rigidity made a very pliable shell until the ends were fixed. The photograph showing these shells on top of each other demonstrates the necessity of maintaining circular boundaries for proper cone and cylinder behavior.

NOT REPRODUCIBLE

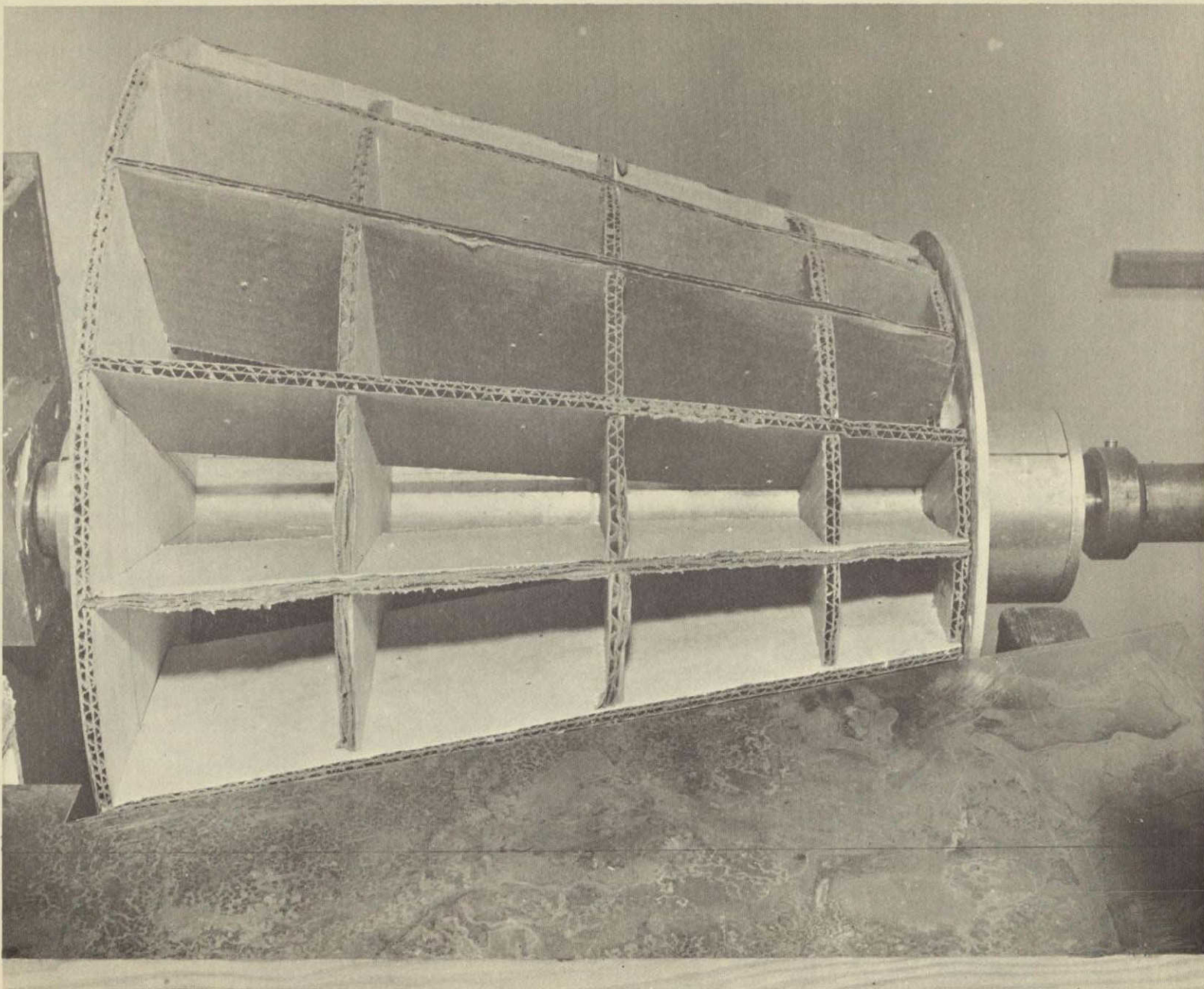
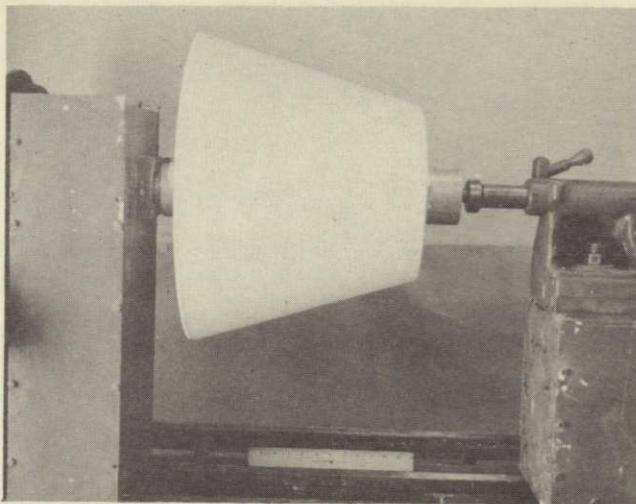
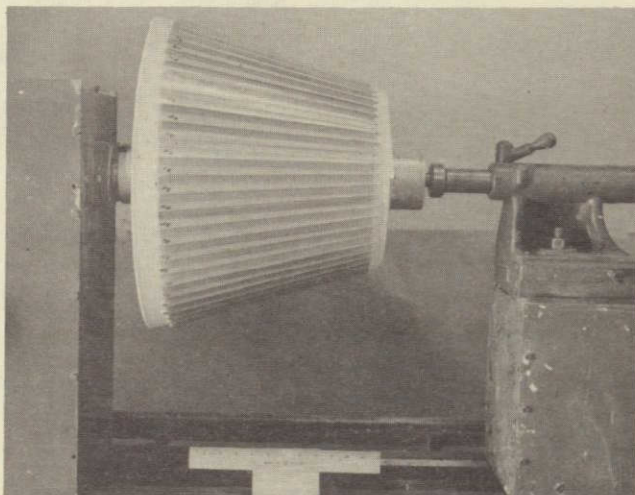


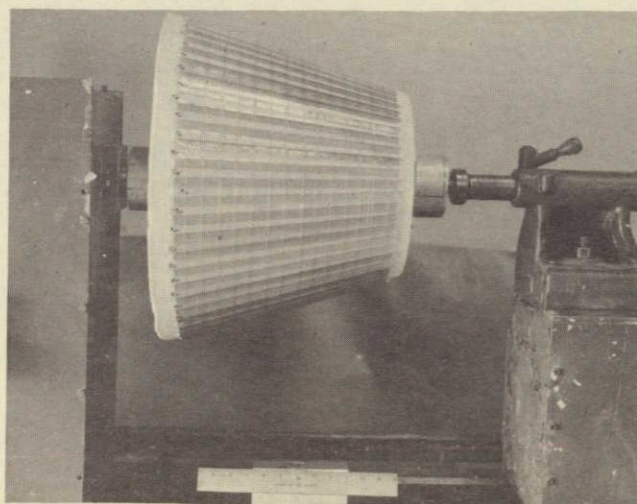
Figure VII-2 Cardboard Structure for Support of Plaster Mandrel



a. Mandrel Made of Plaster



b. Flexible PVC on Mandrel and Spaces Between Ribs Filled with Wood Wedges



c. Glass Filaments Wound on Cone C

Figure VII-3 Steps in Applying Glass Filaments on Cone C

ГОС. НАУЧНО-ИССЛЕДОВАТЕЛЬСКИЙ ЦЕНТР

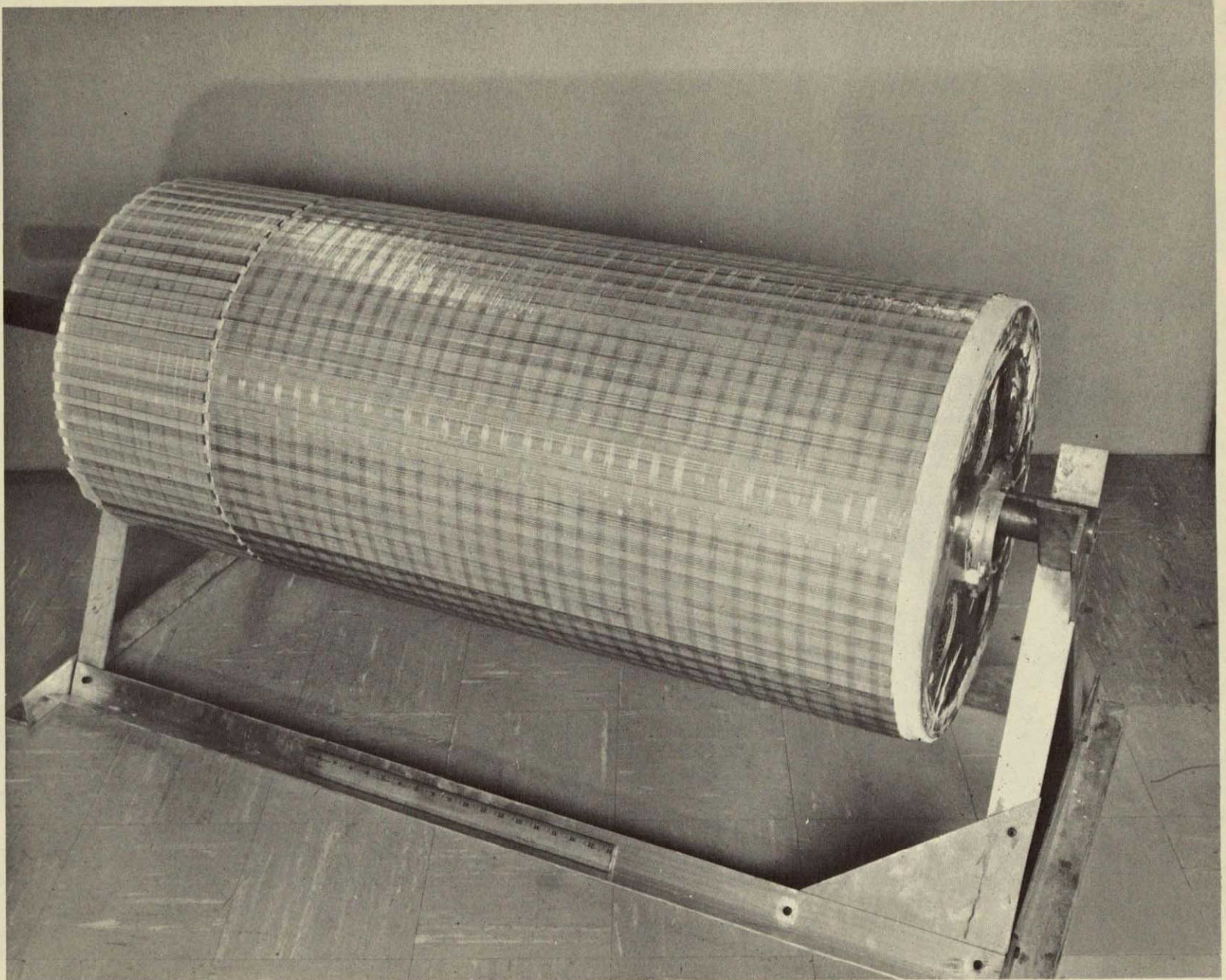


Figure VII-4 Cylinders A and B on Mandrel After Glass Filaments Wound at Intervals

MCR-68-87

VII-7

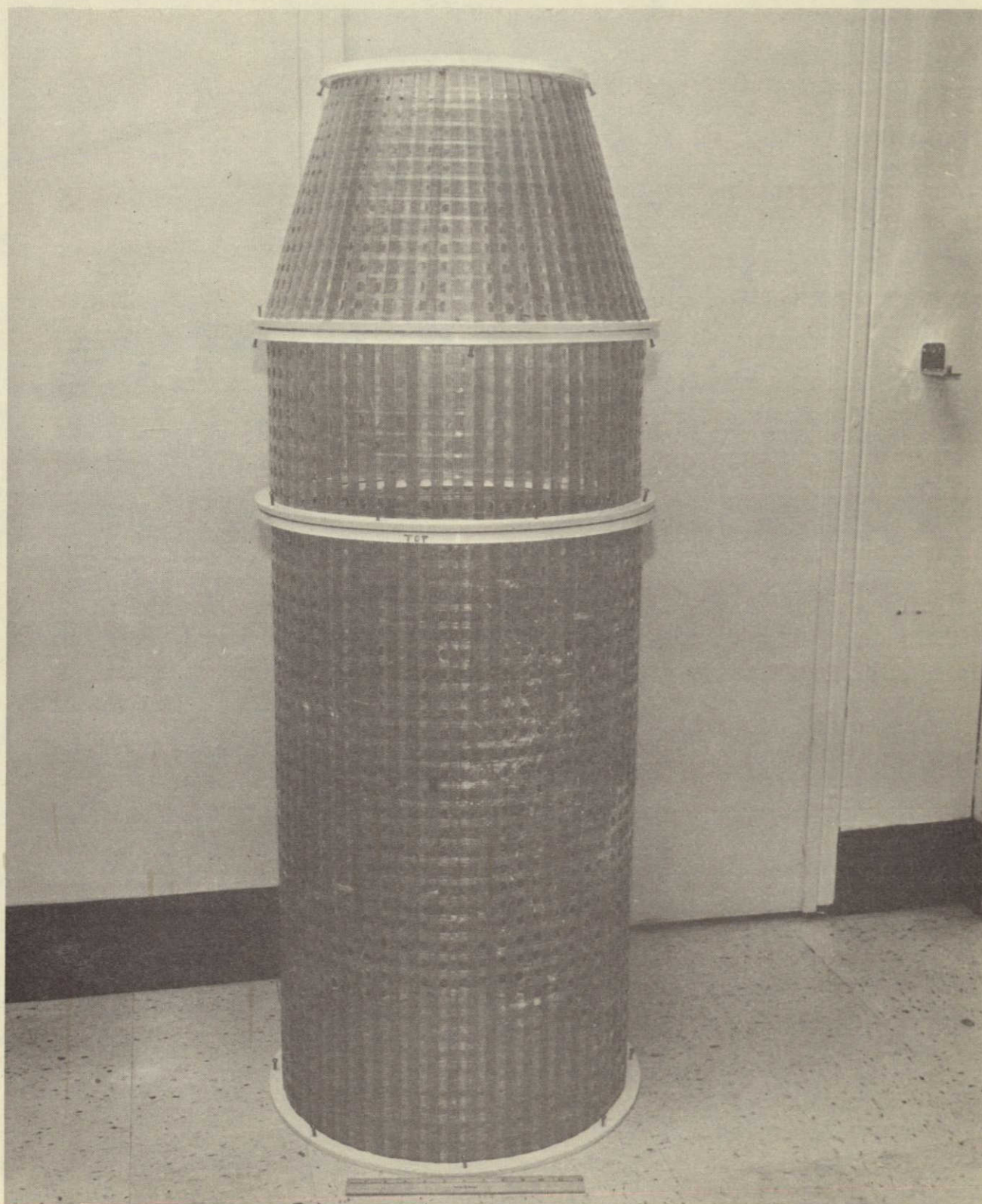


Figure VII-5 Flexible Polyvinyl Chloride Cylinders and Cone

NOT REPRODUCIBLE

3. Summary of Cylinder and Cone Models

Some departures were noted from the design drawings and the finished shells. The most significant deviation occurred in Cylinder A where the generators of the cylindrical surface were not all straight lines but showed an observable curvature and each section was not circular.

When making developable surfaces, as these were, in the developed position, care must be exercised not to stretch or distort the flat sheet and to maintain flat finished construction. This is particularly true of material like cellulose acetate for it acts as a structural material maintaining its fabricated shape. A soft material such as flexible PVC is more forgiving of distortions introduced during fabrication.

Table VII-1 is a summary of the compliance to details of the cellulose acetate models and their design drawings. Noted are such data as gauges, numbers of stiffeners, etc.

Table VII-1 Summary for Cellulose Acetate Models

Shell	Skin Gauge (in.)		No. of Stiff.		Stiff. Size (in.)		Test Length (in.)	
	Design	Model	Design	Model	Design	Model	Design	Model
Cyl. A	.009	.010	60	61	.004 x .080	.005 x .080	32 $\frac{1}{2}$	32 $\frac{3}{4}$
Cyl. A	.003	.005	60	60	.090 x .050	.090 x .040	8.2	8 $\frac{1}{4}$
Cone C	.004	.005	60	60	.070 x .060	.070 x .060	11 $\frac{7}{8}$	12 $\frac{1}{8}$

Similarly for the flexible PVC there were some departures between the design and the completed models. A summary of sizes and numbers is given in Table VII-2.

Several recommendations can be made for producing high quality stiffened plastic models from the experiences gained on this program. These are divided into the subjects of bonding and methods of fabrication.

Table VII-2 Summary for Flexible PVC Models

Shell	Skin Gauge (in.)		Rib Size (in.)		No. of Ribs		Wires/Rib		Glass/Ring		Test Length (in.)	
	Design	Model	Design	Model	Design	Model	Design	Model	Design	Model	Design	Model
Cyl. A	.066	.075	.140 x 1/2	.150 x 1/2	62	62	4	4	30	30	32 $\frac{1}{2}$	32 $\frac{3}{4}$
Cyl. B	.025	.030	.200 x 1/2	.225 x 1/2	62	61	3	4	11	11	8.2	8 $\frac{1}{4}$
Cone C	.027	.030	.210 x 1/2	.210 x 1/2	60	60	3	4	10	10	11 $\frac{7}{8}$	12

A serious effort should be undertaken to note and classify the effects of bonding agents on the joints. Strength, local distortion, and effects of time on integrity are among the items that require study. Structural use of reinforced sheet plastics requiring bonding techniques to attach the reinforcements has not been studied as much as monocoque construction. An example of unreinforced shells are mylar cones and cylinders with a taped seam. Another example of unreinforced shells is spin cast cylinders made of birefringent plastic and studied photoelastically.

Fabricating a reinforced developable surface as a flat reinforced sheet may be acceptable only when the attachments are applied without distortion to the surface. A recommended procedure for cylinders and cones is to make a mold, form the basic shell in the mold, then attach stringers, rings, reinforcements, etc. to the shell wall while being restrained in the mold.

For the low cost of plastic material and ease of fabrication the investment required to produce geometrically excellent specimens appears to be justified.

B. BOUNDARY CONDITIONS

Cellulose acetate and flexible PVC shells had clamped boundary conditions. Displacements and rotations at either end were prevented. This was accomplished by encapsulating about a 1/2-in. of each end in a circular epoxy ring about 1-in. thick. The epoxy material was a very heavily filled, high strength, high modulus laminating resin from Furane Plastics, Inc. To 100 parts by weight of Epocast Resin H-1468 were added 15 parts by weight of Hardener 9816.

Clamping plates for both ends are shown in Fig. VII-6. The process of encapsulation was the same for each end. With the shell in the groove and notches cut along its edge, a circular cardboard disc (with a hole for the 2 1/4-in. diameter pipe and spaces for the stiffeners) held the encapsulating end centered and circular. The 24-in. diameter plate was made level and epoxy was poured along the outer edge between the shell and the groove. Because of the notched edge of the shell the epoxy ran into the area behind the shell and filled the back portion of the groove on the inside of the shell. The 1/2 x 1 in. channel groove in the 24-in. diameter plates had small locating holes drilled in the bottom and in a different pattern for each groove. After the epoxy ring was removed, the shell was returned to the same groove and in the same position for testing.

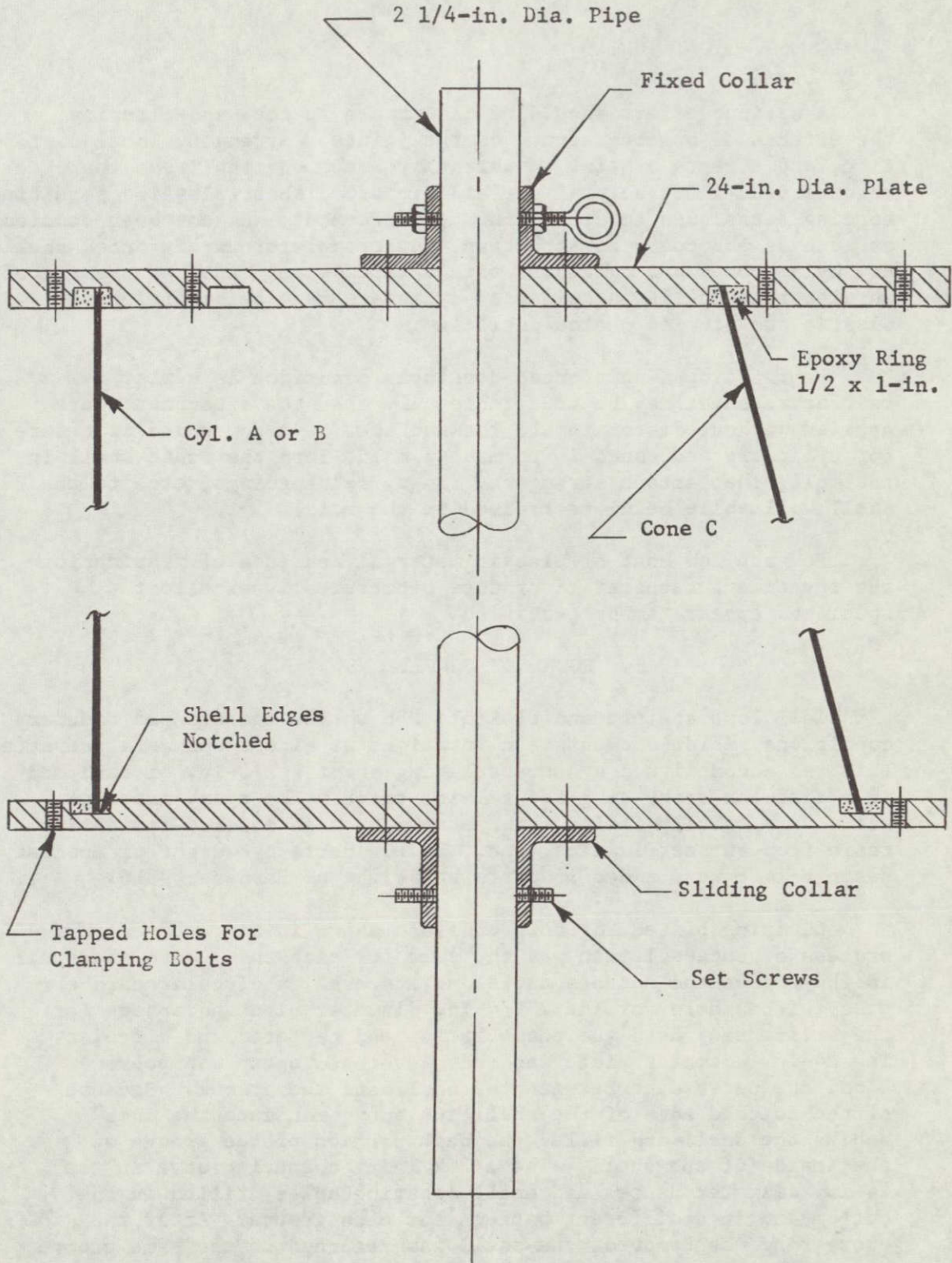


Fig. VII-6 Clamping Plates Showing Cylinder on Left Side and Cone on Right Side

Epoxy rings were cured at least 16 hours at room temperature and the ring was removed from the channel groove. Release was accomplished by using a wax mold release agent. Each channel groove had a 10 degree taper to ease ring removal. In addition, a series of bolts were put in the wet epoxy to be used as jack points to help free the rings. This avoided strain on the shell when removing the ring from the channel groove. These bolts can be seen in the white epoxy rings in Figs. VII-1 and VII-5.

When the shells were replaced on the end plates, a clamping device was used to ensure seating the epoxy ring in the channel groove. Details of this arrangement are shown in a later figure.

C. EXCITATION AND MEASURING

Cylinders A and B and Cone C were excited acoustically by a speaker driven with a signal generator and an amplifier. The sound energy from the speaker was directed onto the specimen through a horn with large end over the speaker and small end held near the shell. A sine wave was produced by the signal generator and the amplitude was controlled by the gain on the amplifier. As required, a very large or a small quantity of air could be pumped by the horn. The baffle tended to prevent wave cancellation between the front and back of the speaker cone.

In Fig. VII-7 a schematic representation of the experimental arrangement identifies all major components used in finding the natural frequencies. The method used to determine resonance was by Lissajous figures on an oscilloscope. As shown in the figure a strain gauge was mounted to act along a generator at about one-third the distance from one end. This gauge responded to vibrations in the axial direction and its amplified output (200,000 times) was recorded as a vertical output on the oscilloscope. Along the horizontal axis of the oscilloscope the output from the signal generator was recorded as a horizontal point undergoing simple harmonic motion. When resonance occurred, the result was an ellipse (axis either horizontal or vertical depending on relative magnifications) that remained stable.

The strain gauge was positioned about 135 degrees from the point of excitation. Rotating the specimen when at a natural frequency had little effect on the Lissajous figure, and was demonstrated for one specimen.

Circumferential waves were determined by using a crystal phonograph cartridge excited by a mechanical device touching the surface. Again a Lissajous figure was used to find nodal lines

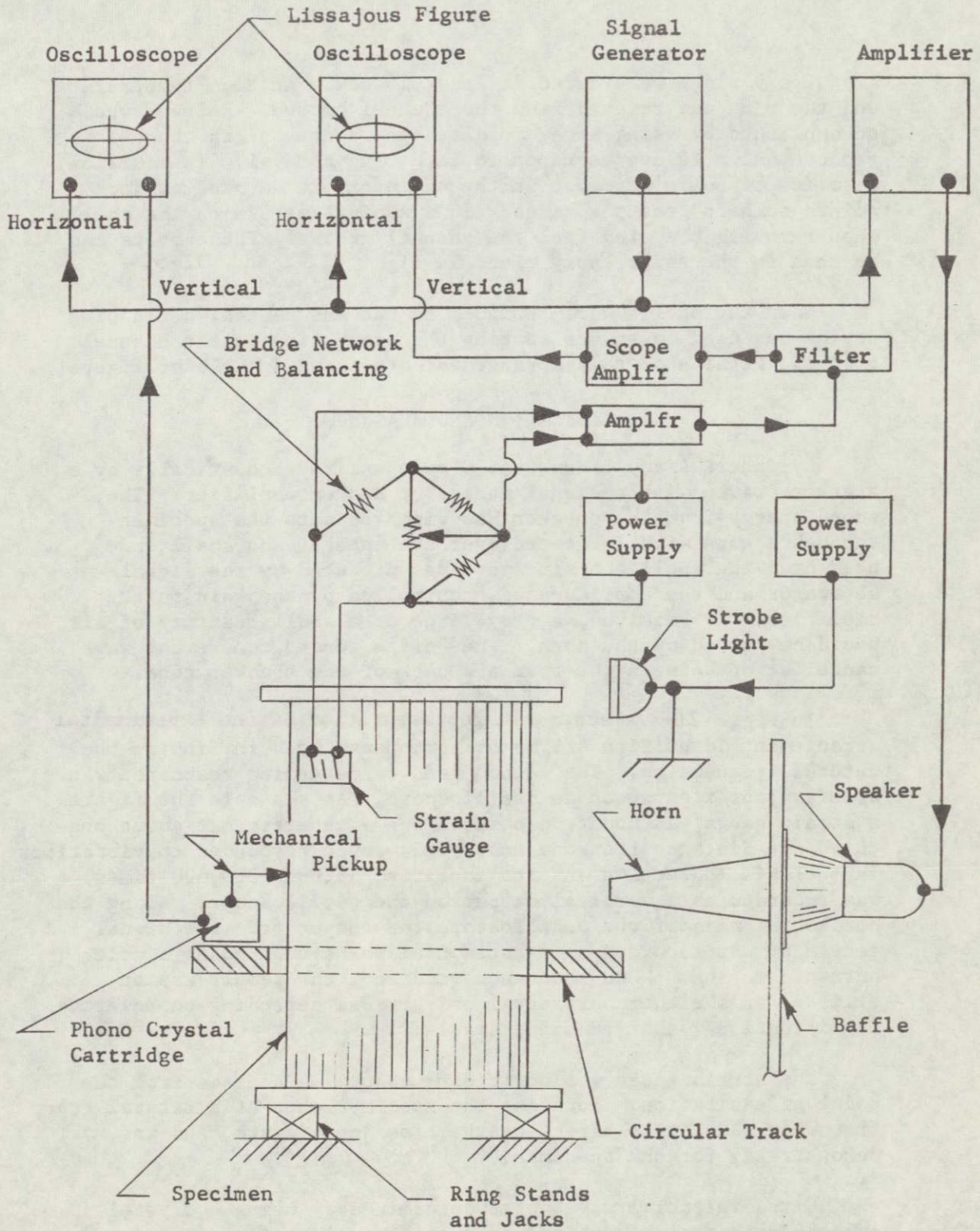


Fig. VII-7 Schematic of Instrumentation and Acoustic Speaker

and points of maximum amplitude by recording the response of radial motion. The crystal output was on the vertical axis and the frequency from the signal generator was on the horizontal axis. When the strain gauge output indicated a resonance on its oscilloscope the phonograph cartridge produced elliptical figures. When the specimen was not at resonance the figures from the radial motion were not regular and generally did not show an elliptical pattern. The relative amplitude as measured by the vertical scale of the oscilloscope was recorded to indicate the amount of radial motion.

In Fig. VII-8 the baffle is shown in front of the speaker and the horn is fastened to the baffle. The assembly was mounted on a cart permitting back and forth movement to bring the end of the horn near the specimen.

Cellulose acetate Cylinder A is shown in Fig. VII-9 fastened to the lower clamping ring with bolts through an angle-like clamping device. Also shown is the strobe light used to observe the overall motion during vibrations. Whenever the strobe light fired the strain gauge circuit would record a blip on the oscilloscope. At perfect synchronization a single blip remained stationary on the Lissajous figure. For a slight mismatch in synchronization the blip from the strobe would travel around the Lissajous figure at the mismatch frequency. When producing a double image, once at each extreme of the vibration two blips would appear on the oscilloscope face. Thus by watching the oscilloscope it was possible to synchronize and single strobe or multiple strobe the vibrating model and the know exactly what condition was in effect.

The major pieces of electronic equipment are shown in Fig. VII-10. The oscilloscope, amplifiers, power supplies, and signal generator were the items necessary to excite and to record. Strobe, bridge network and filters are also included.

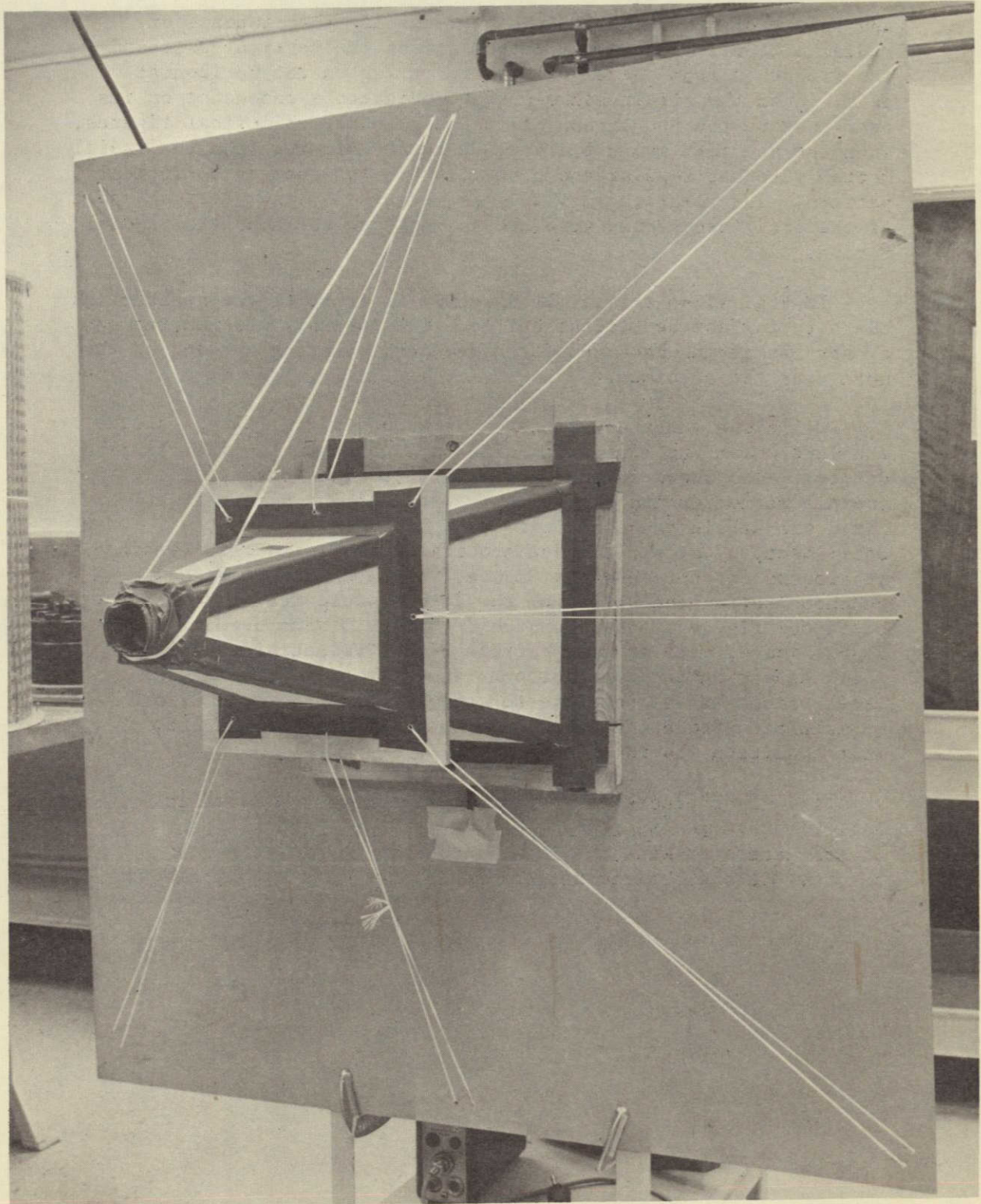


Figure VII-8 Baffle and Horn in Front of Speaker Cone

NOT REPRODUCIBLE

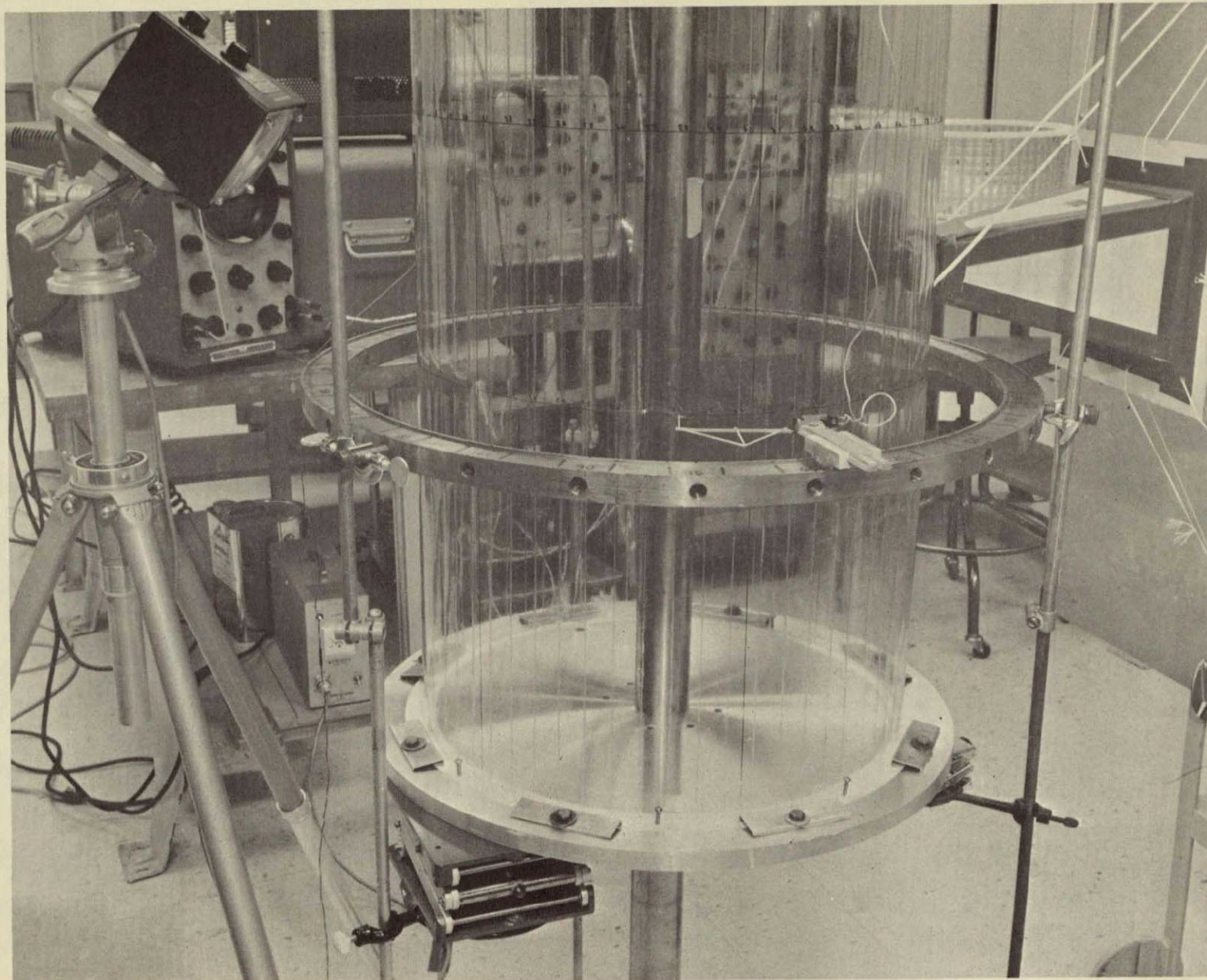


Figure VII-9 Cylinder A in Test Setup with Associated Measuring Devices

MCR-68-87

VII-17

NOT REPRODUCIBLE

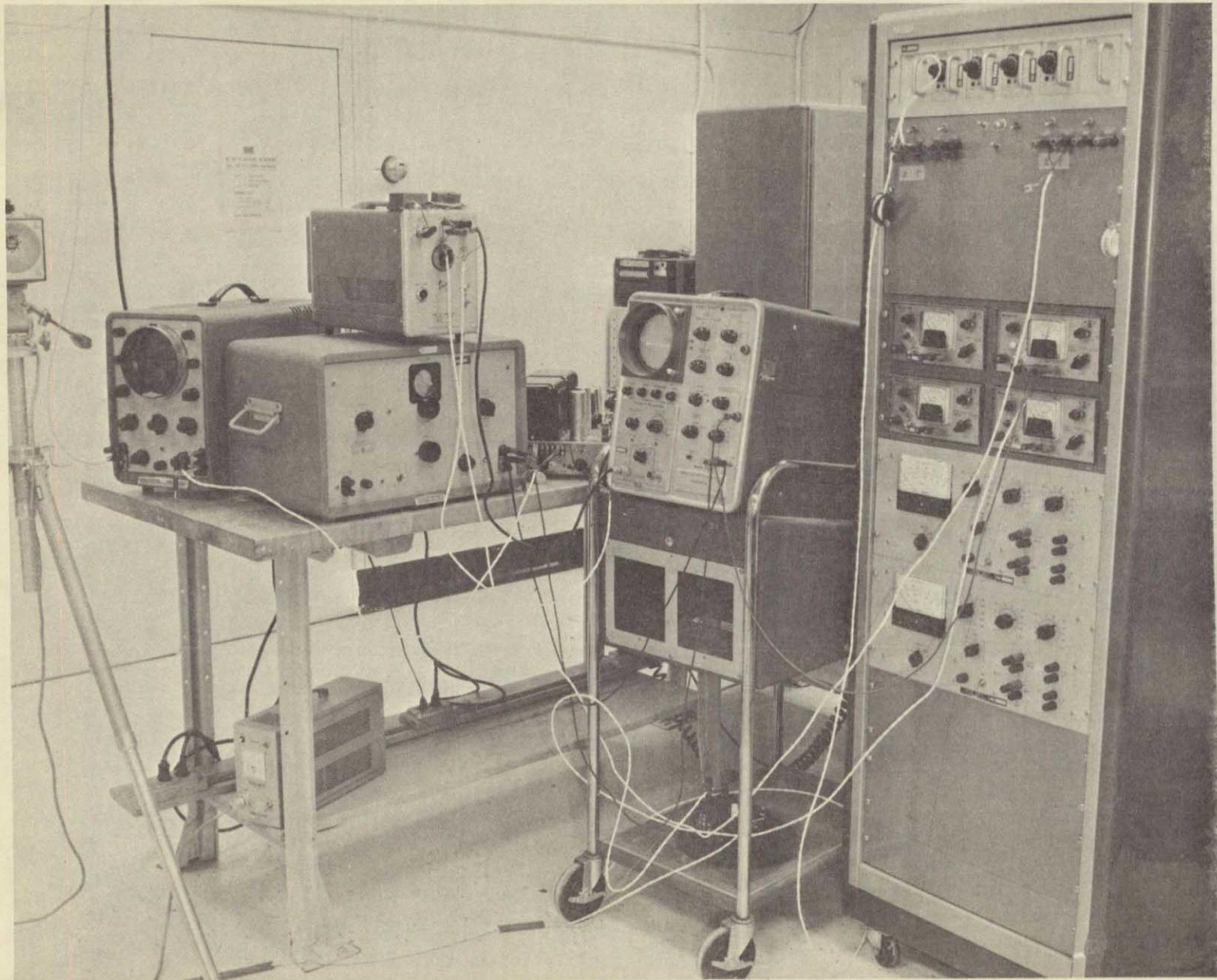


Figure VII-10 Electronics Equipment for Exciting and Measuring Dynamic Response

VIII. RESULTS

A. EXPERIMENTAL DATA

Using the techniques described in Section VII data were acquired for the vibrating cylinders and cones. Boundary conditions were clamped, excitation was at one point from an acoustic driver. Extensive use was made of Lissajous figures and stroboscopic light, and a phono cartridge pickup measured radial motions.

A list of the observable frequencies up to 1300 cps for cellulose acetate shells is given in Table VIII-1. About 90 frequencies are listed for the three shells, however, data on wave number is given for 14 frequencies. These frequencies were designated by a Lissajous figure from the response of a strain gauge mounted axially on the shell and from the signal generator exciting the speaker. Resonance was clearly identified as an elliptical figure stable during the time of test.

Each of the shells was illuminated by a strobe light and an attempt was made to count the nodal lines both axially and circumferentially. Limited success was possible using this system, however, the most useful condition was found to be a strobing frequency twice the fundamental frequency. This provided a double image on clearly defined lines.

The frequencies given in Table VIII-1 are a combination of motions. Because the shells are stiffened, the wall portions between stringers respond as plates between flexible supports. In addition, the behavior similar to the monocoque response is also present. The data given in the table are not considered to be complete, however, they are intended to indicate that cellulose acetate shells can be excited to produce complex vibrational patterns.

In an attempt to provide distorted modeling the flexible PVC shells were designed to provide vibration data. The walls of PVC were assumed to scale the flexural rigidity, steel wires the longitudinal extensional rigidity, and glass filaments the circumferential extensional rigidity. For the two cylinders and one cone a total of eight frequencies were observed. Cylinder A had five frequencies ranging from 12 to 59 cps, Cylinder B had only one frequency at 42 cps and Cone C had two frequencies, 25 and 29 cps. A list of these observations is given in Table VIII-2.

By using the strobe light it was possible to count the axial and circumferential waves for two of the frequencies for Cylinder A. Comparing the frequencies at $n=4$ and $n=5$ for $m=1$, on the inextensional curve for the Cellulose Acetate Cylinder A we find that:

Table VIII-1 Observed Frequencies for Cellulose Acetate Shells

Cylinder A	Cylinder B	Cone C
39* cps	140**cps	99***cps
44*	158**	132***
46*	188**	140***
54*	198	150***
64*	231	189***
68*	248	216
75	260	226
83	290	241
102	295	252
113	327	259
124	410	279
136	436	308
153	454	324
176	486	347
188	499	377
205	505	396
214	527	405
253	608	422
262	655	443
279	665	481
285	960	490
291	1026	532
315	1103	548
323		615
342		643
369		702
400		769
407		816
437		839
473		894
543		908
579		927
764		1020
		1110
		1340

*See Fig. VIII-1

**See Fig. VIII-2

***See Fig. VIII-3

Table VIII-2 Observed Frequencies for Flexible PVC Shells

Cylinder A	Cylinder B	Cone C
12 cps, $m=1$, $n=4^*$	42 cps	25 cps
20 cps, $m=1$, $n=5^*$		29 cps
34 cps		
43 cps		
59 cps		

*Observed with stroboscope

For $n=4$, PVC measured = 12 cps

CA calc. = 10 cps

For $n=5$, PVC measured = 20 cps

CA calc. = 16 cps

For this response to be excited around the cylinder the displacements at the point of forcing were about a half inch. At higher frequencies although at the point of forcing the shell may have been deflecting on the order of an inch the diametric point was not responding. The flexible PVC offered too much damping and the interaction between rigidities did not appear to occur.

B. COMPARISONS WITH OTHER DATA

For the several frequencies that were surveyed for the Cellulose Acetate shells comparisons have been made to the data presented by Arnold and Warburton [8] for fixed end cylinders. The cone was included as an equivalent cylinder. Also included is the inextensional vibrational mode [1] that becomes a bound for all other modes. For the relatively long length to radius ratio of Cylinder A the more exact and the inextensional modes are nearly the same as shown in Fig. VIII-1.

For a short length to radius ratio as for Cylinder B the more exact solution accounts for the effects of boundaries at the lower wave numbers as shown in Fig. VIII-2.

Treating Cone C as a cylinder with an average radius of the two end radii, the curves in Fig. VIII-3 are given for $m=1$ and $m=2$. For low wave numbers the effects of boundaries become apparent. Although these appear to be frequencies considerably below the 99 cps first observed for Cone C these could not be observed on the oscilloscope. From the experimental points on the figure the cone appears to be undergoing very complex motions.

To indicate the effect of longitudinal stiffening, the work of Sewall and Nauman [9] has been included. Fig. VIII-4 shows that when the stiffener area is about equal to the skin area there are no large differences in the response for the first axial wave, $m=1$. Neither internal nor external arrangements are particularly influential as shown by the crossover points. For Cylinder B and Cone C the stiffener area and the skin area are nearly the same. Therefore, the comparisons made with Arnold and Warburton [8] are felt to be good comparisons and are based on the unstiffened shell.

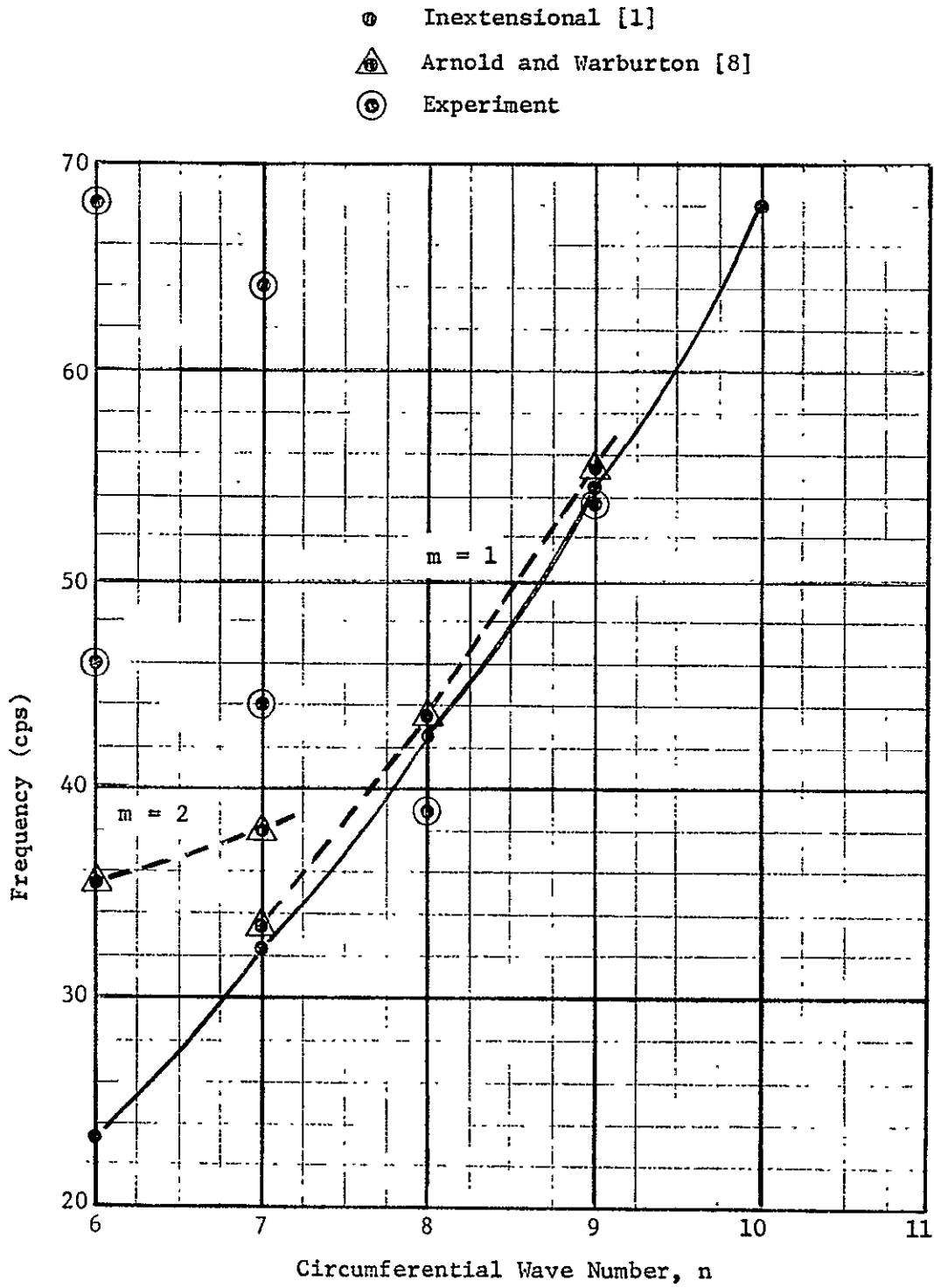


Fig. VIII-1 Frequencies for Cylinder A, Cellulose Acetate

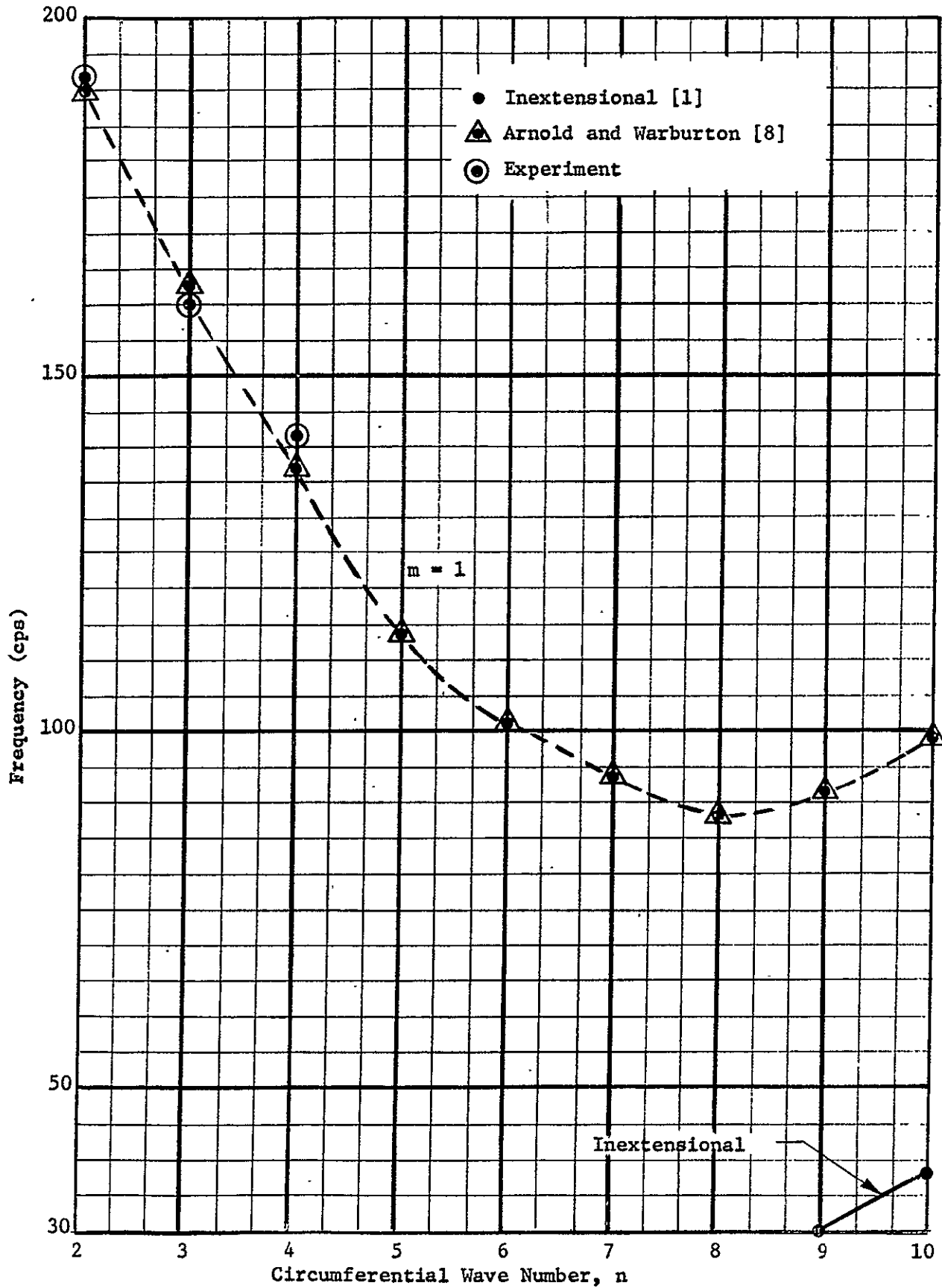


Fig. VIII-2 Frequencies for Cylinder B, Cellulose Acetate

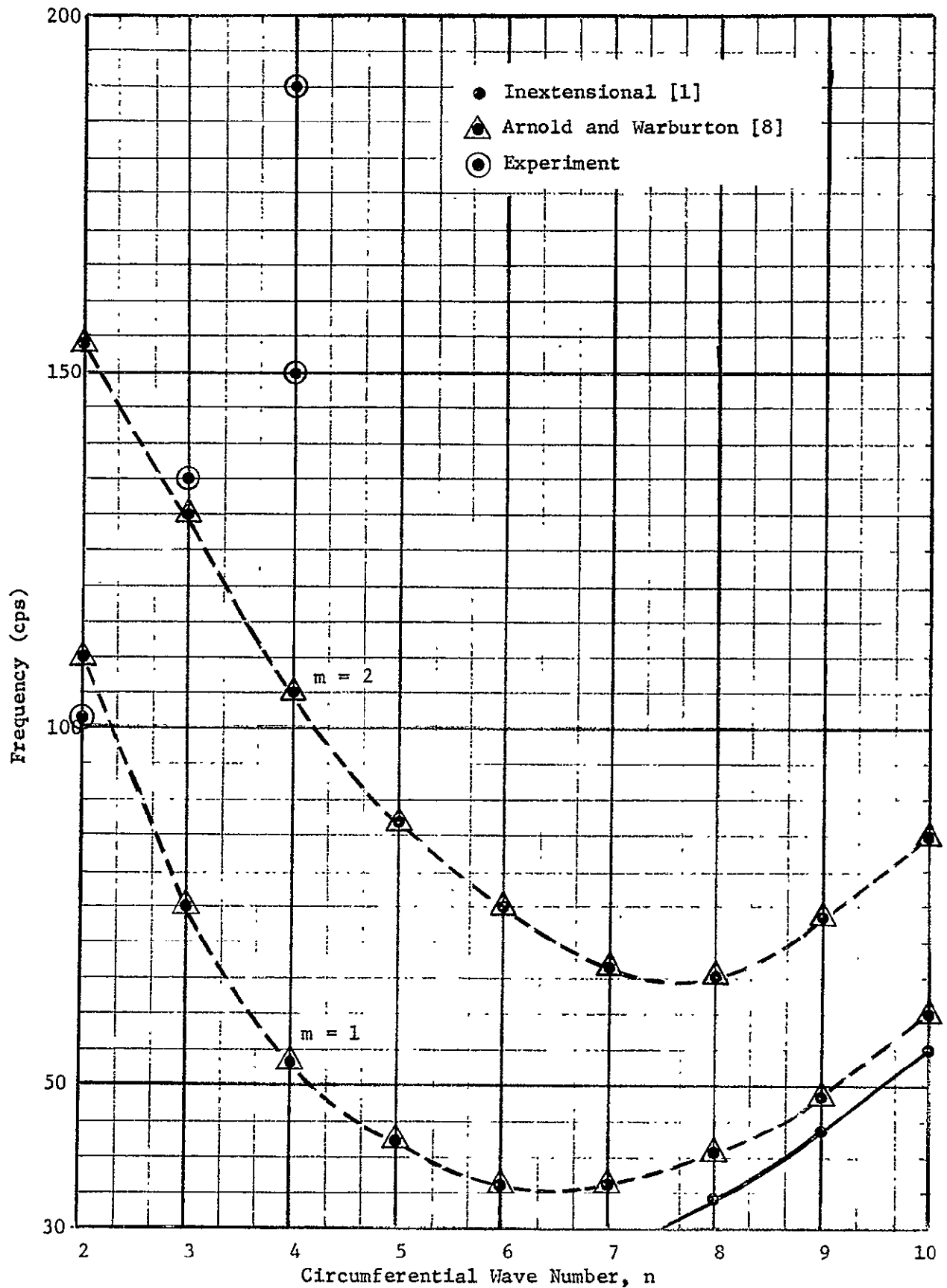


Fig. VIII-3 Frequencies for Cone C, Cellulose Acetate as an Equivalent Cylinder

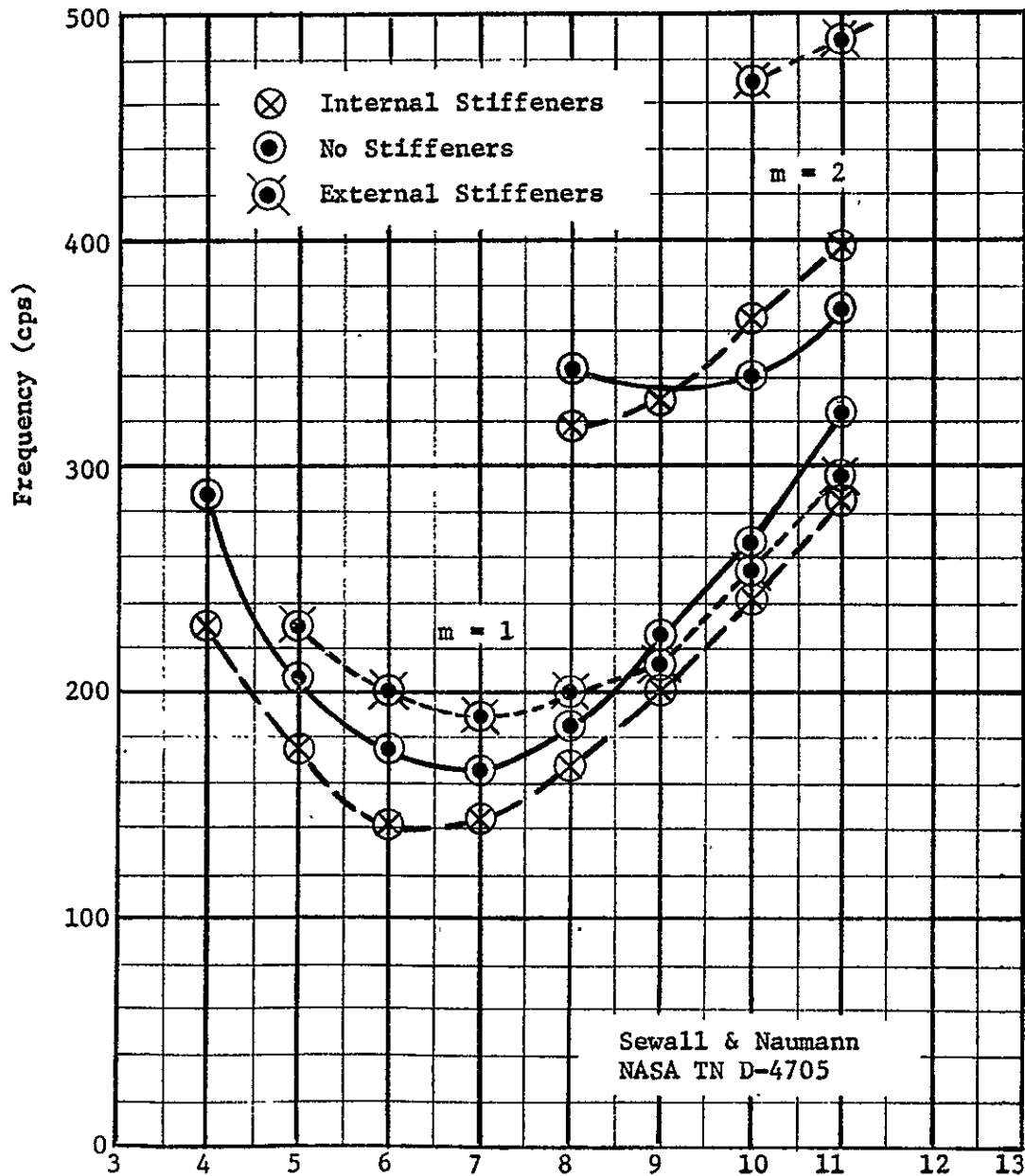
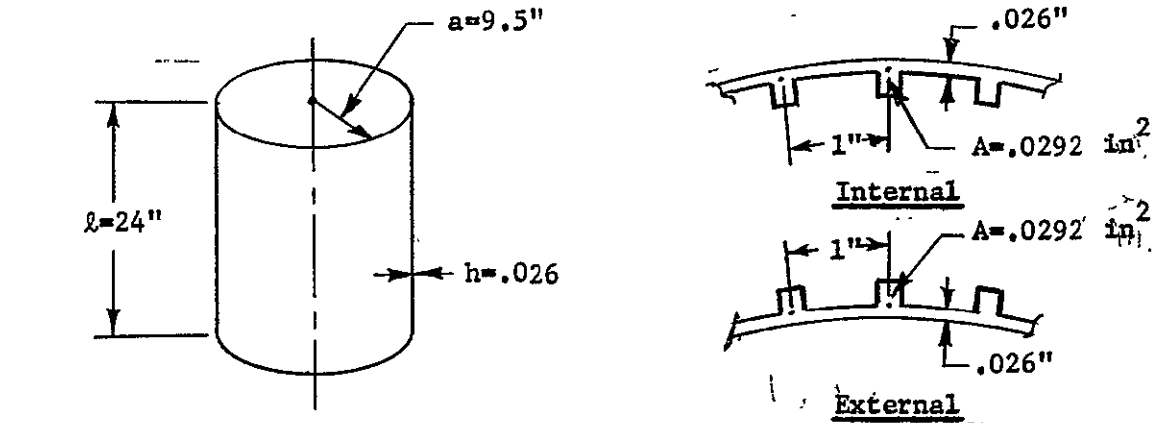


Fig. VIII-4 Frequencies for Simply Supported Aluminum Cylinders with Internal, External and No Stiffeners

To convert the response found for the 1/20 size plastic models to the full size aluminum prototype, the mode shapes are the same but the corresponding prototype frequencies are lower by 0.223 times the model frequency. For the basis of this factor see Equation (V-4).

C. CONCLUSIONS

Distorted scaling as applied to three-dimensional shell problems has limited application. For two dimensional shell problems where the shell is treated as a beam distorted scaling can be applied with confidence. When interactions between the longitudinal and circumferential, flexural and extensional rigidities become important, the model can provide this requirement when it is geometrically similar to the prototype.

For free vibrations of unloaded three-dimensional shell structures the most important scaling parameter (other than geometry) is the modulus to density ratio. When the prototype is made of an isotropic material with orthotropic construction, then the model, to be applicable, must be made similarly.

Plastic materials can be used for model construction, however, the tolerances required must be as good as or better than tolerances on metal models. All circular sections must be circular and concentric. All straight line generators must be maintained as straight line generators. Irregular surfaces caused by bonding produce a much more complicated structure than one of straight lines and circles. This more complicated structure vibrates in a more complicated manner than simple sine waves converging the surface.

The most difficult problem encountered was measuring wave numbers. Many useful techniques have been developed for metal shells and shells with smooth surfaces. The absence of a well defined reference surface from which to measure relative amounts of motion was the largest handicap. A technique that shows great promise and should be very useful is the use of holography to produce interference patterns. Other non-contacting, very sensitive devices applicable to nonmetallic surfaces are necessary.

With the ease of fabrication and low cost of the material modeling with dissimilar materials appears feasible. Strict adherence to the π terms particularly modulus to density and the several extensional and flexural rigidities can provide good scaling for three-dimensional vibrating shell problems.

IX. REFERENCES

1. A. E. H. Love, "A Treatise on the Mathematical Theory of Elasticity," Fourth Ed., Dover Publications, New York, 1944.
2. R. N. Arnold and G. B. Warburton, "Flexural Vibrations of the Walls of Thin Cylindrical Shells Having Freely Supported Ends," Proc. Royal Society of London, Vol. 197 A, 1949, pp. 238-256.
3. L. I. Sedov, "Similarity and Dimensional Methods in Mechanics," Academic Press, New York and London, 1959.
4. W. Flügge, "Stresses in Shells," Springer-Verlag, Berlin, 1962.
5. Structural Analyses, Scaling Analyses and Design of Models, NAS1-3382 Contract Report, North American Aviation Report SID 64-1331.
6. Materials Engineering, Vol. 68, No. 5, Mid-Oct. 1968.
7. D. F. Miner and J. B. Seastone, eds., "Handbook of Engineering Materials," John Wiley & Sons, Inc., New York, First Ed., 1955.
8. R. N. Arnold and G. B. Warburton, "The Flexural Vibrations of Thin Cylinders," Proc. Inst. of Mech. Engineering (London), Vol. 167, 1963, pp. 62-74.
9. J. L. Sewall and E. C. Naumann, "An Experimental and Analytical Study of Thin Cylindrical Shells With and Without Longitudinal Stiffeners," NASA TN D-4705, September 1968.